Universidad
Autónoma de Madrid

Facultad de Ciencias

Departamento de Física Teórica

Consejo Superior
de Investigaciones Científicas

Instituto de Física Teórica

IFT–UAM/CSIC

Applications of Holography to the Physics of Strongly Coupled Plasmas

Sergio Montero Modino,

Madrid, Enero 2008.

Universidad
Autónoma de Madrid

Facultad de Ciencias
Departamento de Física Teórica

Consejo Superior
de Investigaciones Científicas

Instituto de Física Teórica
IFT–UAM/CSIC

Applications of Holography to the Physics of Strongly Coupled Plasmas

Memoria de Tesis Doctoral realizada por
D. Sergio Montero Modino,
presentada ante el Departamento de Física Teórica
de la Universidad Autónoma de Madrid
para la obtención del Título de Doctor en Ciencias.

Tesis Doctoral dirigida por
Dr. D. César Gómez López,
Profesor de Investigación del Consejo Superior de Investigaciones Científicas,

y

Dr. D. Karl Landsteiner,
Investigador Ramón y Cajal.

Madrid, Enero 2008.

Contents

Preface

In this thesis we will find ourselves in a difficult situation: it is definitely a string theory work, but with a very strong motivation and *truly direct* relation to the experimental world. Being this such a (difficult) mixture, we should also say it is therefore quite challenging and very fun to work on it. We hope we have been able to present sensible things that do not clash with the present knowledge in any of them.

This thesis is about how to compute certain properties of a plasma, when this plasma happens to be non-Abelian and, more importantly, when it is strongly coupled. Basically we will say in this paragraph that string theory, and in particular the Anti-deSitter/Conformal Field Theory correspondence (AdS/CFT), has turned out to be quite an interesting tool, to say the least. That is so because using this correspondence one can even perform quantitative computations which in some cases give incredibly close numbers to those in the experiment. In this sense we can connect the experimental part with our string theory approach. Of course, and as we will see, this 6-year old approach still needs to develop until it reaches the maturity.

Building a bit more on that, why non-Abelian strongly coupled plasmas? There are very good motivations to study this kind of plasmas, being the prominent example the first microseconds after the Big Bang. The timeline of our Universe has a set of different periods, starting with the first 10^{-43} seconds where quantum gravity effects dominated. Before the onset of inflation at around 10^{-35} seconds the medium was already an extremely hot and dense soup made of *free* quarks and gluons, among other particles. As it evolved from the initial state it expanded and cooled down (and still cools), losing part of its symmetries. As a consequence it went through a series of phase transitions. The first one took place about 10^{-11} seconds after the bang and it is the so-called electroweak phase transition, which means that the weak and electromagnetic forces were no longer in disguise. The plasma of quarks and gluons continued cooling reaching the next transition, this one of much importance to us: the quark/hadron transition, also known in the more theoretical world as the *confinement/deconfinement transition.* This one set up the scale for hadron formation, the protons and neutrons as we know them appeared, and quarks and gluons were no longer free in "normal" conditions, i.e. those of the surrounding medium. It took place after the first ten microseconds, when the temperature was around 200 MeV. This fancy way of measuring temperatures can be translated to Kelvins using Boltzmann's constant, giving a resounding 2×10^{12} K; that is pretty hot indeed. After a couple of minutes neutrons and protons formed deuterium and Helium nuclei, i.e. nucleosynthesis initiated,

even though most protons remained uncombined as hydrogen nuclei; some 380,000 years later radiation decoupled from matter and neutral atoms formed; afterwards basically all we have had is structure formation like stars, galaxies and the like.

Thus, going back to the period roughly between inflation and the deconfinement transition, studying non-Abelian plasmas of quarks and gluons is no more but no less than partly studying the first microseconds of our Universe.

Of course there are more down-to-Earth approaches, and these are the so-called "Little Bangs". These explosions with very hot and dense matter have been produced colliding nuclei in the Relativistic Heavy Ion Collider (RHIC) at Brookhaven National Laboratory, USA. The outcome is a *fireball* mostly made of quarks and gluons, that thermalizes and cools down by expanding. This plasma has been named the Quark-Gluon Plasma (QGP), and it certainly resembles the process described two paragraphs above. The study of these fireballs have already told us many things about the underlying theory, Quantum Chromodynamics (QCD), above the deconfinement temperature. Understanding them may as well play a role in our understanding of the primordial plasma.

However, it turns out that describing the QGP is a hard task. It is not easy to extract *dynamical* information from them, e.g. the transport parameters. Robust collective phenomena in it seems to indicate that it is strongly coupled, enforcing the idea that computations from first principles —QCD computations— are hard to perform. And indeed this may be an opportunity for string theory, as we will try to show.

Our aim in the body of the thesis is two-fold. Firstly, we do not want to make this long. This means we do not plan to talk about every detail, much more information and technical parts may be found in the quite extensive literature. This leads to the second objective, namely that this is balanced with pedagogy and simplicity. We hope this has been achieved.

The work we present is split in two parts. In the first one we introduce the subject of study and provide the tools we will be using to obtain the results too:

Chapter 1 is devoted to presenting a motivation for the QGP through the deconfinement transition; explaining some basic notions of plasmas like the introduction of temperature, the description of small perturbations and some of the collective modes which can be found; and finally dealing in more depth with the RHIC experiment, which is our new tool to study the plasma phase.

Chapter 2 explains the basics of the Maldacena conjecture and its relevant generalizations to the present work, namely (a) how to put the gauge theory at finite temperature by addition of a black hole to the background geometry and (b) how to compute quantities coming from two-point functions in a real-time formalism and its

relation to the so-called *quasinormal modes.* These are complex eigenfrequencies associated to boundary-value differential equations subject to very peculiar boundary conditions.

Chapter 3 analyzes all the constraints that can be formally put on retarded Green's functions and on the quasinormal spectrum. It also makes an analysis of stability for different perturbations of the background.

Our results are in turn analyzed and commented in the second part, consisting of:

Chapter 4 presents basic results on the contribution of each collective mode to a gluon plasma. We compute the residues of the spectral function at the first four quasinormal modes for vector perturbations and for different values of the momentum. Whenever they exist, we follow as well the hydrodynamic modes, which are purely imaginary quasinormal modes. The results have an interesting interpretation as the time of thermalization τ_{therm} of the plasma.

Chapter 5 shows the computation of absorption lengths in a gluon plasma. The key point is to complexify the momentum instead of the frequency; thus one has complex momentum modes as a function of frequency ω instead of quasinormal modes as a function of momentum q. The absorption lengths are given by the inverse of the imaginary part of the complex momenta, and are shown to decay exponentially. In the zero frequency case, the complex momentum modes are connected to the spectrum of glueball masses in QCD$_3$, for which we compute some of them.

Chapter 6 considers a more phenomenological plasma through the addition of fundamental degrees of freedom, i.e. "quarks". Our results model the late time stages of the process of melting for collective excitations in a plasma. This process is set up in the gravity dual as a flavor brane falling through the black hole's horizon. It is argued that the picture drawn may be of use for studying charmonium suppression at RHIC.

I do not make any claim of originality concerning the first part of this thesis. Most of chapters 1 and 2 has been shaped through the reading of many original and review papers, plus one's own perspective. The original work I present concerns part two, and is based on our preprint paper [1] and our published papers [2–4].

Part I

Plasma Physics and Holographic Duality

Chapter 1

Strongly coupled plasmas

In this chapter we will be interested in QCD plasmas that are strongly coupled. How do they arise? We will devote the first section to the common lore on the phase structure of QCD. It will become clear that QCD not only exists "in vacuum", that is, as single excitations that pop out of it, but in other dresses that correspond to different phases. In particular, we will motivate some limits in which one can obtain the QGP. However, what is a plasma? So far we have mentioned it several times but have said nothing about it: section 1.2 tries to explain some of the key features that define and describe it, focusing at the end in non-Abelian plasmas for which the QGP is an example. One of the big motivations for studying these systems is that they are now accessible in ultrarelativistic heavy-ion collisions, so it looks like a good idea to describe those processes. This will be done in section 1.3, explaining how it is created, which is the evidence for its thermalization, and some of the observables that can be measured to explain its properties. Some results will be commented, trying to make the case for applying string theory to these phenomena.

1.1 The QCD phase diagram

Quantum Chromodynamics is an example of a non-Abelian gauge theory, that is, a quantum field theory whose interactions are governed by a local internal symmetry group with a non-commutative structure; for real-world-QCD this symmetry group is the *colour* SU(3), hence the prefix "Chromo" in its name. The carriers of the force, called the *gluons,* take values on the adjoint representation of its algebra, whereas *quark* matter appears in the fundamental representation. In our case this translates into the following: each quark comes in three colours, where three is the dimension of the fundamental representation and gluons come in eight different combinations of a colour and an anti-colour, where eight is the dimension of the adjoint. This is a qualitative difference with Abelian theories like Quantum Electrodynamics (QED), namely that the messengers of the force are charged under the gauge group. It is clearly not the case for the photons and the electric charge. In addition, in QCD we have six different *flavours* or types of quarks. Of course each of them comes in three colours.

Let us build a bit more on the charge since it will motivate further discussion in this

section. Suppose the coupling is small. As a quantum theory, QCD has corrections arising in the loop expansion that sometimes are divergent. If lucky enough, we can still make sense of the physics *renormalizing* the quantities that appear in the bare action to yield finite results; this renormalization procedure leads to a dependence on the energy scale of the processes, also called *running*. Take our gauge coupling g_s as the example. From the renormalization group equation, i.e. invariance of the renormalized effective action under changes in the regularization parameter μ, one obtains that the coupling must fulfill [5]

$$\mu \frac{\partial}{\partial \mu} g_s(\mu) = \beta(g_s) \ , \tag{1.1}$$

where $\beta(g)$ is the perturbative *beta-function* of the theory as a function of the coupling. Therefore we see that the running depends on whether this function vanishes or not. Now, the beta-function is a consequence of the effect of gauge interactions: had we not them we would find a vanishing $\beta(g)$, whereas distinct gauge interactions lead to different forms of $\beta(g)$. In this sense we expect a different qualitative behaviour between Abelian and non-Abelian theories, or QED and QCD for instance.

And indeed that is the case. In perturbation theory it is possible to expand the beta-function as a power series which reads as

$$\beta(g) = \beta_0 \, g^3 + \beta_1 \, g^5 + \dots \ . \tag{1.2}$$

Notice that g being small, each term contributes less than the preceding ones so a few terms may be enough to describe the behaviour of β. It turns out that for Abelian theories like QED, the coefficients β_i in the expansion are positive. Recalling eq.(1.1) this leads to a coupling that increases with the energy scale μ, eventually becoming big or even infinite in the so-called *Landau pole*.[1] In the case of non-Abelian theories like QCD we find just the opposite [6]; now the β_i coefficients are negative. For example, the first term for QCD [7,8] is obtained from the general SU(N_c) case imposing $N_c = 3$ and $N_f = 6$ in

$$\beta_0 = -\frac{1}{16\pi^2} \left(\frac{11}{3} N_c - \frac{2}{3} N_f \right) \ . \tag{1.3}$$

This coefficient is negative as long as $N_f \leq 16$ for $N_c = 3$, but our $N_f = 6$ is far below that. This leads to a totally different qualitative picture. We can solve approximately eq.(1.1) taking just β_0. Indeed, we give the solution for the strong fine structure constant $\alpha_s := g_s^2/(4\pi)$, since it is who governs the strength of the interaction and appears in the observables:

$$\frac{1}{\alpha_s(\mu)} \simeq \frac{1}{\alpha_s(\mu_0)} - 4\pi\beta_0 \, \log(\mu^2/\mu_0^2) \ , \tag{1.4}$$

where μ_0 is an arbitrary scale set for the renormalization upon which physics do not depend.

[1] However, this may not be the case since in that regime perturbation theory cannot be applied.

Here we can see the two well-known facets of QCD at different energies. At large momentum transfer μ, the strength of the interaction becomes small, and eventually goes to zero where quarks and gluons behave as free particles; this is ultraviolet *asymptotic freedom.* In that case perturbative computations have proved to be of much use and helped establish QCD as the theory governing the strong interactions. In the opposite regime, when μ becomes small enough the interaction as measured by α_s becomes big, and a perturbative expansion loses its predictable power. Below that scale the interaction is sufficiently strong to force quarks and gluons to clump together in hadrons in a sort of infrared slavery. This feature is often used to suggest *confinement.* How small is that scale? We can use eq.(1.4) to approximate the scale $\mu \approx \Lambda_{\text{QCD}}$ where α_s becomes $\mathcal{O}(1)$

$$\Lambda^2_{\text{QCD}} \approx \mu_0^2 \, \mathrm{e}^{1/\beta_0 g_s^2(\mu_0)} \ . \tag{1.5}$$

This clearly shows that Λ_{QCD} has a relevant physical interpretation, setting the scale of non-perturbative interactions. It can be seen as a true non-perturbative effect since it is proportional to an exponential of $\sim 1/g_s^2$ which cannot show up in Feynman diagrams. We will be interested in the following on phases other than the confinement phase. To grasp the qualitative difference it is thus important to understand confinement better, for which we say a few words below.

Confinement is often presented as the statement that partons, i.e. quarks and gluons, cannot escape the hadron since that would take an infinite amount of energy because the strong coupling increases. The process is described as the formation of a flux of chromoelectric force that ties the parton to the hadron; hence they are *confined* to live inside it. But is there true confinement in real QCD? In this theory not all the masses are bigger than $\Lambda_{\text{QCD}} = 216^{+25}_{-24}\,\text{MeV}$,[2] which roughly sets the size of nucleons. For instance, u and d quarks are $\mathcal{O}(1 - 10\,\text{MeV})$ and even s still is $\mathcal{O}(100\,\text{MeV})$. Imagine one kicks hard one of the quarks in the hadron. The object departs so much that the chromoelectric flux energy becomes big, of order $\Lambda^4_{\text{QCD}} \sim (200\,\text{MeV})^4$, allowing to form light (u, d, s) quark-antiquark pairs that eventually break the flux tube: the quark that departs may combine with one of the components of these pairs to form a new hadron and escape. Only if *all* quark masses where well above Λ_{QCD} it would be almost impossible for the chromoelectric flux tube to break into quark-antiquark pairs. Indeed, confinement has more to do with the statement that the chromoelectric flux does not spread out all over the space, at least no more than regions of radius around $\Lambda^{-1}_{\text{QCD}}$.

So effectively the quark has released itself; however, it does so as a constituent of a *new* hadron, not as an asymptotic single state. Thus, a new question arises: can we add more ingredients to the theory, i.e. enlarge the phase diagram of QCD, such that we achieve a different picture(s)? For example, may it be that quarks and gluons are not anti-screened

[2] We note this value was obtained for $N_f = 5$ active flavours at $\mu_0 \equiv m_Z \simeq 91\,\text{GeV}$ in the $\overline{\text{MS}}$ scheme [9].

but screened? A phase where quarks and gluons do not even have to depart from the hadron since they are already asymptotic states? The rest of this section is devoted to an overview of the current understanding of these issues. We will deal with a diagram that has the temperature T and the baryon chemical potential μ_B as representative parameters. Let us start by rising the temperature.

High temperatures. Telling this story is actually quite involved. Conceptually, one could trace back to Pomeranchuk [10], who suggested that a hadron can be called so if it has an independent volume to exist. This idea is better understood or sharpened through *Hagedorn's limiting temperature* [11]. The point is to consider a hadron gas which is being heated: at low temperature the vacuum excites pions, kaons, and the like. However, at temperatures above 100 MeV or so, massive resonances —hadrons other than those before— start to contribute, and around $150 - 170$ MeV they start dominating. Furthermore, extra energy fed into the system is consumed in exciting more and more massive resonances without really increasing the temperature. The system thus reaches a stage where hadrons overlap so much that they lose their identity, and instead one sees the constituent quarks and gluons.

This was really understood with the advent of asymptotic freedom in QCD, at least at very high energies [12,13]. It became clear that the critical temperature we just mentioned was actually signaling a phase transition to a new state of QCD matter; a soup of *deconfined* quarks and gluons which turned to be called the Quark-Gluon Plasma or QGP [14–16]. Research on this transition is still actively pursued. In fact, QCD lattice computations at $\mu_B = 0$ show a steep rise in thermodynamical quantities like the entropy, pressure and energy density, thus backing the arguments in the paragraph before (see figure 1.1). Moreover, recent studies [17, 18] show that such a change is not quite a phase transition of first or second order kind, but a rapid crossover, i.e. as opposed to a jump it is a rapid change as the temperature is varied which does not proceed through any singularity. Nevertheless, one still talks about phases in the sense of regions with different dominant degrees of freedom. Thus, the "critical" temperature T_c is described as a region between $150-190$ MeV where different values correspond to different observables used to extracting it, at least at zero baryon chemical potential [19].

So at (really) high temperatures, where thermal fluctuations carry a lot of momentum, one recovers asymptotic freedom and obtains a weakly coupled plasma gas of quarks and gluons; this can be studied analytically in thermal perturbation theory. Meanwhile, below the critical temperature the system is better described as a hadron gas. What is the situation around T_c? Recall the rise in quantities, much more pronounced for the energy density than for the pressure, so the sound velocity defined as $c_s^2 = \partial P/\partial \varepsilon$ drops below the ideal gas value $c_s = c/\sqrt{3}$. Also, even though ε increases fast it is not clear whether one

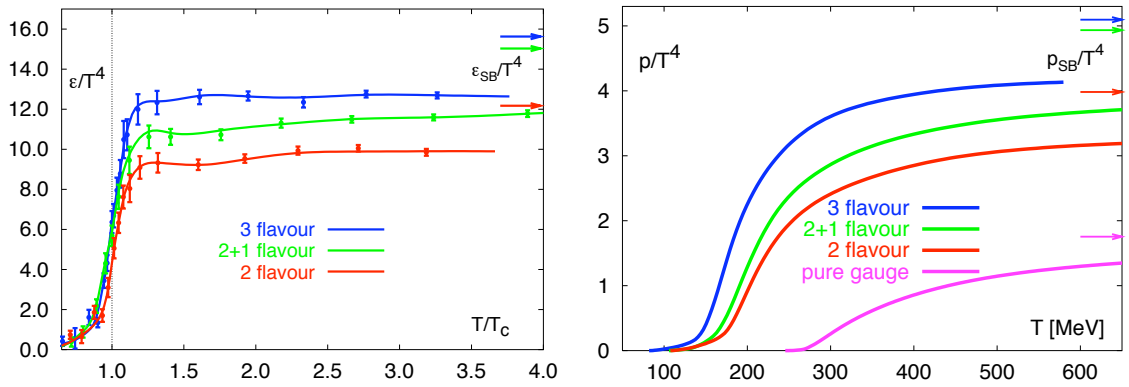

Figure 1.1: *Plots of the energy density and pressure in* QCD *normalized to* T^4 *for different simulations. It is also shown the asymptotic value corresponding to the Stefan–Boltzmann contribution of an ideal non-interacting gas of quarks and gluons. From [20].*

may claim that the new system will be at weak coupling. It is not clear if the asymptotic regime of a gas of deconfined quarks and gluons can be pushed too much towards the region around the critical temperature. As the plot shows, the energy density rises a lot past T_c, but stays practically constant up to temperatures of $4\,T_c$ and amounts to about an 80% of the ideal gas.

This and other reasons have led to a new paradigm, namely the strongly coupled quark-gluon plasma or sQGP. While many people in the community were pointing to a weakly coupled gas, some other thought the remaining 20% contribution was actually pointing to the effect of strong interactions in a non-perturbative system. So it could be possible that at temperatures $T \gtrsim T_c$ one finds a crossover plasma liquid of deconfined quarks and gluons, instead of a gas. That is one reason for studying strongly coupled plasmas, which motivates the title of this chapter.

Moving to non-zero chemical potential. The arguments given above are by themselves pretty exciting; however, the regions of physical interest move a bit or a lot —depending on what one wants to study— to $\mu_B \neq 0$. One can give an heuristic argument for a transition in the same spirit as that for high temperatures. In this case think of a hadron system composed of baryons inside a volume that can be compressed using a piston while keeping the temperature fixed. As one proceeds, the baryons get closer and closer, and eventually lose again their identity to become a liquid of quarks. The main difference is that now the state has a high number of quarks n_q and a low number of anti-quarks $n_{\bar{q}}$, whereas the populated high temperature system was producing meson excitations, so it had both an equal number of quarks and anti-quarks. At low T this transition is thought to appear around $5-10$ times the normal nuclear matter density, and the physically relevant situation is that of compact stars in astrophysics. Continuing

to higher densities one eventually jumps to other phases which will not be relevant for the thesis, like the *colour superconductor* where colorful bound states form.

Let us focus on smaller μ_B's. It turns out that the most powerful tool for studying non-perturbative QCD, namely the lattice approach, has a hard time when introducing a finite chemical potential. This is related to the so-called *sign problem:* the action for $\mu_B \neq 0$ ceases to be positively defined and turns complex. This poses problems since it is used to weigh field configurations when evaluating the path integral. In recent years there has been some improvements though, and one can reach out to small values. This is somehow enough for part of our interests, since close to the T axis one finds the path followed by the early Universe when it suffered the quark/hadron transition. These lattice calculations seem to show again a crossover instead of a sharp phase transition, and this information might be relevant for our understanding of that physical setup.

What happens for bigger chemical potentials? Here the lattice is still poorly understood, but we will see in section 1.3 that we have at our disposal the most important tool among all: experiments in the form of *relativistic heavy ion collisions.* The idea is to collide heavy nuclei in the hope that one creates the quark-gluon plasma going through the crossover region. These experiments will be good to analyze such crossover at bigger μ_B, and to even study the so-called QCD *critical point:* it is expected from effective models that the crossover transition becomes a true first order phase transition for larger chemical potential. To summarize, the state of the art has been depicted in figure 1.2.

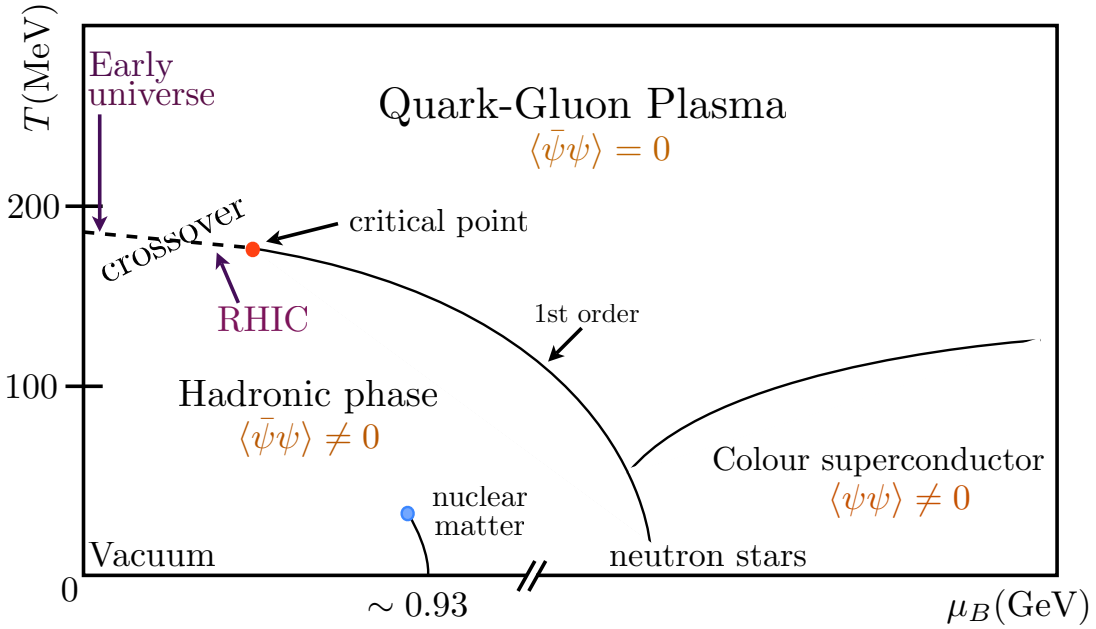

Figure 1.2: *A bird's eye view of the* QCD *phase diagram as currently understood.*

1.2 What is a plasma?

Looking back to the preceding section we have already cited the word 'plasma' ten times. One thing that comes right to our minds nowadays are plasma TV's. Well, that is right: there is a "plasma at work" there. Indeed, there are estimations pointing out that nearly 99% of the visible matter in the whole universe can be considered a plasma (c.f. [21]). This plethora of examples ranges from the man-made one cited above or the QGP, passing through terrestrial plasmas like the polar aurorae and reaching to astrophysical ones like stars, solar wind or even the interstellar and intergalactic mediums. But all of them, with no exception, share a common feature: it is matter where charges are screened due to the presence of other moving charges.

For example, for a QED plasma the electrons have been separated from the then ionized atoms, and due to this mobility they modify Coulomb's law to yield a distance-dependent charge. In the QGP, one would talk instead of the "ionization" of quarks and gluons from the hadrons. However, there is a big difference because now it is the color charge of the quarks and gluons who is screened. This is important since this charge is non-Abelian, and poses noticeable dissimilarities with Abelian plasmas.

In this context, transitions to the plasma phase as the one we studied in section 1.1 can be easily seen in electromagnetic examples. Take for instance a gas of hydrogen atoms at thermal equilibrium, for which the binding energy of electrons is 13.6 eV. In such equilibrated statistical systems Boltzmann's constant k_{B} serves as a bridge between microscopic and macroscopic physics, and one can relate the energy to temperature roughly as $E \sim k_{\mathrm{B}}T$. If one heats the gas to a temperature where thermal fluctuations have an energy of the order of the binding energy, the electrons can be released from the atom. In this example that happens for

$$T_c \simeq \frac{13.6\,\mathrm{eV}}{8.617 \times 10^{-5}\,\mathrm{eV/K}} \simeq 1.6 \times 10^5\,\mathrm{K}\ . \tag{1.6}$$

In QGP's the situation is more difficult, and as we have seen one has to resort to other techniques. Moreover, in electromagnetic plasmas one can define the strength of the interaction through the so-called $\Gamma_{\mathrm{e.m.}}$ parameter given by the ratio of the average potential to kinetic energies, $\Gamma_{\mathrm{e.m.}} = \langle \mathrm{PE} \rangle / \langle \mathrm{KE} \rangle$, whereas in relativistic plasmas like the QGP the notion of potential (or ionization) energy can not be well formulated [22]. This forces to consider other possibilities, like the ratio of the shear viscosity η (a measure of the mean free path of particles) to the entropy density in volume s (a measure of the average separation between particles).

We will see more of this on the following section, but now we turn to a more theoretical description of these systems, introducing temperature in a quantum field theory and showing the relevant scales and the treatment of small perturbations.

(Near-)equilibrium plasmas and linear response theory. Relativistic quantum field theories have an undetermined number of particles from pair creation, but here their number is related to the charge, which we keep fixed, so one should describe its statistical physics in the canonical ensemble. The partition function in such an ensemble is

$$Z = \mathrm{Tr}\ \mathrm{e}^{-\beta\hat{H}} = \sum_{\text{states}} \langle E_n|\mathrm{e}^{\beta\hat{H}}|E_n\rangle = \sum_{\text{states}} \mathrm{e}^{-\beta E_n}\ , \tag{1.7}$$

where the temperature $\beta := T^{-1}$ appears as a Lagrange multiplier for the mean energy $\langle\hat{H}\rangle$. Now, the very presence of the Hamiltonian suggests a possible interpretation of the exponential as a time evolution operator provided one has *imaginary* times $t = -i\beta$. Thus, we can now connect to path integrals since we know how to represent time evolution in them. For imaginary times we have the Euclidean action so

$$Z = \int [\mathcal{D}\varphi]\, \mathrm{e}^{-S_{\mathrm{E}}[\varphi]} = \int [\mathcal{D}\varphi]\, \mathrm{e}^{-\int_0^\beta \mathrm{d}\tau \int \mathrm{d}^3\mathbf{x}\, \mathcal{L}[\varphi]}\ , \tag{1.8}$$

with an important proviso: the implementation in the statistical description of the trace over states translates here to imposing (anti-)periodic boundary conditions on the fields

$$\varphi(0,\mathbf{x}) = \pm\varphi(\beta,\mathbf{x})\ , \tag{1.9}$$

with the plus sign for bosonic excitations and the minus sign for fermionic ones. Therefore, introducing temperature in the field theory in this way corresponds to compactifying time in an Euclidean time circle and imposing certain boundary conditions on the fields. This is the *Matsubara* formalism. It should be noted however that there is an equivalent but quite distinct method which operates in real-time. It is the *Keldysh* formalism where the time contour is chosen differently from the Matsubara one.

In the thermal medium the interactions "dress" the particles converting them in general in collective modes with a mass and a decay width. A nice thing is that one can organize physics by length scales *à la* Wilson, at least at weak-coupling g or very high temperature [3]

- The first scale is $1/T$, associated with the typical energy $E \sim T$ of individual quasi-particles, i.e. particles just slightly modified which can be somehow connected to the elementary excitations.

- However, already at one-loop there are modifications, like the appearance of a thermal mass $\sim gT$ for the excitations which for instance modifies the initial dispersion relation as $E(\mathbf{p}) \sim \sqrt{\mathbf{p}^2 + m_{\mathrm{th}}^2(T)}$. Thus the scale is $1/(gT)$, where g is from one loop and T is the dimensionful parameter. It is associated with collective motion of individual particles and sets the scale for the damping of (chromo-)electric fields, i.e. *Debye screening*. In chapter 5 we study this for a strongly coupled gluon plasma.

[3] It should be said that in thermal field theory the natural expansion parameter is g and not $\alpha = g^2/(4\pi)$.

- One can ask what happens at larger length scales (for non-Abelian theories). In such cases one cannot resolve the time circle and effectively sees a three-dimensional theory, expanded as

$$S_{\rm E} = \frac{1}{g^2}\int_0^\beta \mathrm{d}\tau \int \mathrm{d}^3\mathbf{x}\ \mathrm{tr}\, F_{\rm 4d}^2 \simeq \frac{\beta}{g^2}\int \mathrm{d}^3\mathbf{x}\ \mathrm{tr}\, F_{\rm 3d}^2 + \dots\ , \tag{1.10}$$

  so the three-dimensional coupling $g_{\rm 3d}^2 = g^2 T$ is now dimensionful. For such theory confinement is known, so beyond $1/(g^2T)$ there are no magnetic forces. Also, thermal widths of collective excitations are proportional to this scale so only at weak-coupling one may call them quasi-particles.

All of these physics is obtained studying the response of the theory to small external perturbations that do not change significantly the state of the plasma. The time evolution of such small disturbances of the equilibrium system is determined by the correlation functions of pairs of observables; this is the domain of *linear response theory,* and formulated in real-time. To apply this method one has to extract the effect of the perturbation on an observable, measured as

$$\delta\langle\hat{\mathcal{O}}(t)\rangle = \langle\overline{\Psi}_{\rm S}(t)|\hat{\mathcal{O}}|\overline{\Psi}_{\rm S}(t)\rangle - \langle\Psi_{\rm S}(t)|\hat{\mathcal{O}}|\Psi_{\rm S}(t)\rangle\ , \tag{1.11}$$

where the barred state vector is suffering the perturbation and the unbarred one is not, and subscripts (S,H) stand for Schrödinger and Heisenberg as usual. If the perturbation is small as said, it can be modelled through an expansion in a potential term $\hat{V}_{\rm H}(t)$

$$|\overline{\Psi}_{\rm S}(t)\rangle = \mathrm{e}^{-i\hat{H}t}\left(1 - i\int_{t_0}^{t}\mathrm{d}\tau\,\hat{V}_{\rm H}(\tau) + \dots\right)|\Psi_{\rm H}\rangle\ , \tag{1.12}$$

where picking just the first term corresponds to the unperturbed evolution $|\Psi_{\rm S}(t)\rangle$. A bit of algebra yields the following form for the effect of the perturbation on the quantity $\mathcal{O}$

$$\delta\langle\hat{\mathcal{O}}(t)\rangle = -i\int_{t_0}^{+\infty}\mathrm{d}\tau\,\langle\Psi_{\rm H}|\,\theta(t-\tau)\,[\hat{\mathcal{O}}_{\rm H}(t),\hat{V}_{\rm H}(\tau)]\,|\Psi_{\rm H}\rangle + \text{higher } \hat{V}\ . \tag{1.13}$$

This is the linear response. We will be interested in examples where the perturbation is introduced by a source, so that we can compute two-point correlation functions. Then $\hat{V}(\tau) = \int \mathrm{d}^3\boldsymbol{\xi}\, j_b(\tau,\boldsymbol{\xi})\,\hat{\mathcal{O}}_{{\rm S},b}(\boldsymbol{\xi})$ and the linear response is

$$\delta\langle\hat{\mathcal{O}}_a(t,\mathbf{x})\rangle := -\int \mathrm{d}\tau\,\mathrm{d}^3\boldsymbol{\xi}\ G_{{\rm R},ab}(t-\tau,\mathbf{x}-\boldsymbol{\xi})\,j_b(\tau,\boldsymbol{\xi})\ , \tag{1.14}$$

where we have introduced the definition of the retarded Green's function. The appearance of the retarded function is clear from causality: the system will respond only *after* the perturbation starts. Possible sources $j(\tau,\boldsymbol{\xi})$ that we will use in this thesis involve *dissipation* if the perturbations are localized in time or *absorption* if they are localized in space.[4]

[4]There can also be diffusion effects if conserved charges are involved.

Dissipation is related to correlations in time that describe how lumps of energy are lost in the system. The absorption is directly related to spatial correlations in the equilibrium state. At high temperatures the system is in a very disordered phase, so measurements made in different parts of the plasma give uncorrelated results. For the same reason, a small perturbation cannot travel too far in the plasma before being washed out by thermal fluctuations. How far this can be depends on the details of the plasma, but in general one expects that the characteristic absorption lengths decrease as the temperature increases.

Plasma hydrodynamics. A possible description of the evolution of the fireball produced at RHIC supported by the data is in terms of hydrodynamics, so let us have a brief look at it here.

Hydrodynamics is about the dynamics and thus near-equilibrium behaviour at large distances and time scales. To formulate it one uses directly equations of motion instead of an action principle. This is so because, as we said before, in the thermal medium the collective excitations have an associated decay width and thus one has to accommodate in a simple way for dissipation phenomena. We may start with an easy example: the hydrodynamic equation of motion for a conserved charge. Imagine we have some symmetry; in this context we study the diffusion of the charge associated to it given by the continuity equation

$$\partial_\mu j^\mu = 0 \ , \tag{1.15}$$

where the current j^μ can be expressed in terms of the relevant quantities for the medium through the so-called constitutive equations

$$j^\mu = \rho\, u^\mu - D(g^{\mu\nu} + u^\mu u^\nu)\, \partial_\nu \rho \ , \tag{1.16}$$

with ρ the charge density, u^μ the local fluid velocity and D the diffusion constant.

To gain full insight into the effect of such a current one has to compute the full real-time retarded Green's function, as seen from linear response theory, in the hydrodynamic limit, i.e. low momentum and low frequency. In particular, the transport parameters can be expressed in terms of the retarded function through the Green–Kubo relations. For our charge diffusion

$$D = -\,\text{factor} \times \lim_{\omega\to 0} \frac{2T}{\omega}\, \text{Im}\, \widetilde{G}^{j-j}_{\text{R}}(\omega, \mathbf{k} = 0) \ . \tag{1.17}$$

Of course one can be somehow more ambitious, and be interested in the location of the poles of the retarded Green's functions to study the dispersion relations for these collective modes. In this limit, one must look for normal modes of the form $\mathrm{e}^{-i\omega t + i\mathbf{k}\mathbf{x}}$, named the *hydrodynamic modes.* In our example, using equations (1.15) and (1.16) one arrives at the equation for charge diffusion

$$\partial_t \rho - D\Delta\rho = 0 \ , \tag{1.18}$$

which for our particular modes has solution $\omega = -iD|\mathbf{k}|^2$. Therefore, this pole in the retarded Green's function of two currents encodes the diffusive behaviour of the charge in the thermal medium.

We end this section with the most important transport parameters, which in this case are tied to the energy-momentum tensor. They describe the flow of energy and momentum in the medium, but in spirit the steps one must take are the same. The conservation equation is $\partial_\mu T^{\mu\nu} = 0$ and the constitutive relation to first order in dissipation

$$T^{\mu\nu} - T^{\mu\nu}_{\text{ideal}} = -P^{\mu\alpha}\, P^{\nu\beta} \left[\eta\Big(\partial_\alpha u_\beta + \partial_\beta u_\alpha - \frac{2}{3}\, g_{\alpha\beta} \partial_\lambda u^\lambda \Big) + \zeta\, g_{\alpha\beta} \partial_\lambda u^\lambda \right] \ , \tag{1.19}$$

with η and ζ the two transport parameters, called *shear* and *bulk* viscosities, respectively. $P^{\mu\nu}$ is a projector onto directions transverse to u^μ. The corresponding hydrodynamic modes are —choosing $\mathbf{k} = (0, 0, k)$

- *Shear modes,* for fluctuations of $T^{0\perp}$ and $T^{3\perp}$ where $\perp = (1, 2)$. They are related since $T^{3\perp} = -\frac{\eta}{\varepsilon + P}\, \partial_3 T^{0\perp}$, and the evolution can be encoded in $T^{0\perp}$, for whom it is diffusive: $\partial_t T^{0\perp} - \frac{\eta}{\varepsilon + P}\, \partial_3^2 T^{0\perp} = 0$. This yields the shear mode

$$\omega = -i\, \frac{\eta}{\varepsilon + P}\, |\mathbf{k}|^2 \ , \tag{1.20}$$

  for diffusion of momentum in a given direction to the transverse ones.

- *Sound modes,* for fluctuations of T^{00}, T^{03} and T^{33}. Now there are two conservation equations, which upon diagonalization yield the sound mode

$$\omega = c_s |\mathbf{k}| - \frac{i}{2} \left(\frac{4}{3}\eta + \zeta \right) \frac{|\mathbf{k}|^2}{\varepsilon + P} \ , \tag{1.21}$$

  where c_s is the sound velocity for the propagation of the energy density.

We will see more on these modes and related responses in (quark-)gluon plasmas from string theory in chapters 4 and 5 of this thesis.

1.3 RHIC physics: QGP in more detail

Back to 1974, T.D. Lee suggested one could create a new phase of matter *"by distributing high energy or high nucleon density over a relatively large volume"* [23, 24], and the way to have such high densities and temperatures could be in relativistic heavy-ion collisions [25, 26]. The qualitative difference was that early accelerators collided a few particles at a time, so it made little sense to talk about statistical quantities and a 'macroscopic' state of matter. In simple terms, they were experiments in vacuum.

Some of these facilities were thus modified to accelerate heavy ions and collide them with a fixed target, like AGS at Brookhaven and SPS at CERN. Even though they produced beams of 10 and 160 GeV per nucleon, the center-of-mass energy was somehow low, 5 and 17 GeV per nucleon pair respectively; and it is this energy the one relevant for collision experiments. The purpose of RHIC was to remove that fixed target by colliding nuclei on nuclei, mainly gold ions. This has been achieved and currently the center-of-mass energy reaches to 200 GeV, and in LHC it will be an order of magnitude above! That is a lot of total energy indeed, around 39 TeV since for gold $A = 197$. But much more important is the fact that it will produce energy densities above the critical one $\varepsilon_{\rm crit} \approx 1\,{\rm GeV/fm}^3$, where the energy density of the medium is that of matter inside hadrons.

The ions after accelerated to 99.995% of the speed of light enter two rings, one for each beam direction, which intersect at six different points. At four of them there are detectors, named STAR [27], PHENIX [28], PHOBOS [29] and BRAHMS [30], whereas the other two intersections are left for future experiments. Each of the detectors focus mainly on different aspects of the system formed in the collision, although there is some overlap in the analysis to allow for cross-checking.

Creation and evolution. How does the collision look like? As said above, at RHIC the heavy ions are travelling at light speeds, and for those quoted the corresponding Lorentz factor is $\gamma \simeq 100$. In Bjorken's own words, one has two *"highly Lorentz-contracted pancakes"*. After approximating they eventually collide and recede leaving in between a very hot and dense medium. The shortest time scale for the collision comes from the simple estimation of the overlapping time between the pancakes in the laboratory/center-of-mass frame

$$t_{\rm min} = 2\,\frac{R}{\gamma c} \simeq 2\,\frac{7\,{\rm fm}}{100\,c} = 0.14\,{\rm fm}/c\ , \tag{1.22}$$

where R is the average size of the nucleus. Some estimates point to an energy density of about $30 - 40\,{\rm GeV/fm}^3$. The medium inside comes from a lot of secondary particles produced in the collision, where 'slow' ones are first formed in the central region whereas 'fast' ones —large momentum suffering time dilation— are produced later towards the external part where the pancakes are receding. The production of these particles has an associated time scale called *formation time*, $t = \tau_{\rm form}$; they are those that later will form the QGP. Some estimates gives $\tau_{\rm form} \simeq 0.35\,{\rm fm}/c$, which is causally good since it is bigger than $t_{\rm min}$, and a peak energy density for created particles of about $15\,{\rm GeV/fm}^3$.

By later one means above that the system has to thermalize, and the way to achieve this is through collisions between the formed particles. This is important since one of the criteria for QGP formation at RHIC is that matter must be to a good approximation in a thermal state. A partial positive result is the fact that the particle yields on the detectors can be fit to a thermal distribution. So provided this is the case one could use hydrody-

namics to describe the further evolution of the system, first being one-dimensional where one can use Bjorken's cylindrical picture [31] and later three-dimensional and anisotropic, as seen from the spectrum of particles transverse to the longitudinal collision line (see below). Moreover, the thermalization time can be obtained matching data to collective parameters in hydrodynamical simulations, giving $\tau_{\text{therm}} \simeq 0.6 - 1.0\,\text{fm}/c$. This number is pretty small, and indeed it should not be much less than $1\,\text{fm}/c$ since that is the typical time taken by a signal from a parton to travel out of a hadron.

All of this picture has an associated cooling by expansion so eventually the energy density and temperature will drop below $\varepsilon_{\text{crit}}$ and T_c, going through the deconfinement crossover, producing jets by hadronization which are those actually measured on the detectors. The full movie is depicted in figure 1.3.

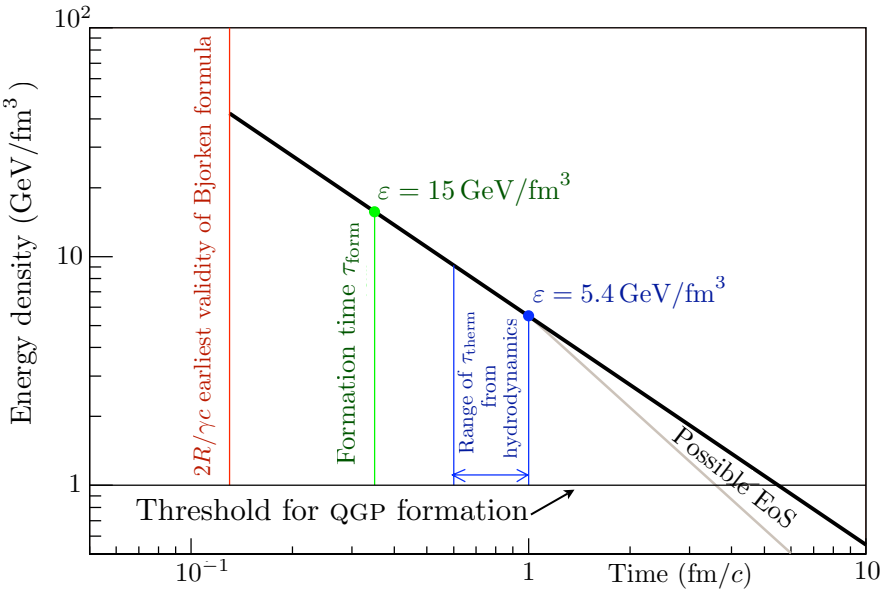

Figure 1.3: *Representation of the energy density versus time as follows from the Bjorken picture.*

Apart from creating the QGP one would like to study its properties too, and some of these are at the same time giving an insight into e.g. thermalization. That is the case of viscosity η. We mentioned that there is an anisotropy effect in the transverse distribution of particles, which is most impressive when the collision between the nuclei is not head-on; in this case the initial QGP region is "almond-shaped", and its evolution suffers a gradient pressure that pushes more particles in one directions than in others, called the *elliptic flow* (see left of figure 1.4). The experimental anisotropic distribution can be fitted in an expansion in terms of the azimuthal angle [27–29], where the first and most important term is the elliptic flow parameter v_2. To reproduce its value in the hydrodynamic simulations [32–35] it is necessary to introduce viscosity, in particular a very small value of η/s [36]. This ratio is basically mean-free-path over interparticle-distance,

so a low value corresponding to large interactions even though being separated means being at strong coupling, strengthening the liquid sQGP picture. As said above, this also gives a short thermalization time.

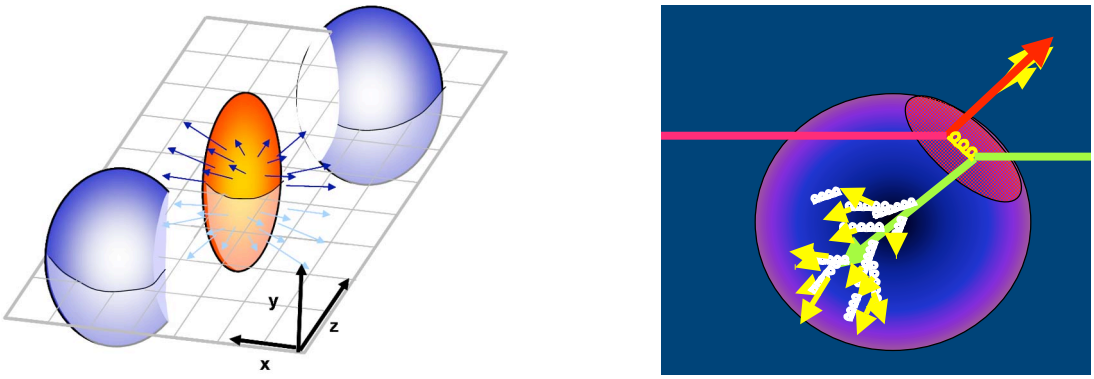

Figure 1.4: *(Left) Initial configuration of a non-central collision that then flows elliptically. From [37] (Right) Effect of jet quenching in the interior of the plasma: the red parton escapes and hadronizes whereas the green one is lost in the medium through collisions and gluon radiation. From [38].*

Other paradigmatic property of the QGP is its large opacity to energetic coloured particles, i.e. large energy losses. The simple idea behind that name is that in such a dissipative medium a charged particle will lose its energy as it moves through it, partly from collisions, partly from gluon radiation. A nice thing is that partons produced in the medium can work as probes of it. At this stage one should distinguish heavy from light particles. For instance, a heavy quark like the charm quark, with a mass notably above T_c, is expected to lose energy more slowly, thus thermalizing more slowly and leading to a smaller elliptic flow. So measuring its energy loss rate help to understand its thermalization time. On the other hand and concerning light quarks, there is an observable effect called *jet quenching*. Imagine a quark anti-quark pair produced close to the boundary of the plasma; it may happen that one of them is produced pointing towards the external region and escapes to later produce a jet seen in the detector. But the recoiling mate will go towards the interior losing its energy and eventually disappearing (see right of figure 1.4). This would lead to a missing jet in that direction, and indeed this is measured at RHIC, so studying its energy loss at strong coupling is important experimentally.

There are of course much more properties which can be studied. For instance the suppression in the yields of heavy bound states like J/ψ, as compared to hadron-hadron and hadron-nucleus collisions where there is no plasma formation that can help them melt. In this thesis we will say nothing about a dual description of the formation time. Concerning the thermalization time, an accurate description in terms of thermal field theory is still lacking, due to the fact that it is in the regime far from equilibrium and linear response theory cannot be applied. Some suggestions have though been made towards an

explanation tied to plasma instabilities [39–46], but this point has to be made much more precise yet. However, even though we do not dive into the mechanisms of thermalization, in chapter 4 we will give an interesting point of view on early thermalization from the application of the AdS/CFT correspondence. Also, in chapter 5 we will study absorption lengths in a gluon plasma, which in the static limit can be seen as screening lengths of the chromoelectric charge. As referred to meson melting and suppression, in chapter 6 we will study the late time stage of the process of melting for low-spin mesons in a supersymmetric quark-gluon plasma.

An interesting connection? So far we have set QCD as the theory behind the physics of the QGP. However, performing first-principles QCD computations is a hard task. As already said, after thermalization one resorts to hydrodynamic models to describe the evolution of the fireball, and much effort is put in computing the relevant parameters that can be related to the observables. Indeed, the value of α_s is usually quoted to be around $1/2$ for RHIC scales. Thus, it is somehow clear that perturbative QCD will not provide accurate results in general. For instance, the perturbative prediction for the Debye mass m_{D} seems to be one third of the measured one at around those energies [47–50]. Concerning hydrodynamic parameters, the famous ratio of the shear viscosity to entropy density η/s is about an order of magnitude higher in perturbative QCD than what seems to be measured at RHIC [51–55]. On the other hand, lattice QCD has proved to be a powerful tool when we play with *static* quantities at strong coupling, which by itself are very important ones. We have talked about some of them, e.g. the pressure and energy. But when it comes to *dynamical* information, i.e. real-time phenomena like the afore-mentioned transport parameters, the lattice has a hard time since it is formulated in the Euclidean. Take for example recent attempts to obtain Lorentzian spectral functions [56–58].

Thus the question is: do we have an alternative tool to describe the dynamical non-perturbative processes that take place in these kind of plasmas? Do we have an alternative description of the hydrodynamical simulations? In fact, can we even go beyond and describe in some way the thermalization process or part of it? Let us think for a moment about string theory.

One of the on-going projects in theoretical high-energy physics today is to develop a finite and sensible theory of quantum gravity. In many cases a classical description is enough; however, there are some extreme situations such as the physics of black holes where it is important to understand the quantum effects, think of the information paradox for instance. These effects would take place at around the *Planck energy scale,* obtained from the three most fundamental constants as

$$m_{\mathrm{P}} = \left(\frac{\hbar\, c}{G}\right)^{1/2} \approx 1.2 \times 10^{19}\,\mathrm{GeV}/c^2 \ ,$$

which is about 10^{20} times the scale of the confinement/deconfinement transition. Being string theory a candidate for such an ultraviolet completion of gravity (plus the other interactions), in the simplest approaches the characteristic mass m_s of string excitations will be around $m_{\rm P}$. Most of the "stringy" physics will occur at around that huge scale. Therefore, and back to the original thought: how is it that we could use string theory to address questions about strongly-coupled plasmas like ours, who operate around QCD energy scales?

The answer for us in this thesis comes from the AdS/CFT correspondence.[5] In its weakest formulation, this correspondence is a conjectured duality, or map, relating two seemingly different theories: a classical supergravity theory and a quantum gauge theory. Of particular interest to us is the fact that it is a *strong/weak* coupling duality. Supergravity computations on a weakly curved background (which we know how to do) correspond to strong coupling computations in the dual gauge theory. In order that the gauge coupling is large the processes in the latter theory must be at sufficiently "low" energies, precisely those of the plasmas above. This is something remarkable. Were the plasma weakly coupled, there would be no need for strong coupling computations; we could perform first-principles perturbative QCD calculations. However, it really seems to be strongly coupled, so by the particularities of the duality AdS/CFT may be of much use.

This interesting connection between string and gauge theory physics will hopefully allow the community to gather new information about some non-perturbative dynamical quantities, which where not accessible using the methods we talked about before. It feels like we are the heart of a research "phase transition". Indeed, the reference list in this thesis may seem outdated in a couple of months.

[5] Particularly, a partial version of it with Lorentzian signature. See section 2.3 for an extended discussion.

Chapter 2

AdS/CFT correspondence

Holography in high energy physics is introduced as the statement that quantum gravity in some region may be described in terms of a non-gravity theory living on its boundary [59, 60]. How may one explicitly realize this idea? On parallel, it is been long since 't Hooft suggested that a gauge theory might have a dual description in terms of effective strings [61]. It turns out that both these ideas can be given a precise meaning through the AdS/CFT correspondence [62]. As it will be described below, a version of this duality shows how to relate a string theory in a product of two five-dimensional spaces with a gauge theory on the conformal boundary of one of those two manifolds. Thus, it is *holographic* since it relates theories living on spaces of different dimensionality, and it implements as well 't Hooft's idea in terms of *real* and not just effective strings.

Originally the duality was conceived as a non-perturbative definition of M-theory. Even though this may be quite suggesting, we will use the correspondence in this thesis as a tool; hence our title. This also means that we are mainly interested in some partial aspects of it and thus the first section is devoted to presenting the very basics of it. Much more thorough explanations can be found in the famous three papers [62–64] and in the ever increasing list of reviews [65].

In the next section we will be interested in some generalizations of the correspondence to theories which bear more resemblance to QCD, since it is the one underlying the QGP. In this direction one may start by introducing temperature, which it is done by putting a black hole in the geometry [66–68]. This is nice too because the resulting theory is no longer supersymmetric nor conformal, two features not present in the QGP. Now some properties like the confinement/deconfinement transition for the dual theory explained in section 1.1 appear geometrized [68], and can be modelled in terms of classical results like the Hawking–Page transition in gravity [69].

We made though a strong point in the preceding chapter about the lack of non-perturbative computations of dynamical quantities in strongly coupled plasmas. It turns out that the original correspondence was formulated in the Euclidean, so like the lattice it has proven good in computing static quantities such as entropies [66, 67], Wilson loops giving the energy of a quark-antiquark pair [70], etc. On the other hand, formulating the duality with Lorentzian signature has some problems, mainly tied to the non-uniqueness

of supergravity fields solutions given a set of boundary conditions [71–76]. Of course one could argue that first one calculates in the Euclidean to afterwards continue analytically to Lorentzian signature, but in practice this is not possible because one needs the *exact* expression of the Euclidean correlators. Fortunately, a kind of breakthrough in our opinion came from work by Son and Starinets [76, 77], who proposed a recipe for computing Minkowskian correlators. This allows to obtain out-of-equilibrium quantities describing for instance transport properties of a plasma, and will be studied in section 2.3.

2.1 Zero temperature case

We shall start this section by drawing a simple picture for a connection between gauge and gravity degrees of freedom, to later present a precise example concerning a supersymmetric gauge theory and a closed string theory.

The motivation. Black hole solutions in general relativity have been known for a long time. Introducing local supersymmetry in these theories gives rise to supergravity, which will also contain this type of solutions. In general they need not be constrained to a point, and their mass may be spread out over p-dimensional surfaces plus time. These became known as black p-branes, in analogy with membranes but with the full range of dimensions. In some cases, called extremal solutions, the horizon shrinks to zero size so effectively the adjective *black* for the p-brane disappears. Notice this is not the case for extremal black holes.

Being supergravity a low-energy effective theory of strings, it is natural to think that these solutions will be present in the latter theory as well. If so, how do they look like? The tension or energy per unit p-volume for this kind of solutions is split in two different and broad classes: those for which it goes like $1/g_s^2$ (with g_s the closed-string coupling) and those for which it behaves as $1/g_s$. We will be concerned in the thesis with the second class; however, it is clear that for perturbative string theory, i.e. $g_s \ll 1$ they are both very heavy objects and can be seen as hyperplanes placed on the string background.

The microscopic or "stringy" description for these objects is that they provide the place where *open* strings can end. This is like a Dirichlet condition for them on the transverse directions to the brane; hence they are called D(irichlet)-branes. This is very nice since we will be considering type IIb theory, which is a theory of closed strings, but through D-branes one is able to introduce open strings as well. Even though they are very heavy, they are dynamical objects in the sense that open string excitations make the D-brane fluctuate. At low energies $E \ll \ell_s^{-1}$, and more precisely for massless open string excitations, these modes scatter like gauge bosons or other types of matter. This is understood as the fact that in the world-volume of the brane there is a gauge theory living

in it. In the same way, at those low energies the massless closed string modes behave as the graviton and other particles which comprise the content of ten-dimensional supergravity.

Thus we have a two-fold description of the brane system. In one of them we have a hyperplane with open strings attached to it whose low-energy world-volume theory is an Abelian gauge theory. Indeed, one can obtain a non-Abelian gauge theory by placing a stack of parallel branes. In this case open-string endpoints may be anchored on different branes, so the possible permutations give rise to a U(N) gauge theory. This stack is stable since there is a balance between the attractive and repulsive forces that arise through the exchange of closed NS-NS and R-R string modes. The other point of view comes from the supergravity description which motivated us to think of these objects in string theory. The connection from the string version is that the open strings on the brane couple to bulk closed string modes (as gravity couples to everything) and act as a source of gravitons, dilatons, etc. which in turn source Einstein equations, effectively curving the geometry from this backreaction to yield the metric and the other fields obtained in the supergravity solutions.

Provided the underlying configuration is the same, it is tempting to consider limits of the two descriptions to gather new insights from them. A clear limit which one may take is that of low energies, i.e. $E \ll \ell_s^{-1}$, or equivalently fix E and send $\ell_s \to 0$ so that it effectively costs infinite energy to see string excitations. In the following we will be setting $p = 3$ to consider 4-dimensional gauge theories:

- *The D-brane picture.* One may see the total action of the system as the sum of the bulk, brane and interactions terms. At low energies the gravitational coupling $\kappa \sim \sqrt{G} \sim g_s \ell_s^4$ goes to zero, so the closed-closed and closed-open string interactions vanish. Since we are at low energies we focus on the light degrees of freedom; this leaves us with free supergravity in the bulk which is also decoupled from the theory on the branes. At these low energies we have come to agree that the theory on the stack is a supersymmetric gauge theory, which as opposed to the bulk supergravity it is interacting. The precise coupling can be extracted from the Born–Infeld action of the branes, where for $p = 3$ is independent of the $\ell_s \to 0$ limit

$$\frac{g_{\rm SYM}^2}{4\pi} = g_s (2\pi \ell_s)^{p-3} \qquad \stackrel{p=3}{\longrightarrow} \qquad g_{\rm SYM}^2 = 4\pi g_s \ . \tag{2.1}$$

- *Strings in curved background picture.* In this case there are no branes, and one rather has closed strings propagating on the curved background given by a throat where the source is, but asymptotically flat when afar from it —in the brane picture this is also true, but in that case the gravitational radius of the throat is incredibly tiny at weak string coupling g_s. So again the closed strings in the flat region become free supergravity at low energies, and decouple from the modes inside the throat since

their wavelength becomes so big as to notice it. In technical terms, the absorption cross section for the 'out' modes by the brane vanishes [78]. On the other hand, low energies are now measured by an observer at the asymptotically flat region! This means that closed string excitations of arbitrary fixed energy in the throat appear red-shifted to the asymptotic observer. So the limit is compatible with low energies, even though in the throat we have interacting closed strings.

Therefore, and just by comparison, if we match the two free supergravities in the two descriptions, we are lead as well to match the interacting quantum gauge theory on the branes with the interacting quantum string theory on the throat. This is the *strong* version of the Maldacena conjecture, namely that a *quantum* gauge theory is dual to a *quantum* string theory. In the following we make this a bit more precise with a particular example central to the whole thesis.

The precise setup. Let us focus on the example set by a stack of N D3-branes in type IIb string theory, and consider its low-energy limit. The corresponding gauge theory on the world-volume is $\mathcal{N}=4$ SU(N) super Yang–Mills in four dimensions [79], containing a gauge field, four Weyl fermions and six real scalars, all of them in the adjoint representation of the gauge group and connected through supersymmetry transformations. On the other hand, how does it look like for the 3-brane solution and its low-energy limit? The metric is given by

$$\mathrm{d}s^2 = \left(1+\frac{L^4}{r^4}\right)^{-1/2}\cdot \mathrm{d}x_\parallel^2 + \left(1+\frac{L^4}{r^4}\right)^{1/2}\cdot \mathrm{d}x_\perp^2 \quad \text{with } L^4 = 4\pi g_s N \ell_s^4 \ , \tag{2.2}$$

where r parametrizes the radial coordinate in the transverse space. If one sets $r \gg L$ then recovers asymptotically 10-dimensional Minkowski space ($\mathrm{d}x_\parallel^2$ has Lorentzian signature). Concerning the excitations in the throat, the red-shift factor relates its energy measured at asymptotic Minkowski, E_∞, with its proper energy in the throat, E_p, through

$$E_\infty \sim \sqrt{-g_{00}}\, E_\mathrm{p} = \left(1+\frac{L^4}{r^4}\right)^{-1/4} E_\mathrm{p} \quad \overset{\text{throat}}{\longrightarrow} \quad E_\infty \sim \frac{r}{L} E_\mathrm{p} \ ,$$

so the low-energy limit ($E_\infty \to 0$) corresponds to $r \ll L$. This is why it is called the *near-horizon* limit, since one gets arbitrarily close to $r=0$, even though in the extremal case there is no such horizon. In this limit the metric takes the form

$$\mathrm{d}s^2 = \frac{r^2}{L^2}(-\mathrm{d}t^2 + \mathrm{d}\mathbf{x}^2) + \frac{L^2}{r^2}\mathrm{d}r^2 + L^2 \mathrm{d}\Omega_5^2 \ , \tag{2.3}$$

which is $\mathrm{AdS}_5 \times \mathrm{S}^5$, and doing $r \equiv L^2/z$ gives the anti-de Sitter (AdS) part in the so-called Poincaré coordinates. These spacetimes are maximally symmetric solutions to Einstein's equations with a negative value of the cosmological constant. Thus, in this particular case the AdS/CFT correspondence reads:

Type IIb closed string theory on $\mathrm{AdS}_5 \times \mathrm{S}^5$ *with* N *units of R-R flux on the 5-sphere is equivalent to* $\mathcal{N}=4$ $\mathrm{SU}(N)$ *gauge theory in four dimensions.*

Even though the low-energy limit described above would lead one to consider supergravity instead of strings, as Maldacena pointed out one should still think of the $\mathrm{AdS}_5 \times \mathrm{S}^5$ space as the background for the string theory. This was the strong statement about the equivalence of quantum gauge and string theories. Being this such an inspiring connection, one must tell a bit of bad news: we presently do not know how to quantize the string theory on that background, we do not know the precise spectrum that comes out. But at least it has been shown to be solvable, and much progress has been recently made in an approach where one can determine the spectrum beyond the supergravity limit, provided some quantum numbers like e.g. the spin become large [80–85].

Of course, even though the conjecture has not been totally proven there are hints that point to its correctness, and one should start by looking at the symmetries of both theories for instance:

- The string background has isometries, which are $\mathrm{SO}(2,4)$ for the AdS part and $\mathrm{SO}(6)$ for the sphere, and since there are spinors present it is better to talk of their covering groups $\mathrm{SU}(2,2)$ and $\mathrm{SU}(4)$, respectively. It is further possible to see that they combine in the super-Lie group $\mathrm{SU}(2,2|4)$. The $\mathcal{N}=4$ theory is conformal, which means that has vanishing beta-function, and in four dimensions translates to an $\mathrm{SO}(2,4)$ symmetry. Since the theory is supersymmetric, it has an R-symmetry, which for the $\mathcal{N}=4$ theory it is $\mathrm{SO}(6)$. This supersymmetry enhances as well the conformal group to its superconformal version $\mathrm{SU}(2,2|4)$. Hence the two symmetry groups agree, where there is a mapping from gauge transformations in the gravity side to global symmetries on the gauge theory; this is a key feature of gauge/string dualities.

  It is nice to see how the RG-flow is geometrized in the string picture. Scale transformations are trivial in the $\mathcal{N}=4$ theory, meaning that the action is quantum invariant under $(t,\mathbf{x}) \mapsto D\,(t,\mathbf{x})$. In the gravity side, this is the same provided one scales not only the world-volume directions but also the radial coordinate as $r \mapsto r/D$. Therefore, ultraviolet or short-distance physics tied to $D \to 0$ map to $r \to \infty$, i.e. the boundary of the AdS space —this really means going to the "boundary of the throat", not escaping to the asymptotically flat region. Alternatively, infared physics corresponding to $D \gg 1$ map to $r \to 0$. Thus, the radial r coordinate acts as the renormalization group scale! Defining the supersymmetric gauge theory at the ultraviolet fixed-point means that it is living on the boundary of anti-deSitter space, and that its flow to the infrared is obtained falling down the throat, which as we said corresponds to lower and lower energies. If one forgets for a moment

about the S^5 or does dimensional reduction on it, this sets in the idea of holography with supergravity in five dimensions and the gauge theory in four, arising as the conformal boundary in the $r \to \infty$ limit of the metric (2.3).

- One may also look at non-perturbative dualities of the theories like the $SL(2,\mathbb{Z})$ S-duality of type IIb strings, which acts on the axion-dilaton coupling $\tau = \chi + i\,e^{-\Phi}$. In the gauge theory the same S-duality is acting, now on the complexified gauge coupling $\tau = \frac{\theta}{2\pi} + \frac{4\pi i}{g^2_{\text{SYM}}}$, where θ is the vacuum theta-angle related to the strong CP-problem. This one is known as Montonen–Olive duality.

So indeed it seems possible that they are equivalent in the strong sense. However, we want to *apply* the correspondence, that is to compute some quantities. It turns out that the weaker statement of the duality where one replaces string theory by supergravity is quite fruitful, provided one puts some constraints on the gauge theories considered. Recalling equations (2.1) and (2.2) one can connect the gravitational radius of the background and string length with the 't Hooft coupling ($\lambda := g^2_{\text{SYM}} N$) of the gauge theory

$$L^4 = \lambda\, \ell_s^4 \ . \tag{2.4}$$

In order that supergravity is applicable, one needs a weakly curved space. This means that the gravitational radius or size of the throat must be quite big when measured in terms of the string length, leading to the constraint $\lambda \gg 1$. In the 't Hooft large N expansion of gauge theories it is this parameter who governs the interactions, and as such it appears in the amplitudes. Thus the supergravity limit corresponds to infinite 't Hooft coupling. This is good since the QGP seems to be strongly coupled, even though not infinitely. Now, since supergravity corresponds to the low-energy limit of the tree-level string action one must suppress string loop corrections and thence must send $g_s \to 0$. Provided we have a fixed background radius, i.e. fixed λ, this translates into the fact that we are at very large N in the gauge theory; this is the *planar* limit in its 't Hooft expansion.

Therefore, "stringy" corrections correspond to a $1/\sqrt{\lambda}$ expansion in the gauge theory, whereas string quantum loops correspond to $1/N$ corrections in the gauge theory. To summarize, our tool will be classical supergravity on a weakly curved background, which in turn will let us compute quantities in the multicolor limit of the gauge theory at infinite strong coupling. As a first approximation it looks good, the question is how good it is for the purpose of applying it to the QGP.

The field-operator dictionary. So far we have shown good motivations for believing in the conjecture, and matching the symmetries in both theories was a starting point. But further checks have been made concerning the spectrum of very particular operators, which does not change as the coupling is varied, and also some correlation functions protected by

supersymmetry were shown to match. How was all this made? In order to do so, one had to go beyond the previous presentation and provide a computational recipe for correlators, and a matching between gauge theory operators and string excitations [63, 64]. This is important since it converts the AdS/CFT correspondence into a quantitative tool.

In string theory, the string coupling g_s ($\propto g^2_{\text{SYM}}$ here) is given by the expectation value of the string dilaton Φ. Varying this field yields a modification of the coupling, and in this spirit one may connect fields on the string side with operators on the gauge theory. Even more explicitly, one can deduce for instance from the 3-brane Born–Infeld action the coupling of dilatons, R-R scalars and gravitons to $\operatorname{tr} F^2$, $\operatorname{tr} F\widetilde{F}$ and $T_{\mu\nu}$, respectively, where $F_{\mu\nu}$ is the field-strength for the non-Abelian gauge field and $T_{\mu\nu}$ is the energy-momentum tensor of the gauge theory. From the geometrical point of view, those couplings come from absorption of asymptotic excitations which tunnel into the throat. Therefore, these can be seen as perturbations of the AdS boundary and can be encoded into boundary conditions for the supergravity fields.

It turns out that there are two kinds of small fluctuations: *normalizable* and *non-normalizable* ones. The former are quantized and used to construct the Hilbert space of the boundary theory, whereas the latter are fixed by the conditions at the boundary and are dual to the insertion of operators. This is the case since it is the non-normalizable ones who under $r \mapsto r/D$ transform as a source does, whereas the normalizable transform as vev's. They are distinguished by their asymptotic behaviour at the boundary, scaling as $r^{-\Delta_+}$ and $r^{-\Delta_-}$ respectively, with $\Delta_+ > \Delta_-$ the characteristic exponents which depend on the nature of the operator. For Euclidean AdS normalizable modes are not independent of the non-normalizable ones so boundary conditions are enough to determine both. Therefore, in the supergravity approximation of interest to us, the precise statement is that its non-normalizable modes at the boundary will act as sources for the gauge theory operators. The AdS/CFT correspondence is thus formulated in this language as

$$\left\langle \mathrm{e}^{-S_{\text{CFT}}+\int \mathrm{d}^4x\, j(x)\,\mathcal{O}(x)} \right\rangle = \mathcal{Z}_{\text{CFT}}[j] \equiv \mathcal{Z}_{\text{sugra}}[\phi_{\text{cl}}] = \mathrm{e}^{-S_{\text{sugra}}[\phi_{\text{cl}}]} \ , \tag{2.5}$$

where S_{sugra} is the classical action for the classical solution ϕ_{cl} to its field equations, subject to the boundary condition

$$\lim_{r\to\infty} \frac{\phi_{\text{cl}}(x^\mu, r)}{r^{-\Delta_-}} = j(x^\mu) \ . \tag{2.6}$$

Moreover, correlators in the Euclidean gauge theory are obtained by functional variation of the classical supergravity action with respect to the boundary fields who act as sources as seen in equation (2.6), e.g. the two-point Euclidean correlator comes from two variations

$$G_{\text{E}}(x-y) = \langle T_{\text{E}}\, \mathcal{O}(x)\mathcal{O}(y)\rangle = \frac{\delta^2 S_{\text{sugra}}}{\delta j(x)\,\delta j(y)} \ . \tag{2.7}$$

It is important to stress that all of the above was formulated in the Euclidean regime. In Lorentzian signature normalizable modes are independent, posing an ambiguity when computing the correlators. Of course, at zero temperature the difficulties can be overcome by an analytic continuation to Lorentzian signature. However, once finite temperature is present it does not work any more, and one needs to refine the arguments; we will deal with these issues in section 2.3. These are important if one wants to describe real-time phenomena.

2.2 Finite temperature case

We have seen how to construct the gravitational description of a very particular theory, conformal and supersymmetric, in a very peculiar regime: the planar and infinite 't Hooft coupling limit. But as stated we want to use the duality as a tool, and the physical setup is a theory which among other things is not conformal but confining, is not supersymmetric and is at finite temperature. In this section we describe a little step which can be taken to get closer to the physical situation of interest.

The step consists in taking the decoupling limit on the *non-extremal* black 3-brane, which has a black hole built in. The new near-horizon gravity background is

$$\mathrm{d}s^2 = \frac{r^2}{L^2}\left(-f(r)\,\mathrm{d}t^2 + \mathrm{d}\mathbf{x}^2\right) + \frac{L^2}{r^2}\frac{\mathrm{d}r^2}{f(r)} + L^2\,\mathrm{d}\Omega_5^2\ , \tag{2.8}$$

with $f(r) = (1 - r_+^4/r^4)$. Notice that in contrast to the usual Schwarzschild metric the horizon has three flat directions $\mathbf{x}$, and hence one calls it the planar AdS-Schwarzschild background. The presence of such horizon allows to talk about Hawking radiation and temperature, so in the dual field theory the temperature is given by that on the black hole's horizon. To see it properly we can proceed as in section 1.2, rotating to the Euclidean and compactifying time in a circle. Since this "time" circle shrinks to zero size at $r = r_+$ one has to demand regularity of the metric in that limit, which in turn fixes the value of the temperature. Moreover, in such circle one may impose supersymmetric (periodic) boundary conditions for fermions or thermal (anti-periodic) ones. Since we want a thermal field theory we choose the latter, thereby breaking supersymmetry in the scenario.

To obtain the temperature we focus on the effect of the limit $r \to r_+$, i.e. the Euclidean time τ and radial r parts. In that limit we may write $r = r_+(1+\epsilon)$, with $\epsilon \ll 1$, so the metric becomes

$$\mathrm{d}s^2_{\mathrm{E,horizon}} = \frac{L^2}{4\epsilon}\,\mathrm{d}\epsilon^2 + \frac{4\epsilon\, r_+^2}{L^2}\,\mathrm{d}\tau^2\ . \tag{2.9}$$

This metric can be expressed in the form $\mathrm{d}\rho^2 + \rho^2\mathrm{d}\varphi^2$, so matching the coordinates and

demanding the absence of a conical singularity, i.e. that φ has period $\beta_\varphi = 2\pi$, one obtains the temperature as

$$T_{\text{gauge}} := T_{\text{BH}} = \beta_\tau^{-1} = \left(\frac{L^2}{2r_+}\beta_\varphi\right)^{-1} = \frac{r_+}{\pi L^2} \ . \tag{2.10}$$

Now we focus on conformal symmetry. Remember that the decoupling limit on the non-extremal 3-brane leads to a modification of the AdS part through the introduction of a black hole. Thus, the isometry group of the AdS spacetime is changed, and consequently conformal invariance is not present in the gauge theory. Only in the far ultraviolet region, with $r \to \infty$, the black hole factor values one and we recover the $\text{AdS}_5 \times \text{S}^5$ space. In the dual gauge theory this is just the statement that at large enough energies the temperature plays no role, and one recovers conformal symmetry. Recall the theory has a fixed-point there. This is nice, since now there exists the possibility of confinement and of a transition between the confined and deconfined phases, even though the metric (2.8) is not suitable for describing it (see below). Therefore, the question is which phase of the finite temperature gauge theory is dual to the chosen background. It turns out to be the deconfined (or plasma) phase [68], so all in all this allows to model a non-Abelian, not conformal, not supersymmetric multicolor gluon plasma —of infinite extent— at very strong coupling. Let us build a bit more on this in the next part of this section.

A natural question that might pop up is whether the gauge/gravity equivalence continues to hold at finite temperature. Many of the symmetries in the zero temperature theory, which allowed to match quantities in both sides of the correspondence, are now lost so it is more difficult to check it up on. Indeed, results from AdS/CFT at finite T may rather be seen as predictions on the strongly coupled dual gauge theory. We would like to comment on one of these predictions: in refs. [66,67] the entropy of the finite temperature version of the $\mathcal{N}=4$ SU(N) theory at strong coupling was confronted with the result at zero coupling for an Stefan–Boltzmann gas, both obtained from the derivative of the free energy with respect to the temperature. The outcome was that

$$F_{\text{BH}} = \frac{3}{4}\,F_{\text{SB}} = -\frac{\pi^2}{8}VN^2T^4 \ , \tag{2.11}$$

where $\beta_\tau F_{\text{BH}}$ is the Euclidean action of the black hole and SB stands for Stefan–Boltzmann. Now, in figure 1.1 we saw how in QCD closely above T_c the pressure ($P = -\partial F/\partial V$) amounts to an 80% of the ideal gas value, and that it was not clear if one should view it as evidence of almost weak coupling or not. Moreover, results at RHIC commented in section 1.3 seem to push towards strong coupling. So provided one "believes" that AdS/CFT has something to say at least universally on this issue, it should be clear that 75% is not that far from 80%, thus supporting the strongly coupled QGP picture since the $\mathcal{N}=4$ theory is at very large 't Hooft coupling!

Confinement/deconfinement is Hawking–Page. Above we saw that the background (2.8) is dual to the plasma phase of the gauge theory, but we really did not explain why. If AdS/CFT is really stating an equivalence, one should be able to reproduce the transition from confined to deconfined degrees of freedom in the gravitational picture. As explained in section 1.1, it is possible to produce such transition by rising the temperature. Just by analogy, we could start with some gravity background where we would heat the system producing a gas of gravitons, that eventually would collapse to form a black hole when rising the temperature. This is very well known in the context of semiclassical gravity, being the process called a Hawking–Page phase transition [69] where an initially horizonless geometry nucleates spontaneously a black hole, which occurs when the free energies of both configurations are equal. What would be the two backgrounds in this picture?

Recall that in the (Euclidean) correspondence we put boundary conditions on the fields and continue them into the bulk, but for differential equations there can be different solutions with the same boundary conditions. More generally, we could have different metrics in the throat, all of them with the same boundary topology. So when evaluating the right hand side of equation (2.5) it should be done over *all* possible contributions. At large N, the saddle points that dominate are the solutions to the supergravity equations of motion. Also, in such thermodynamical limit the free energies scale with N^2 for the $\mathcal{N}=4$ theory, so any slight difference between the configurations will favour dramatically one of the solutions. In our case, the relevant metrics were given by Hawking and Page [69]

$$\mathrm{d}s^2_{\mathrm{gas}} = \left(1+\frac{r^2}{L^2}\right)\mathrm{d}\tau^2 + \frac{\mathrm{d}r^2}{\left(1+\frac{r^2}{L^2}\right)} + r^2\,\mathrm{d}\Omega_3{}^2 \tag{2.12a}$$

$$\mathrm{d}s^2_{\mathrm{BH}} = \left(1+\frac{r^2}{L^2}-\frac{\mu}{r^2}\right)\mathrm{d}\tau^2 + \frac{\mathrm{d}r^2}{\left(1+\frac{r^2}{L^2}-\frac{\mu}{r^2}\right)} + r^2\,\mathrm{d}\Omega_3{}^2\ , \tag{2.12b}$$

where μ is related to the mass of the black hole. Both metrics share the same topology at the boundary $r\to\infty$, which for compact Euclidean τ is $\mathrm{S}^1\times\mathrm{S}^3$. To compare the free energies of the supergravity theories one has to match the radii of the two S^1 and the two S^3 in order to reproduce the same boundary metric. It turns out that once this is done, at high gauge theory temperature the black hole metric is favoured and dominates, so dual gauge theory properties should be studied within this background. On the contrary, at low temperatures it is the so-called thermal AdS metric (2.12a) which should be used. Just for completeness, let us note that in the limit where one sends the radius of the S^3 in (2.12b) to infinity, thus with boundary topology $\mathrm{S}^1\times\mathbf{R}^3$, it is possible to do a change of variables that takes to the Euclidean version of the AdS part in (2.8). So this last metric can be used as well to study the high temperature behaviour, but unfortunately is not good for studying the transition.

Therefore, to finally answer the question one must study properties of the gauge the-

ory and associate a phase to each background. In this spirit, an order parameter for confinement is the Polyakov loop, corresponding here to a string wrapped around the time direction. This loop is roughly e^{-F} with F the free energy of a probe static quark, so a vanishing loop means that it costs infinite energy to place it in the medium, i.e. confinement, whereas a non-vanishing loop value means it is possible to put it and thus deconfinement. In the string description the value of the loop is proportional to the area of a string worldsheet. At low temperatures the time circle is non-contractible and not the boundary of a disc, so that the Polyakov loop vanishes. After the transition, this circle becomes contractible because the S^1 shrinks, resulting in a non-zero expectation value for the Polyakov loop (see left panel on figure 2.1). Thus we see that the black hole geometry corresponds to the deconfinement phase! Another thing that can be studied is

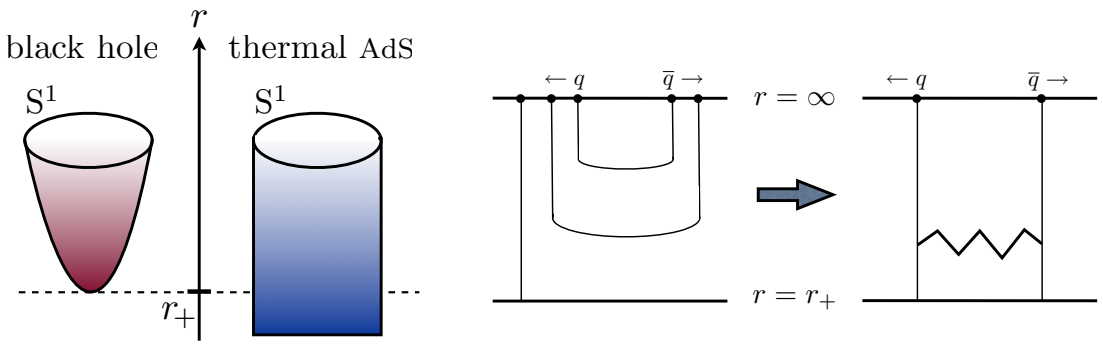

Figure 2.1: *(Left panel) On the left the high temperature black hole metric, with the* S^1 *shrinking. The cigar can be deformed to a disc. On the right the* S^1 *does not shrink since it has no black hole factor multiplying and cannot be deformed to be the boundary of a worldsheet. (Right panel) String splitting leading to deconfinement and glueball exchange.*

the potential between probe quark anti-quark pairs, related to the string tension (in the lattice sense). Let us take the black hole background, and model this by an open string hanging on the boundary whose stretching is proportional to the energy. Of course, since the boundary is at infinity one has to regularize the quantity by subtracting the value for a sole string hanging from that boundary till the horizon; in the gauge theory this is seen as the free energy of a static probe quark. As the pair separates, the equations of motion for this string can be solved to find that the intermediate part sinks towards the horizon more and more as they go. Eventually the string touches the horizon and splits in two single strings stretching from the boundary down to the horizon, which happens when $E \sim T \propto r_+$ (the whole process is depicted on the right panel on figure 2.1). This means that in the gauge theory it is favoured a configuration with the deconfined quark and anti-quark. There can still be interactions between the two hanging strings through the interchange of supergravity fields, seen as glueballs in the gauge theory. In chapter 5 we will compute some of these glueball (masses) as the static limit of absorption lengths in the deconfined plasma.

2.3 Going Lorentzian

In section 2.1 we showed the recipe to compute Euclidean correlators from the gravity dual, but the major point of this thesis is to study real-time properties relevant for strongly coupled plasmas. In particular, we saw that near-equilibrium properties can be computed in linear response theory, provided one knows the structure of the real-time retarded Green's functions. Recall for example the use of the Green–Kubo formula (1.17) to express the charge diffusion parameter in terms of the Lorentzian $\widetilde{G}_{\rm R}$. Other examples can be given: imagine one wants to follow a hydrodynamic mode, corresponding to low frequency ω (and momentum). In the Euclidean prescription the frequencies associated to the compact time circle appear as Fourier modes called *Matsubara frequencies,* which for bosons are $\omega_n = 2\pi i T n$. If one continues analytically these values, even the smallest of them turns out to be $2\pi T$, which can be far above the values for the hydrodynamic mode.

Thus, it is clear that the Euclidean recipe needs to be generalized to the Lorentzian case, where the new one should allow for a direct computation of real-time correlators. Moreover, and since for our purposes we are interested in the retarded Green's function, we need to isolate which is the precise boundary condition on the gravity fields that corresponds to the retarded function in the dual gauge theory.

The recipe for Lorentzian correlators.[1] The Euclidean recipe for correlators (2.5) builds on the ability to express the supergravity action in terms of the solutions to the field equations. The idea is that providing a condition for the field at the boundary, say $\phi|_\partial = \phi_0(x)$, and demanding regularity at the horizon completely fixes the solution. This allows to feed it back into the action to evaluate it on-shell, such that correlators come as variations with respect to that solution. Let us illustrate it in the simplest example of a massless scalar on the black hole background. We will work with the coordinate $z = r_+/r$, where the AdS part of the (Euclidean section of the) metric (A.1) is

$$\mathrm{d}s^2 = \frac{L^2}{z^2}\left(f(z)\,\mathrm{d}\tau^2 + \mathrm{d}\mathbf{x}^2 + \frac{\mathrm{d}z^2}{f(z)}\right) \ , \tag{2.13}$$

with the boundary at $z = 0$ and the horizon at $z = 1$. The equation of motion for the massless scalar on this (Euclidean) background is that given in eq.(A.2) with a change of sign in the $\ddot{\phi}$ term and $m = 0$. As explained in appendix A.1 we can Fourier transform ϕ, also with a sign change in ω

$$\phi(z,\tau,\mathbf{x}) = T\sum_n \int \frac{\mathrm{d}^3\mathbf{k}}{(2\pi)^3}\,\mathrm{e}^{i\omega_n\tau + i\mathbf{k}\mathbf{x}}\,\Phi_k(z)\,\phi_0(k) \ , \tag{2.14}$$

[1] The following argument will be based on the black hole background since we are interested in finite temperature gauge theories, even though the final prescription for Lorentzian two-point functions is valid at zero temperature as well.

and again $\Phi_k(z=0) := 1$ to reproduce $\phi|_\partial = \phi_0(x)$. The equation of motion in terms of $\Phi_k(z)$ thus is

$$\Phi_k''(z) + \left(\frac{f'(z)}{f(z)} - \frac{3}{z}\right)\Phi_k'(z) - \left(\frac{\omega^2}{f(z)^2} + \frac{\mathbf{k}^2}{f(z)}\right)\Phi_k(z) = 0 \ . \tag{2.15}$$

One can study the behaviour of the solution close to the boundary and the horizon using the typical Frobenius method. At the boundary there are two solutions, which go like 1 and z^4, respectively. On the other side and up to irrelevant numerical factors in the exponents, the two solutions at the horizon behave as $(1-z)^{+\omega}$ and $(1-z)^{-\omega}$. The requirement of regularity demands one throws away the latter since it blows up in the limit $z \to 1$ (we choose $\omega > 0$). Thus, from the ordinary theory of differential equations one can match the behaviour at the horizon with those at the boundary and obtain the solution to later compute the correlator. What happens when we perform the same study on the Lorentzian background? The difference is basically a change of sign for the term in ω^2, but a dramatic one. Again, one finds the same characteristic exponents at the boundary while at the horizon they change; now they give the behaviours $(1-z)^{+i\omega}$ and $(1-z)^{-i\omega}$. These are oscillatory solutions which do not explode, so one finds that demanding regularity at the horizon is no longer enough to obtain an unique solution which can be fed back to compute the correlator.

There is however an outstanding physical boundary condition at the horizon: classical black holes do not radiate so one may choose the oscillation that falls into the horizon. This is clearer if we recover time-dependence and rewrite $(1-z)^{\pm i\omega} = \exp[\pm i\omega \log(1-z)]$. Changing variables as $u \propto \log(1-z) \in (-\infty, 0]$

$$\phi \sim \mathrm{e}^{-i\omega t \pm i\omega u} = \mathrm{e}^{-i\omega(t\mp u)} \ \Rightarrow \ \begin{cases} +i\omega \text{ moves to the right in } u\text{, i.e. “outgoing”} \\ -i\omega \text{ moves to the left in } u\text{, i.e. “infalling”} \end{cases} ,$$

and one should pick $(1-z)^{-i\omega}$. From the gauge theory point of view this is an oscillation of the field sourced on the boundary that then travels to the horizon and disappears, so just from causality it looks natural to associate that condition at the horizon with the retarded correlator on the boundary theory. This allows to obtain an unique solution to be fed back into the action, but unfortunately is not the end of the story.

As said, the solution can be inserted into the action to write it as

$$S_{\text{sugra}} = \int \frac{\mathrm{d}^4k}{(2\pi)^4}\, \phi_0(-k)\, \mathcal{F}(k,z)\, \phi_0(k)\Big|_{z=0}^{z=1} , \tag{2.16}$$

where $\mathcal{F}(k,z) \propto \sqrt{-g}\, g^{zz}\, \Phi_{-k}(z)\, \partial_z \Phi_k(z)$. Notice that it receives contributions from both the boundary and the horizon. If one tries to extend the recipe straightforwardly to the Lorentzian case as

$$\left\langle \mathrm{e}^{iS_{\text{CFT}} + i\int \mathrm{d}^4x\, \phi_0\, \mathcal{O}(x)} \right\rangle = \mathcal{Z}_{\text{CFT}}[j] \equiv \mathcal{Z}_{\text{sugra}}[\phi_{\text{cl}}] = \mathrm{e}^{iS_{\text{sugra}}[\phi_{\text{cl}}]} \ , \tag{2.17}$$

the outcome for the Green's function is

$$\widetilde{G}(k) = \mathcal{F}(k,z)\Big|_{z=0}^{z=1} + \mathcal{F}(-k,z)\Big|_{z=0}^{z=1} . \tag{2.18}$$

Using the equation (2.15) for Φ_k and noticing that $\Phi_{-k} = \Phi_k^*$ one can derive that $\operatorname{Im}\mathcal{F}$ has no dependence on z. This means that the imaginary parts at $z = 0, 1$ in this formula cancel for each term and yields a real $\widetilde{G}(k)$. This is not good since one expects in general that the retarded Green's function be complex. Even if one drops the contributions from the horizon one still obtains a real value, since $\mathcal{F}(-k,z) = \mathcal{F}^*(k,z)$. Thus, it looks like the direct variation of the action does not yield the retarded Green's function.

In ref. [76] a conjecture for the actual formula was put forward without any direct evidence, except to look like the one at zero temperature; this was

$$\widetilde{G}_{\mathrm{R}}(k) \stackrel{?}{=} -2 \lim_{z\to 0} \mathcal{F}(k,z) \ , \tag{2.19}$$

suitable for the computation of real-time two-point functions. It is curious that even though the definition of the retarded correlator relies on the existence of a horizon and on imposing a very precise boundary condition on it, at the end of the day the recipe for that correlator involves just the evaluation of the function $\mathcal{F}(k,z)$ at the boundary. A more rigorous approach was used in [77] building on an earlier suggestion by Maldacena [86], which relies on the Schwinger–Keldysh formalism of finite temperature field theory named in section 1.2, and allows in principle to compute arbitrary n-point functions.

Retarded correlators and quasinormal modes. The prescription outlined above seems useful and, whenever applicable, happens to reproduce the results for correlators obtained from other methods [76]. But for non-extremal backgrounds such as the one we are interested in, applying the recipe is only possible in some limits, for instance very low or very high temperature. Fortunately, there is a way out building on the connection between retarded correlators and the necessity to impose *infalling* boundary conditions in the black hole background.

Infalling boundary conditions are the constitutive ingredient for the calculation of the quasinormal modes of black holes; these are time-dependent solutions to the linearized equations of motion with complex frequency whose imaginary part represents their damping on the background. Thus, quasinormal modes can be seen as excitations that dissipate their energy into the horizon or spread it out to infinity. In our case we have an asymptotic AdS geometry, so all the energy is dissipated into the horizon since its curvature acts effectively as a box. Traditionally these modes have been studied in the context of black holes in asymptotically flat space (see [87, 88] for a review). In the context of the AdS/CFT correspondence they were first studied in [89], and later extended on [90–100]. The picture is quite nice since the dual field theory interpretation is that the inverse of the

imaginary part gives the relaxation time back to equilibrium under a small perturbation of the plasma.

The key point of the authors of ref. [91] was to realize that the quasinormal frequencies of BTZ black holes coincide with the poles of the retarded two-point functions in the dual two-dimensional conformal field theory. In [96, 99] it was shown that this observation extends generally to the Lorentzian AdS/CFT correspondence, i.e. quasinormal frequencies in AdS can be interpreted as the poles of retarded Green's functions in the dual field theory. Let us see this in more detail.

In general, the problem of finding the quasinormal modes can be reduced to a quantum mechanical problem of scattering in a one-dimensional potential. In asymptotically flat spaces the potential vanishes both at infinity and at the horizon, so the solutions are in general a superposition of infalling and outgoing waves, to which we impose the infalling boundary condition at the horizon. In spaces that are asymptotically AdS the situation is similar at the horizon, but the potential does not vanish at infinity and a different set of boundary conditions should be considered. For a scalar field the usual choice is the Dirichlet condition at the boundary. However, for other perturbations like vectors or the metric, which in the boundary couple to conserved currents, such condition is less clear since those quantities are gauge-dependent. The way out is to use gauge-invariant combinations from them (see e.g. the vector field in A.1) and study which are the conditions that need to be imposed in order that their quasinormal spectrum matches the poles of the retarded Green's function. If one calls them Z_k, playing the generalized role of Φ_k above, one can express the infalling solution in terms of those at the boundary as

$$Z_k(z) = \mathcal{A}(\omega, \mathbf{k})\, y_1(z) + \mathcal{B}(\omega, \mathbf{k})\, y_2(z) \ , \tag{2.20}$$

which near the boundary looks like

$$Z_k(z \simeq 0) \simeq \mathcal{A}(\omega, \mathbf{k})\, z^{\Delta_-}(1 + \ldots) + \mathcal{B}(\omega, \mathbf{k})\, z^{\Delta_+}(1 + \ldots) \ , \tag{2.21}$$

with $\mathcal{A}$ and $\mathcal{B}$ the so-called *connection coefficients* of the differential equation, and Δ_+, Δ_- its characteristic exponents close to the boundary. These were for instance 0 and 4 in the massless scalar case above. One can take in general $\Delta_+ > \Delta_-$, with Δ_+ positive. If one rewrites the action to quadratic order in terms of these gauge-invariant variables, the on-shell version reduces reduces to the boundary term

$$S \simeq \lim_{z \to 0} \int \mathrm{d}^4 k\, F(\omega, \mathbf{k})\, g(z)\, Z'(z)\, Z(z) + \ldots \ , \tag{2.22}$$

where $F(\omega, \mathbf{k})$ contains the dependence on the parameters and the normalization of the action, $g(z)$ carries the dependence on the radial coordinate and periods stand for contact terms which do not contain derivatives of Z. Application of the recipe (2.19) to obtain

the correlator of the operator dual to Z yields

$$\widetilde{G}_{\mathrm{R}}(\omega,\mathbf{k}) = 2(\Delta_+ - \Delta_-)\, F(\omega,\mathbf{k})\, \frac{\mathcal{B}(\omega,\mathbf{k})}{\mathcal{A}(\omega,\mathbf{k})} \lim_{z\to 0} \left(g(z) z^{\Delta_+ - \Delta_- - 1} \right) , \tag{2.23}$$

which is valid whenever $(\Delta_+ - \Delta_-) \notin \mathbb{Z}$, though there are cases where one finds an integer difference between the characteristic exponents. When that happens, there is the chance that a logarithm in one of the two boundary solutions appear and the analysis has to be slightly modified. An example of this kind can be found in the longitudinal vector perturbations studied in the absorption lengths chapter 5.

In the cases we will be considering, the last z-dependent term will be regular, so the poles of the retarded Green's function will come as the values of ω and $\mathbf{k}$ which make the connection coefficient $\mathcal{A}$ zero. Holographically this condition is that they should be normalizable modes, so in the gauge theory they correspond to states and not to the insertion of sources or couplings (c.f. [99]). From the gravity point of view, the equation $\mathcal{A} = 0$ imposes a relation between the frequencies and momenta that allows to solve for one of them in terms of the other. This is just the statement that $\mathcal{A} = 0$ defines the quasinormal spectrum for the perturbations on the background. Thus, knowledge of such quasinormal frequencies allows to obtain the poles of the retarded correlators and in turn determine the dispersion relations for near-equilibrium collective excitations of the plasma!

We would not like to end this section without taking one more step, which will be the subject of chapter 5. In the gravity dual picture the dissipative properties of the plasma rely as said on the presence of a horizon, where small classical perturbations end up falling into the horizon either after a finite time or *after travelling a finite distance.* We have just explained how the first are described by complex values of the eigenfrequency: the quasinormal modes. Complementarily, the second class will be described by *complex momentum values.* Both are intimately related, they correspond to solutions of the linearized equations of motion and also satisfy the same boundary conditions. The difference is that quasinormal modes decay exponentially in time while complex momenta describe the decay along the direction of propagation; it is the choice of boundary conditions what restricts the possible values of complex frequency or momentum to a discrete set. So if the first ones are interpreted in the dual gauge theory as inverse relaxation times τ, the second ones will be seen as inverse absorption lengths λ of the plasma. While the relaxation time depends on the (real-valued) wave number k, the absorption length will depend on the (real-valued) frequency ω, i.e. $\lambda = \lambda(\omega)$. In the gravity theory we therefore fix a frequency, impose infalling boundary conditions on the horizon and then search for a solution of the boundary condition at infinity in the complexified momentum plane. In this way we can compute the frequency dependence of the absorption lengths.

Complex momenta are not that odd, and have been studied for horizons of compact spatial geometry, where they correspond to Regge poles [101] of the black hole S-matrix.

Chapter 3

Stability of small fluctuations

In section 1.2 we saw that the effect of a small perturbation can be obtained in linear response theory as the convolution of its source $j(\tau, \boldsymbol{\xi})$ with the retarded Green's function $G_{\mathrm{R}}(t-\tau, \mathbf{x}-\boldsymbol{\xi})$. In particular, provided one knows the shape of the source everything that lacks is the determination of the function G_{R}. In this chapter we will show that even though stability arguments do not determine the precise location of its singularities nor the values at them, they partly constrain the analytic form of these functions. The precise determination of the locations and residues for different kinds of perturbations will be the subjects in the next chapters with different physical motivations.

3.1 General field theory arguments

Let us try in this section to obtain some preliminary results on the structure of the poles and residues of the retarded Green's functions. We can replace in equation (1.14) the quantities by their Fourier transforms, without any recourse to the precise shape of the source. The formula of linear response theory now reads

$$\delta\langle\mathcal{O}(t,\mathbf{x})\rangle = -\int \frac{\mathrm{d}\omega\,\mathrm{d}^3\mathbf{q}}{(2\pi)^4}\,\mathrm{e}^{-i\omega t+i\mathbf{q}\mathbf{x}}\,\widetilde{G}_{\mathrm{R}}(\omega,\mathbf{q})\,\widetilde{j}(\omega,\mathbf{q})\ . \tag{3.1}$$

Constraints on quasinormal modes. At this point we choose to make the analytical continuation to the complex ω-plane and use Cauchy's theorem, with the only assumption that the singularities of the retarded Green's function on the complex frequency plane are single poles, so

$$\widetilde{G}_{\mathrm{R}}(\omega,\mathbf{q}) = \sum_{\text{poles}} \frac{R_n(\omega_n(\mathbf{q}),\mathbf{q})}{\omega-\omega_n(\mathbf{q})}\ , \tag{3.2}$$

where $\omega_n := \Omega_n - i\,\Gamma_n$ and R_n are the residues of $\widetilde{G}_{\mathrm{R}}$ evaluated at them. In order that our integrals converge for $t>0$ we form a closed contour with a semicircle at infinity on the lower-half ω-plane, whereas for $t<0$ we would close it in the upper-half plane. Thus the response is

$$\delta\langle\mathcal{O}(t,\mathbf{x})\rangle = i\,\mathrm{sign}(t)\int \frac{\mathrm{d}^3\mathbf{q}}{(2\pi)^3}\,\mathrm{e}^{i\mathbf{q}\mathbf{x}} \sum_{\omega_n\,:\,\text{poles}} R_n(\mathbf{q})\,\mathrm{e}^{-i\Omega_n(\mathbf{q})t-\Gamma_n(\mathbf{q})t}\,\widetilde{j}(\omega_n(\mathbf{q}),\mathbf{q})\ . \tag{3.3}$$

As an example we may choose a perturbation that is localized in time, i.e. we strike the medium once at time $t = 0$ and with a periodic profile such that $j(t, \mathbf{x}) = \delta(t) \cos(\mathbf{k}\,\mathbf{x})$, to find

$$\delta\langle \mathcal{O}(t, \mathbf{x})\rangle = i \operatorname{sign}(t) \cos(\mathbf{k}\,\mathbf{x}) \sum_{\omega_n} R_n(\mathbf{k})\, \mathrm{e}^{-i\Omega_n(\mathbf{k})t - \Gamma_n(\mathbf{k})t} \ . \tag{3.4}$$

We can now use this equation to derive a restriction on the location of the poles and on the residues. This restriction can be derived either from the condition that the response (3.4) has to be real or from symmetry under time reversal $\rho(\omega, \mathbf{k}) = -\rho(-\omega, \mathbf{k})$, where $\rho(\omega, \mathbf{k}) = -2 \operatorname{Im} \widetilde{G}_{\mathrm{R}}(\omega, \mathbf{k})$ is the *spectral function.* Both conditions lead to the result that the poles come in pairs and that the residues at a pair are related according to

$$\widetilde{\omega}_n = -\omega_n^* \ , \quad \widetilde{R}_n = -R_n^* \ . \tag{3.5}$$

Apart from these ones there can also be unpaired poles lying on the imaginary axis, for which their residues have to be purely imaginary.

We can do more yet. From its very definition, in order to ensure causality the retarded Green's function is proportional to the Heaviside $\theta(t)$, such that for $t < 0$ it vanishes whereas for $t > 0$ it is in general non-zero. Remember that for negative values of time we closed the contour on the upper plane, so the requirement that $\widetilde{G}_{\mathrm{R}}$ vanishes for $t < 0$ translates to the fact that we should find no poles on it. The same arguments applied to $t > 0$ means that at least one pole should be found in the lower plane. To summarize, *all* poles of the retarded Green's function should lie on the lower-half plane.

Since these poles correspond to complexifying the frequencies the dual analysis corresponds to the computation of quasinormal modes in the black hole background. This is indeed the analytic structure that appears in the Lorentzian AdS/CFT correspondence at finite temperature [99]. In general, the analytic structure of retarded two-point functions is of course more complicated and involves also branch cuts. The authors of [102] computed the retarded two-point function of $\operatorname{tr} F^2$ at weak coupling and found a tower of branch cuts with branch points located at $\omega \pm k = -i4\pi nT$. However, we will only consider the strict large N and strong 't Hooft coupling limit in this thesis. Therefore, the response of the system to a perturbation localized in time is determined by the sum over the residues of $\widetilde{G}_{\mathrm{R}}$ at the poles.

Instabilities, i.e. exponentially growing modes, appear as quasinormal frequencies with positive imaginary part. This is consistent with the interpretation as retarded Green's function, where singularities in the upper-half plane would correspond to tachyonic modes travelling backwards in time. A typical arrangement of quasinormal frequencies as they appear in the analysis of small perturbations of asymptotically AdS black hole spacetimes is depicted in figure 3.1.

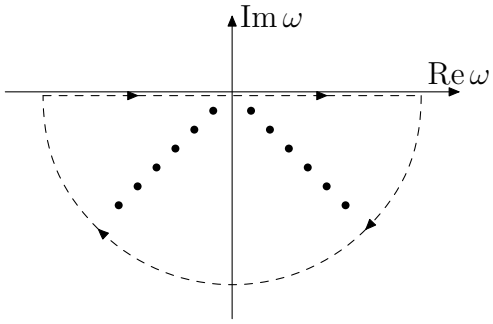

Figure 3.1: *The relevant integration contour for the poles in the ω-plane. All the poles are in the lower-half plane, corresponding to the interpretation of quasinormal modes as the poles of a retarded Green's function.*

Constraints on complex momentum modes. Let us choose now another kind of perturbation. This time we will switch the roles of time and one space coordinate with respect to the discussion above. Of course we proceed again using eq.(3.1) but now assume

$$\widetilde{G}_{\mathrm{R}}(q,\omega) = \sum_{\text{poles}} \frac{R_n(q_n(\omega),\omega)}{q - q_n(\omega)} \ , \tag{3.6}$$

in the spirit of what was motivated at the end of section 2.3, with poles $q_n = q_n^{\mathrm{R}} + i q_n^{\mathrm{I}}$ in the complexified momentum plane. To be more concrete we pick a periodic fluctuation localized in space, i.e. we assume a source of the form $j(t,\mathbf{x}) = \delta(x)\exp[-i(\nu t - \mathbf{k}_\perp \mathbf{x}_\perp)]$. Doing the Fourier transform of the retarded propagator and performing $\boldsymbol{\xi}_\perp$ and τ integrations one finds

$$\delta\langle\mathcal{O}(t,\mathbf{x})\rangle = -\frac{1}{(2\pi)}\,\mathrm{e}^{-i(\nu t - \mathbf{k}_\perp\mathbf{x}_\perp)} \int \mathrm{d}q\ \widetilde{G}_{\mathrm{R}}(\nu,\mathbf{k}_\perp,q)\ \mathrm{e}^{iqx} \ . \tag{3.7}$$

This is the response of the system to a periodic perturbation with frequency ν that is localized in the x-direction and has the form of a plane wave in the perpendicular directions $\mathbf{x}_\perp$. We have assumed that the perturbation has started far in the past such that all transient oscillations have already vanished and the system has reached a stationary state. In the following we will also assume that the perturbation is not further modulated in the $\mathbf{x}_\perp$-directions, i.e. we set $\mathbf{k}_\perp = 0$. Now one can use again Cauchy's theorem, closing in the upper or lower-half planes for $x > 0$ and $x < 0$, respectively. The result is

$$\delta\langle\mathcal{O}(t,\mathbf{x})\rangle = -i\ \mathrm{sign}(x)\,\mathrm{e}^{-i\nu t} \sum_{q_n:\text{poles}} \mathrm{e}^{iq_n x}\, R_n(q_n(\nu),\nu) \ . \tag{3.8}$$

In this case, parity symmetry $x \to -x$ imposes that if $q_n = q_n^{\mathrm{R}} + i q_n^{\mathrm{I}}$ is a pole then $q = -q_n$ has to be a pole too.

For complex momentum modes there is no analogous argument of causality and the Heaviside function. However, we would like the poles in the upper-half to lie in the first

quadrant and those in the lower-half in the third quadrant: with such and arrangement of poles the perturbation is creating damped waves moving to the right for $x > 0$ and to the left for $x < 0$. The waves propagate away from the origin of the perturbation at $x = 0$ and are exponentially decaying with the distance from the perturbation. In section 3.2 we prove that for the holographic retarded two-point functions the poles do indeed fall into the first and third quadrants of the complex momentum plane, and in chapter 5 we check it numerically for different kinds of perturbations. A typical setup with the corresponding integration contours is depicted in figure 3.2.

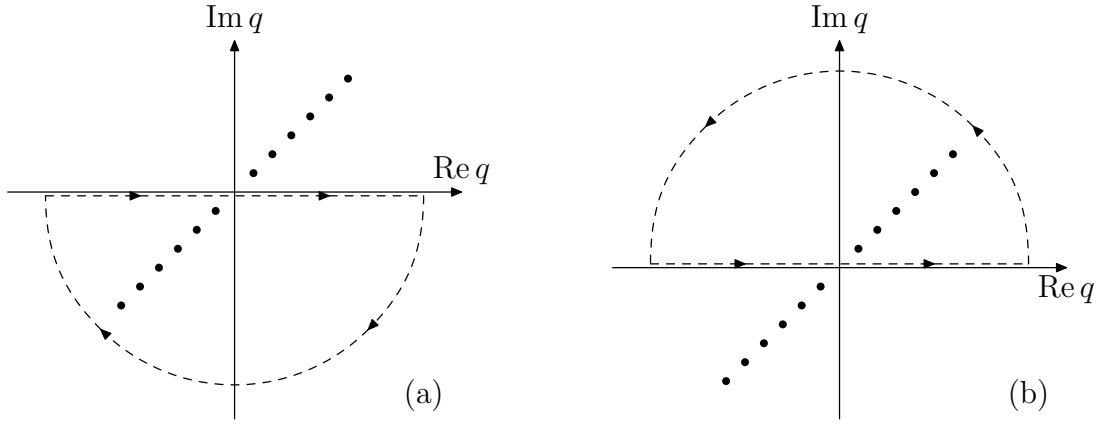

Figure 3.2: *The relevant integration contours for the poles in the complexified momentum-plane. Figure (a) shows the contour for $x < 0$, and figure (b) shows the contour for $x > 0$. In order to obtain exponentially decaying waves travelling away from the origin of the perturbation it is necessary that the poles lie in the first and third quadrants.*

The imaginary part of the complex wave number can be interpreted as the inverse of an *absorption length*. For a given complex momentum pole q_n the right-moving wave has the form $\mathrm{e}^{-i(\nu t - q_n^{\mathrm{R}} x)}\,\mathrm{e}^{-q_n^{\mathrm{I}} x}$. The amplitude of the wave has decayed to a factor of $1/e$ at a distance of $\lambda_n = 1/q_n^{\mathrm{I}}$.

3.2 Gravity arguments for complex momentum

We will now perform a stability analysis analogous to the one for quasinormal modes done in ref. [89]. We will see that the complex momentum wave numbers indeed lie in the first and third quadrants of the complex q-plane for positive frequencies. Note that a pole in the second or fourth quadrants would allow to construct outgoing waves that are exponentially growing with the distance from the perturbation; for the stability of the system under the fluctuation the absence of such poles is therefore crucial. We start recalling from (3.8) that the time and space dependence of the field is given by simple

exponentials

$$\phi(t,x) \sim \mathrm{e}^{-i\omega t}\,\mathrm{e}^{iqx} \ ,$$

where $q := q^{\mathrm{R}} + iq^{\mathrm{I}}$, and we will distinguish between the cases $x > 0$ and $x < 0$.

In the case $x > 0$ stability demands an exponentially decaying wave and therefore $\operatorname{sign} q^{\mathrm{I}} = +1$. We further demand that the wave is outgoing from the origin of the perturbation which imposes $\operatorname{sign}\omega = \operatorname{sign} q^{\mathrm{R}}$. Taking these two facts together amounts to the condition

$$\operatorname{sign}\left(\frac{\omega}{q^{\mathrm{R}}}\right) = \operatorname{sign} q^{\mathrm{I}} \ . \tag{3.9}$$

Doing the same analysis for $x < 0$, one finds that the perturbation moves away to the left if $\operatorname{sign}\omega = -\operatorname{sign} q^{\mathrm{R}}$, whereas the stability condition is now $\operatorname{sign} q^{\mathrm{I}} = -1$. This again amounts to eq.(3.9).

We want to prove now that in the gravity dual the complex momentum modes of the black hole follow indeed the rule given by equation (3.9). As an example we consider a minimally coupled scalar Φ in $\mathrm{AdS}_5 \times \mathrm{S}^5$ with mass m in the background (A.1), modulo the overall L^2 factor. We will set without any loss of generality the momentum to be $\mathbf{k} = (q,0,0)$, and further split the field as $\Phi(z) = \sigma(z)\,y(z)$, in order to find an equation for $y(z)$ that is Schrödinger-like in a 'tortoise' z_* coordinate defined through

$$\mathrm{d}z_* = \frac{\mathrm{d}z}{f(z)} \quad \Rightarrow \quad \Big(\partial_{z_*}^2 + \omega^2 - V(z_*)\Big)y(z_*) = 0 \ , \tag{3.10}$$

provided that $\sigma(z)$ fulfils

$$\frac{\sigma'(z)}{\sigma(z)} = \frac{3}{2z} \ . \tag{3.11}$$

In the z coordinate the Schrödinger potential reads

$$V(z) = \frac{f(z)}{4z^2}\Big(15 + 4m^2 + 4q^2z^2 + 9z^4\Big) := V_0(z) + \mathrm{Re}\,(q^2)\,f(z) + i\,\mathrm{Im}\,(q^2)f(z) \ , \tag{3.12}$$

where we have separated it into its real and imaginary parts. In the z_* coordinate the horizon lies at $z_* \to +\infty$ and the potential vanishes there, so the wavefunction can be described as a superposition of plane waves. The infalling boundary condition corresponds to setting $y(z_*) = \mathrm{e}^{i\omega z_*}\,\chi(z_*)$ with $\chi(+\infty) = \text{const}$. Thus we find

$$\Big(\partial_{z_*}^2 + 2i\omega\,\partial_{z_*} - V_0(z_*) - \mathrm{Re}\,(q^2)\,f(z_*) - i\,\mathrm{Im}\,(q^2)\,f(z_*)\Big)\,\chi(z_*) = 0 \ . \tag{3.13}$$

If we multiply by the conjugate $\overline{\chi}(z_*)$ and pick out the imaginary part of the equation we obtain

$$-\frac{i}{2}\,(\overline{\chi}\partial_{z_*}^2\chi - \chi\partial_{z_*}^2\overline{\chi}) + \omega\,\partial_{z_*}|\chi|^2 - \mathrm{Im}\,(q^2)f(z_*)|\chi|^2 = 0 \ , \tag{3.14}$$

Now we integrate this equation between the boundary ($z_* = z_*^b$) and the horizon. Upon a partial integration the derivative terms cancel each other: $\chi(z_*)$ vanishes at the boundary

due to the Dirichlet boundary condition we impose there, and at the horizon the derivative vanishes $\partial_{z_*}\chi(+\infty) = f(1)\,\partial_z\chi(1) = 0$. The remaining terms in equation (3.14) amount to

$$\omega\,|\chi(z=1)|^2 = \mathrm{Im}\,(q^2)\int_{z_*^b}^{\infty} \mathrm{d}z_*\, f(z_*)|\chi(z_*)|^2 = \mathrm{Im}\,(q^2)\int_0^1 \mathrm{d}z\,|\chi(z)|^2\ , \tag{3.15}$$

The integral on the right hand side is positive definite, which in turn implies that $\mathrm{sign}\,\omega = \mathrm{sign}\,\mathrm{Im}\,(q^2) = \mathrm{sign}(q^{\mathrm{R}}q^{\mathrm{I}})$, i.e. it is precisely the stability condition (3.9).

There is a further stability condition involving the properties of the potential. When $\omega = 0$, we have the condition that $\mathrm{Im}\,(q^2) = 0$, so either $q^{\mathrm{R}} = 0$ or $q^{\mathrm{I}} = 0$. Consider now the real part of the Schrödinger equation (3.13). After multiplying by $\overline{\chi}(z_*)$ and integrating between the boundary and the horizon we find

$$\int_{z_*^b}^{\infty} \mathrm{d}z_* \left(|\partial_{z_*}\chi(z_*) + i\omega\chi(z_*)|^2 + (V_0(z_*) - \omega^2)|\chi(z_*)|^2\right) = -\mathrm{Re}\,(q^2)\int_0^1 \mathrm{d}z\,|\chi(z)|^2\ , \tag{3.16}$$

Clearly, if $V_0(z_*) \geq 0$ between the boundary and the horizon, then, at $\omega = 0$, $\mathrm{Re}\,(q^2) < 0$ and we will have $q^{\mathrm{R}} = 0$ and $q^{\mathrm{I}} \neq 0$. On the other hand, if the potential is negative on some region then there could be solutions with $\mathrm{Re}\,(q^2) > 0$ or equivalently $q^{\mathrm{R}} \neq 0$ and $q^{\mathrm{I}} = 0$. Considering four-dimensional Minkowski slices of AdS_5, these modes can be regarded as tachyonic instabilities of negative mass squared $m^2 = -(q^{\mathrm{R}})^2$. Notice that with our choice the boundary conditions are $\sim \mathrm{e}^{i\omega z_*}$, and fixing ω to be real this condition actually refers to the presence of 'negative energy' modes in the scattering spectrum, so only when the potential is negative at the horizon this kind of instabilities could appear. Besides, other instabilities associated to the presence of bound states could be present; see appendix A.3 for a discussion.

If $\mathrm{Re}\,(q^2) > 0$ instabilities are present in the bulk theory, and the gauge correlation functions associated to the dual operators will show an oscillatory behavior at large separations, as opposed to vanishing, indicating that the plasma is actually out of equilibrium. From the point of view of the effective three-dimensional theory, instabilities will appear as tachyonic states in the spectrum.

Part II

Applying AdS/CFT to compute Plasma Properties

Chapter 4

Weight of collective excitations

In the next two chapters we will focus on the location of the poles of the retarded Green's function —that determine the dispersion relations for collective excitations— for complex momenta defining absorption lengths in a gluon plasma, as well as quasinormal modes on a flavour brane defining dissipation of a meson excitation. Let us though start here with the basic example of quasinormal modes on a gluon plasma, but going a bit beyond by computing not only the location of the poles for a given set of perturbations, but also the residues at them. This is important because it allows in principle for a full determination of the response to the perturbation.[1]

It is helpful to remember the situation at weak coupling for correlators of field components: the poles of the retarded Green's functions correspond to quasiparticle excitations.[2] As explained in section 1.2, a *hard* scale of order the temperature T can be distinguished from a *soft* scale of order gT. Far in the hard scale the relevant excitations are the hard partons, i.e. the quarks and gluons. At the soft scale there are however quasiparticles corresponding to the dressed partons and collective excitations, e.g. the so-called longitudinal plasmon mode. Both types of poles can be distinguished by the behaviour of their residues at short wavelengths: the residues of the particle poles scale like q^{-1} with the momentum q whereas the collective excitations show exponentially decaying residues of the form $\exp(-\alpha q^2/g^2T^2)$, with a mode dependent constant α [103]. To gain a better understanding of the quasinormal frequencies that appear in the holographic model of the strongly coupled plasma it is thus of utmost importance to study the behaviour of their residues. In particular we will concentrate on the transverse and longitudinal R-charge vector current correlators. The corresponding quasinormal frequencies and spectral functions have been studied before in [99] and [104–106], respectively.

Following the arguments presented in section 2.3 we will be able to compute the location of the poles and the value of the residues using the gravity dual. We would like to note that in our numerical calculations we have checked that the stability and time

[1] To know the response *exactly* one would need the values of *all* poles and residues. In practice this is not possible; however, computing some of them is enough since each quasinormal mode is a subleading correction to the preceding ones.

[2] At weak coupling one also finds branch cuts corresponding to e.g. Landau damping.

reversal relations from section 3.1 indeed hold for the quasinormal modes.

Apart from that, in this chapter we present what we see as a nice result concerning heavy-ion physics, which rely on the computation of hydrodynamic modes —such as those presented in section 1.2— whose frequencies vanish as the momentum goes to zero. At sufficiently small momentum the hydrodynamic mode has the smallest imaginary part of all poles and therefore dominates the long time behaviour. Moreover, knowledge of the residues allows us to define the time τ_{H} from when on the system enters the hydrodynamic regime. From (3.4) we find

$$\tau_{\text{H}} = \frac{\log|R_{\text{H}}| - \log|R_1|}{\Gamma_{\text{H}} - \Gamma_1} \ . \tag{4.1}$$

This value restricts the validity of the hydrodynamic approximation to times larger than τ_{H}, where we can expect hydrodynamics to be a good approximation. For shorter times more and more higher poles will contribute. Since hydrodynamic simulations of the evolution of the quark-gluon plasma are at the heart of the new sQGP paradigm, it is therefore important to know the hydrodynamic time scale τ_{H}, which in turn requires knowledge of the residues of the quasinormal modes. At the end of this chapter we give a rough estimate on this value, as computed from the R-current correlators.

4.1 An exactly solvable example

In general the quasinormal modes of the five-dimensional AdS-black hole can be determined only numerically. There are however some special cases where the wave equations simplify and can be solved analytically. Two such cases are the equations at zero momentum for the gauge-invariant variables corresponding to longitudinal and transverse vector field perturbations, $E_{\text{L}} = qA_0 + \omega A_{\text{L}}$ and $E_{\text{T}} = \omega A_{\text{T}}$, given in appendix A.1. In this case we work in the $x = 1 - z^2$ coordinate, whose horizon and boundary sit at $x = 0$ and $x = 1$, respectively. According to the holographic dictionary the vector field in AdS acts as a source for the R-charge currents J^a_μ of the SU(4) R-symmetry in the dual gauge theory. Denoting the retarded correlator of two currents as $G_{\mu\nu}$ one can write for the non-vanishing components [99]

$$\widetilde{G}_{\text{TT}} = \Pi^{\text{T}}(\omega, \mathbf{q}) \ , \qquad \widetilde{G}_{\text{LL}} = \frac{\omega^2}{\omega^2 - \mathbf{q}^2}\, \Pi^{\text{L}}(\omega, \mathbf{q}) \ , \tag{4.2a}$$

$$\widetilde{G}_{t\,\text{L}} = \frac{-\omega|\mathbf{q}|}{\omega^2 - \mathbf{q}^2}\, \Pi^{\text{L}}(\omega, \mathbf{q}) \ , \qquad \widetilde{G}_{tt} = \frac{\mathbf{q}^2}{\omega^2 - \mathbf{q}^2}\, \Pi^{\text{L}}(\omega, \mathbf{q}) \ , \tag{4.2b}$$

so the correlators and consequently the response of the system are thus defined by the transverse and longitudinal polarization tensors $\Pi^{\text{T,L}}(\omega, \mathbf{q})$.

At zero momentum $\mathbf{q} = 0$, the longitudinal and transverse components become indistinguishable from each other, $E_{\text{T}} = E_{\text{L}} \equiv E(x)$, and obey the same wave equation which

in terms of the dimensionless frequency $\mathfrak{w} := \omega/(2\pi T)$ reads

$$E'' + \frac{f'(x)}{f(x)}\,E' + \frac{\mathfrak{w}^2}{(1-x)f(x)^2}\,E(x) = 0\ . \tag{4.3}$$

This equation can be solved exactly and has two solutions, both proportional to the Gauss' hypergeometric function. Choosing the one that reproduces the infalling boundary condition at the horizon as explained in section 2.3, the polarization tensor was found to be [106]

$$\frac{\Pi(\mathfrak{w})}{N^2T^2/8} = \lim_{x\to 1}\frac{E'(x)}{E(x)} = i\mathfrak{w} + \mathfrak{w}^2\left[\psi\left(\frac{(1-i)}{2}\mathfrak{w}\right) + \psi\left(\frac{-(1+i)}{2}\mathfrak{w}\right)\right]\ , \tag{4.4}$$

where ψ is the digamma function and N the number of colors. The locations of the poles and their residues are

$$\omega_n^{\pm} = 2\pi T n(\pm 1 - i) = 2\pi T\,\mathfrak{w}_n\ , \quad R_n^{\pm} = \frac{\pi}{2}N^2T^3n^2(\mp 1 - i) = 2\pi T\,\mathfrak{R}_n\ , \tag{4.5}$$

with $n \in \mathbb{N}$, where the quasinormal modes and residues fulfil the reality conditions (3.5). Notice that at $\mathfrak{q} = 0$ the residues of the non-vanishing retarded Green's functions G_{TT} and G_{LL} equal these above for $\Pi(\mathfrak{w})$. In the general $\mathfrak{q} \neq 0$ case one has to multiply by the preceding factors in equations (4.2) to obtain the true values.

At first glance it looks strange that the residues grow quadratically with the mode number. If we want to write the retarded Green's function as a sum over the poles this leads to a divergent expression. However, we have to remember that the poles determine the Green's function only up to an analytic part and that this analytic part can be infinite. In order to obtain a well-defined pole representation one has therefore to substract a conveniently chosen analytic part. This is made explicit in the well-known pole representation of the digamma function

$$\psi(x) = -\gamma_{\mathrm{E}} - \sum_{n=1}^{\infty}\left(\frac{1}{x-1+n} - \frac{1}{n}\right)\ , \tag{4.6}$$

where $\gamma_{\mathrm{E}} \simeq 0.577$ is the Euler–Mascheroni constant. Using this we can find a pole representation of the polarization tensor as

$$\Pi(\mathfrak{w}) = \frac{N^2T^2}{8}\left\{ - i\mathfrak{w} - 2\gamma_{\mathrm{E}}\,\mathfrak{w}^2 + \mathfrak{w}^3\sum_{n=1}^{\infty}\frac{1}{n}\left(\frac{1}{\mathfrak{w} - n(1-i)} + \frac{1}{\mathfrak{w} + n(1+i)}\right)\right\}\ , \tag{4.7}$$

where the linear term in $\mathfrak{w}$ can be understood as the zero momentum limit of the R-charge diffusion pole. This suggests that the retarded Green's function at non-zero momentum would be a meromorphic function of frequency and momentum and admit an expansion

$$\Pi(\mathfrak{w},\mathfrak{q}) = \sum_n \frac{\mathfrak{R}_n(\mathfrak{w},\mathfrak{q})}{\mathfrak{w} - \mathfrak{w}_n(\mathfrak{q})}\ , \tag{4.8}$$

where $\mathfrak{R}_n(\mathfrak{w},\mathfrak{q})$ are analytic functions. Notice this was a bold assumption in section 3.1 whereas here it looks a bit more natural. We will do a numerical evaluation of the residues at the pole $\mathfrak{R}_n(\mathfrak{w}_n(\mathfrak{q}),\mathfrak{q})$. This implies that our method does not disentangle the frequency from the momentum dependence.

A rather interesting point is to ask what is the spectral line produced by a single isolated quasinormal mode. Due to the fact that the residue is complex the line spectrum of an isolated quasinormal mode does not have the shape of a Lorentzian function. Writing $Y = \mathrm{Im}\,(R)/\mathrm{Re}\,(R)$, we find

$$\rho_{\mathrm{QNM}}(\mathfrak{w}) \propto \frac{\Gamma - Y(\mathfrak{w}-\Omega)}{(\mathfrak{w}-\Omega)^2+\Gamma^2}\ . \tag{4.9}$$

For non-vanishing imaginary part of the residue the peak is higher than that of a Lorentz curve with $Y = 0$, and it is shifted to lower frequencies if $Y > 0$ or to higher frequencies if $Y < 0$. In the case at hand where the $\Gamma/\Omega \approx 1$ the quasiparticle approximation is not valid and the line spectrum of an isolated quasinormal mode does not approximate the full spectral function in any range of the frequency. In cases where $\Gamma/\Omega \ll 1$ and Y different from zero it would show up as an asymmetry in the form of the observed resonance in the spectral function and a correct interpretation is possible only if the residue is known.[3]

The expression found as a sum over poles and the exact one differ only by some contact terms, coming from the analytic pieces we have neglected. Neglecting the contact terms, the Green's function in position-space diverges at $t = 0$ as t^{-3}, coinciding with the zero-temperature result. This shows that the sum over poles is enough to recover most of the dynamical information and only the contact terms require a more detailed analysis. In principle they should be related to the Schwinger terms of the $T = 0$ theory.

4.2 Numerical computation

According to the holographic dictionary the retarded Green's function can be computed as the ratio of the connection coefficients that relate the local solution at the horizon with infalling boundary conditions to the non-normalizable ($\mathcal{A}$) and normalizable ($\mathcal{B}$) solutions at the boundary. Defining $_{(\alpha)} := (\mathrm{T},\mathrm{L})$ as the two components, the connection is

$$E^{\mathrm{h}}_{(\alpha)}(x) = \mathcal{A}_{(\alpha)}\, E^{1}_{(\alpha)}(x) + \mathcal{B}_{(\alpha)}\, E^{2}_{(\alpha)}(x)\ . \tag{4.10}$$

The retarded polarization tensors are given then by [99]

$$\Pi^{(\alpha)} = -\frac{N^2T^2}{8}\,\frac{\mathcal{B}_{(\alpha)}}{\mathcal{A}_{(\alpha)}}\ . \tag{4.11}$$

[3] Narrow peaks in holographic spectral functions have been recently observed in [106, 107].

As seen in section 2.3, the quasinormal modes are normalizable solutions where the connection coefficient $\mathcal{A}_{(\alpha)} = 0$. Using eq.(4.10), the polarization tensor follows from demanding the solution to be smooth at a matching point in the interior of the interval $x \in (0, 1)$

$$\frac{\mathcal{B}_{(\alpha)}}{\mathcal{A}_{(\alpha)}} = \frac{E^{\rm h}_{(\alpha)}(E^1_{(\alpha)})' - (E^{\rm h}_{(\alpha)})' E^1_{(\alpha)}}{E^2_{(\alpha)}(E^{\rm h}_{(\alpha)})' - (E^2_{(\alpha)})' E^{\rm h}_{(\alpha)}} \,. \tag{4.12}$$

We computed the Frobenius series up to $\mathcal{O}(x^{50})$. Matching the series expansions, one can see numerically that the ratio (4.12) remains constant for a fair interval in the radial coordinate. We chose $x = 0.53$ to evaluate the ratio and checked that the spectral function agrees with previous numerical (for non-zero momentum) and exact (for zero momentum) results [104–106]. In appendix A.2 we show that the residue can be computed as

$$R_n^{(\alpha)} = -\frac{\pi}{4} N^2 T^3 \left[\frac{\partial}{\partial \mathfrak{w}} \left(\frac{\mathcal{A}_{(\alpha)}}{\mathcal{B}_{(\alpha)}} \right) \Big|_{\mathfrak{w}=\mathfrak{w}_n} \right]^{-1} \,. \tag{4.13}$$

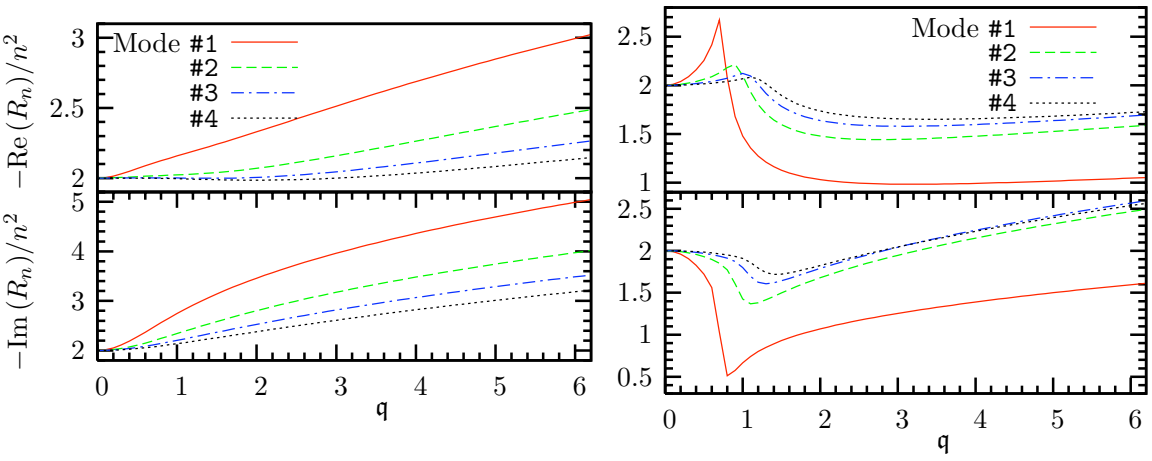

Figure 4.1: *(Left) Real and imaginary parts of the residues for the first four quasinormal modes in the transverse component $E_{\rm T}$ (right) Idem for the longitudinal component $E_{\rm L}$. The apparent non-analyticity in the first mode is due to a lack of resolution at that point. The n^2 scaling is necessary to recover the asymptotic behaviour of the spectral function at large frequencies. Close to the crossing with the diffusion mode $\mathfrak{q} \sim 1$, the residues of the longitudinal component present peaks. The residues grow with momentum, this is also reflected in the growth of the spectral function.*

Our results for the residues (normalized by $[(-\pi N^2 T^3 n^2)/4]^{-1}$) of transverse and longitudinal vector fluctuations are plotted in figure 4.1. The longitudinal fluctuations show an interesting behaviour related to the diffusion mode. The peaks and dips in figure 4.1 appear roughly at the locations where the hydrodynamic mode [4] crosses the imaginary part

[4] We continue calling it like this even outside the regime where the actual hydrodynamic approximation is valid.

of the quasinormal frequency. The hydrodynamic mode behaves in a completely different way. The diffusion pole quickly moves towards negative imaginary frequencies, while the residue first grows according to hydrodynamics and later goes as a damped oscillation. Numerically the zeroes coincide with $\mathfrak{w} = -in$. On the other hand, the location of the other quasinormal modes remains fairly constant until the diffusion pole reaches an integer value that coincides with the imaginary part of the quasinormal pole at zero momentum. After this point, the quasinormal pole starts approaching the real axis. This first happens at $\mathfrak{q}^2 = 1/2$, when the diffusion pole is at $\mathfrak{w} = -i$. For larger momentum, the long time behaviour of the fluctuations will be dominated by the first quasinormal mode and not by the hydrodynamic mode.

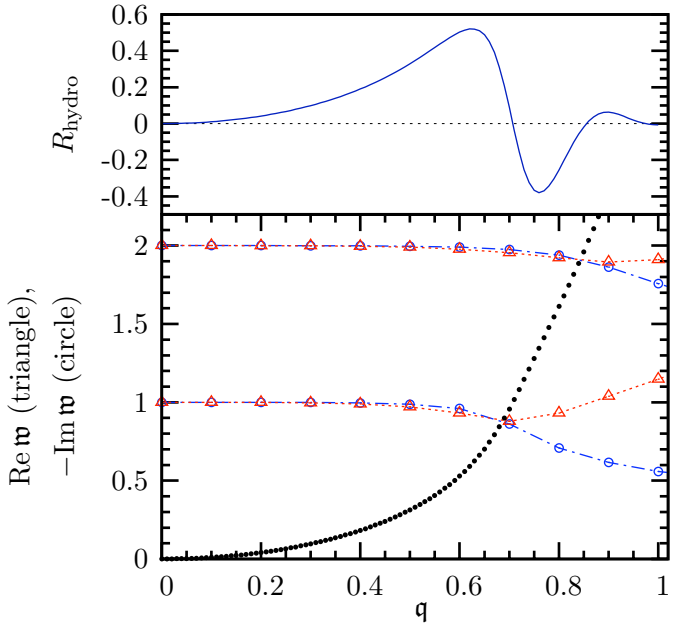

Figure 4.2: *In the lower figure, we show the real and imaginary parts of the quasinormal frequencies in the longitudinal channel and the value of the frequency for the diffusion mode. The quasinormal frequencies remain fairly stable as momentum increases, until there is a 'crossing' with the diffusion mode (it reaches a special value $\mathfrak{w} = -in$). Then, there is a qualitative change in the behaviour of the quasinormal frequency that starts approaching the real axis. The residue of the diffusion mode, shown in the upper figure, has a zero at each crossing value, and shows and oscillatory and decaying behaviour with momentum. Quasinormal frequencies in the transverse channel approach smoothly the real axis as momentum increases.*

We also find some interesting analytic structure related to the zeroes of the residue of the hydrodynamic pole (see figure 4.2). When $\mathfrak{w} = -in$, the exponents of infalling and outgoing solutions at the horizon differ by an integer. The infalling solution should then develop a logarithmic term since it has the lower exponent. However, for very special values of the parameters, i.e. the momentum $\mathfrak{q}$, it can happen that the coefficient of the logarithm

vanishes. We found numerically that the zeroes of the residues of the hydrodynamic mode coincide with these special values at $(\mathfrak{w}, \mathfrak{q}^2) = (-i, 1/2)$, $(-2i, \sqrt{3}-1)$, $(-3i, \sqrt{6}-3/2)$ and $(-4i, 1.4436)$.

4.3 Conclusions

The analytic structure we have found for the R-charge correlator at finite temperature is very interesting. At zero momentum, an infinite set of evenly spaced poles on the complex frequency plane is a generic feature of correlators. At weak coupling, they lie on the imaginary axis [102], but according to the AdS/CFT computation they move away at strong coupling. The right ultraviolet behavior, that is analytic at zero temperature, is recovered after summing over all the poles. The value of the residues is crucial, and especially the vanishing of the hydrodynamic mode at zero momentum. When we consider momentum dependence, the analytic form of the diffusion residue in the hydrodynamic approximation $\sim q^2$ will induce a singularity in the correlator at short times, on top of the usual ultraviolet singularity. This clearly cannot be the right answer, and we can understand this as a limit in the validity of the approximation. The damped and oscillatory behavior of the hydrodynamic residue can cure this problem, making the contribution from the diffusion mode smooth at short times. The hydrodynamic mode effectively decouples for momenta $q > 1$, and in this respect behaves as the collective modes present at weak coupling. In this sense, our results go beyond the hydrodynamic approximation. In principle, we expect that other hydrodynamic modes appearing in the stress-tensor two-point functions, the shear and the sound mode presented in section 1.2, to have a similar collective mode behavior.

We observe that as the momentum increases, diffusion becomes less important and other collective excitations of longitudinal modes describe charge density fluctuations. In contrast with the dressed partons of the weak coupling regime, they do not decouple at high momentum. The behaviour is also different from the poles found for gauge invariant operators. At weak coupling, these poles open up in branch cuts at fixed positions in the imaginary axis, while the holographic computation predicts that at infinite coupling the only singularities are poles that come closer to the real axis. Eventually a new peak appears in the spectral function, located close to $\mathfrak{w} = \mathfrak{q}$. This peak persists at higher momentum, and can be interpreted as a quasiparticle excitation of charge density fluctuations. This shows a change of behaviour of the system as we increase the momentum, from diffusive to reactive. Transverse fluctuations are comparatively featureless, there are no quasiparticle excitations appearing; this reflects the fact that there are no propagating modes in the zero temperature conformal theory.

Now, as suggested in the introduction to this chapter we may apply our results to

the calculation of the hydrodynamic time scale $\tau_{\rm H}$. Recalling eq.(3.4) we can estimate the moment where the diffusion mode's contribution is on par with that of the first quasinormal mode

$$|R_{\rm H}(q)\,\mathrm{e}^{-i\Omega_{\rm H}(q)\tau_{\rm H}-\Gamma_{\rm H}(q)\tau_{\rm H}}| \simeq |R_1(q)\,\mathrm{e}^{-i\Omega_1(q)\tau_{\rm H}-\Gamma_1(q)\tau_{\rm H}}|\ , \tag{4.14}$$

which after some algebra leads to q-dependent formula (4.1)

$$\tau_{\rm H} = \frac{\log|R_{\rm H}/R_1|}{\Gamma_{\rm H}-\Gamma_1} = \frac{1}{2\pi T}\,\frac{\log|\mathfrak{R}_{\rm H}/\mathfrak{R}_1|}{\mathrm{Im}\,(\mathfrak{w}_1-\mathfrak{w}_{\rm H})}\ .$$

Using our numerical results we plot $\tau_{\rm H}$ as a function of $\mathfrak{q}$, to find that in units of $(2\pi T)^{-1}$ the minimal time scale is $\tau_{\rm H}=3.7-3.2$ in a rank $\mathfrak{q}=0.3-0.48$, rapidly growing for higher values of the momentum. For lower values it also grows, but this is due to the fact that the charge distribution is already quite uniform, so we can take this value as the onset of diffusion. In fact, the dispersion relation starts to deviate from the hydrodynamic approximation for $\mathfrak{q}\approx 0.45$ which corresponds to Compton wavelengths of 1.2 fm, roughly the size of a proton. As a model for the sQGP at RHIC described in section 1.3, let us pick $T\simeq 2\,T_c\simeq 350\,\mathrm{MeV}$. The hydrodynamic time scale is then $\tau_{\rm H}\approx 0.3\,\mathrm{fm}/c$. This is a remarkable short time, even a bit smaller than $\tau_{\rm form}$. In fact it indicates that the hydrodynamic approximation is valid from very short times on. Recall that at RHIC the thermalization time is $\tau_{\rm therm}\approx 0.6-1.0\,\mathrm{fm}/c$ and the hydrodynamic approximation is therefore valid already for $t\lesssim 1\,\mathrm{fm}/c$ [108]. We expect that the values for shear or sound modes related to momentum and energy flow will be slightly different, but it is reassuring to find the right orders of magnitude even for $\mathcal{N}=4$.

Chapter 5

Absorption lengths

At the end of section 2.3 we saw the possibility of having complex momentum modes in the gravity background instead of quasinormal ones. The associated complex wave numbers corresponded in the dual gauge theory to poles of the retarded Green's function in the complex q-plane, where the inverse of their imaginary part plays the role of an absorption length in the medium. In the gravity side we have to solve wave equations with purely infalling boundary conditions at the horizon just as in the calculation of quasinormal modes. At the boundary of AdS we have to specify the same boundary conditions that have been described in refs. [96, 99] for the quasinormal modes. The imaginary part of these complex momentum wave numbers give absorption lengths characteristic of the black hole. After having travelled a distance λ_n a part of the wave has fallen into the black hole such that the amplitude is diminished by a factor of e^{-1}.

In the following we will be interested in computing these absorption lengths and their frequency dependence in the holographic dual of the $\mathcal{N}=4$ supersymmetric gauge theory in the gluon plasma phase. We will do this for different kinds of perturbations corresponding to certain gauge-invariant operators, namely we compute the largest correlation lengths for scalar operators of conformal dimension $\Delta = 4$ in section 5.2, global currents in section 5.3, and the transverse and shear channels of the stress-energy tensor in section 5.4, respectively. To achieve this we will map all of our equations of motion to a so-called *Heun equation,* i.e. a second order linear ordinary differential equation with *four* regular points. There is a method, which we will describe, that allows to obtain the absorption lengths in a semi-analytical treatment. Recall that in the preceding chapter the analysis performed was wholly numerical. This method based on the Heun equation will also be used in one of the cases addressed in chapter 6.

Finally, there is also a particular limit in the absorption lengths obtained above of interest for the three-dimensional reduced theory. If one takes their zero frequency limit, one will be computing the screening lengths for a static field in the plasma. These are directly related to the glueball masses in the dimensionally reduced theory, which are bound states made of gluons with a mass of order the confinement scale, but not much above since one should start to see the gluons, which are massless. We point out that the longest screening length corresponds to an operator with non-vanishing R-charge, and thus

does not have an interpretation as a QCD$_3$ glueball. In the AdS/CFT correspondence, part of the glueball masses of QCD$_3$ had already been analyzed, as computed in refs. [109–111].

5.1 Another exactly solvable case

It is clear from the discussion above that in both cases —relaxation times and absorption lengths— the gravity waves are subject to the infalling condition at the horizon. The question is simply which parameter of the retarded Green's function is analytically continued to complex values, either the frequency or the momentum. To compute these complex momentum wave numbers one can therefore follow the same strategy that is used for the calculation of quasinormal frequencies, but fixing the frequency ω to be real-valued instead of the momentum q.

This switch of roles is particularly clear in the case of the AdS$_3$/CFT$_2$ correspondence, where a solvable two-dimensional conformal field theory is dual to the three-dimensional BTZ black hole background. In this case the exact retarded Green's functions can be calculated in both sides of the correspondence and seen to match [91]. Let us consider a particular case to see how such a switch of roles takes place. For a field with conformal dimension $\Delta = 2$, the retarded two-point function is

$$\widetilde{G}_{\mathrm{R}}^{(2\mathrm{d})}(\omega, q) = \frac{\omega^2 - q^2}{4\pi^2} \left[\psi\left(1 - i\,\frac{\omega - q}{4\pi T}\right) + \psi\left(1 - i\,\frac{\omega + q}{4\pi T}\right) \right] \ , \tag{5.1}$$

where ψ is again the digamma function. Thus, the poles of such function determine the quasinormal frequencies $\omega_n = \pm q - 4\pi i T(n+1)$. For each quasinormal mode the dispersion relation $\omega_n = \omega_n(q)$ is linear. Because of this linearity the poles can also be interpreted in a different way by writing

$$q_n = \pm[\omega + 4\pi i T(n+1)] \ , \quad n \in \mathbb{N} \ , \tag{5.2}$$

where we see explicitly that the complex momentum modes lie in the first and third quadrants for the right- and left-movers respectively, as it was shown both from field theory as well as gravity arguments in chapter 3.

In higher dimensions the dispersion relations for the quasinormal frequencies are not linear and can be computed only numerically. At zero momentum, the position of large frequencies in the complex momentum plane has been estimated using semiclassical methods [112, 113]; it would be interesting to extend those analysis to non-zero momentum. Since the dispersion relation for the quasinormal modes is known only numerically we also have to resort to numerical methods to find the complex wave numbers and absorption lengths. The only exception is given by the hydrodynamic modes that appear for small frequency and wave numbers [93, 95] presented in section 1.2. We will see that our numerical results are in agreement with the analytic dispersion relations of these modes.

5.2 Numerics I: scalar operators

As a first example we want to compute the absorption lengths of a scalar operator $\mathcal{O}(t, \mathbf{x})$ of conformal dimension $\Delta = 4$. We choose this particular case because it is the simplest setup we can use to illustrate the method, since the dual supergravity field corresponds to a minimally coupled, massless scalar. A possible example is given by $\mathcal{O} = \mathrm{tr}F^2$, that maps to the dilaton in the holographic dual.

Consider the retarded two-point correlation function in the theory at temperature T

$$G_{\mathrm{R}}(t - t', \mathbf{x} - \mathbf{y}) = -i\,\theta(t - t')\,\left\langle [\mathcal{O}(t, \mathbf{x}), \mathcal{O}(t', \mathbf{y})] \right\rangle \ . \tag{5.3}$$

At large distances $|\mathbf{x} - \mathbf{y}| \gg T^{-1}$, the Green's function decays exponentially due to thermal screening. As we have explained, this behaviour is determined by a set of discrete lengths that in linear response theory describe the *absorption* of out-of-equilibrium perturbations. For the theory in equilibrium they are identified with *correlation lengths* in the plasma, as proposed in ref. [114], with the squared inverse of the zero frequency correlation lengths regarded as the glueball masses[1] of a three-dimensional effective theory in the high-temperature limit [109–111]. Via the AdS/CFT correspondence we can reduce this complicated non-perturbative problem in the gauge theory to finding the complex momenta that allow the dilaton fluctuations to obey infalling boundary conditions on the horizon, and Dirichlet ones on the boundary. In this example, and in the other cases we consider in this thesis, after a suitable transformation the equations of motion can be reduced to Heun equations, which we can solve using semi-analytic methods.

The Heun equation method. The equation of motion for this field (A.4) was already derived in appendix A.1. Throughout the chapter we use dimensionless frequency and momentum. In order to recover the dimensionful quantities it is enough to make the substitution $(\omega, q) \mapsto \pi T\,(\omega, q)$, where we have set without loss of generality the momentum along one of the three spatial directions. Changing coordinates from z to $x = 1 - z^2$, the equation now reads

$$\Phi'' + \frac{1 + (1 - x)^2}{x(1 - x)(2 - x)}\,\Phi' + \left(\frac{\omega^2}{4x^2(1 - x)(2 - x)^2} - \frac{q^2}{4x(1 - x)(2 - x)} \right) \Phi(x) = 0 \ . \tag{5.4}$$

This equation has four regular singular points at $x = 0, 1, 2, \infty$, with characteristic exponents from the Frobenius expansion

$$\{0; -i\omega/4, +i\omega/4\} \ , \quad \{1; 0, 2\} \ , \quad \{2; -\omega/4, +\omega/4\} \ , \quad \{\infty; 0, 0\} \ .$$

Therefore, we can transform it into a Heun equation and we can follow the analysis described in [94]. To compute the complex wave numbers we simply have to analytically

[1] In this particular example we are considering $J^{\mathrm{PC}} = 0^{++}$ glueballs.

continue the momentum instead of the frequency. It is interesting to observe that none of the characteristic exponents at the singular points depend on the momenta. If we factorize $\Phi(x)$ as

$$\Phi(x) = x^{-i\omega/4}\,(1-x)^2\,(2-x)^{-\omega/4}\,y(x)\ , \tag{5.5}$$

then we are allowed to write the equation of motion in the standard form of a Heun equation for $y(z)$

$$y''(x) + \left(\frac{\gamma}{x} + \frac{\delta}{x-1} + \frac{\epsilon}{x-2}\right) y'(x) + \frac{\alpha\beta x - Q}{x(x-1)(x-2)}\, y(x) = 0\ , \tag{5.6}$$

with parameters

$$\alpha = \beta = 2 - \frac{\omega}{4}(1+i)\ , \quad Q = 4 + \frac{q^2}{4} - (1+7i)\frac{\omega}{4} - (2-i)\frac{\omega^2}{8}\ , \tag{5.7}$$

$$\gamma = 1 - i\frac{\omega}{2}\ , \quad \delta = 3\ , \quad \epsilon = 1 - \frac{\omega}{2}\ . \tag{5.8}$$

All the other perturbations we will consider in this chapter can be transformed to Heun equations in a similar manner. Just in the same way as we saw in section 2.3 for quasinormal modes and applied in chapter 4, we can compute the poles of the retarded Green's function

$$\widetilde{G}_{\rm R}(\omega, q) \propto \frac{\mathcal{B}(\omega, q)}{\mathcal{A}(\omega, q)}\ ,$$

as the solutions to the equation $\mathcal{A} = 0$, i.e. solutions that are analytic in the interval $x \in [0, 1]$. These boundary conditions determine a discrete set of complex momentum eigenvalues if we fix the frequency ω to real values.

We can find local solutions that define $\mathcal{A}$ and $\mathcal{B}$ using the Frobenius method close to the singularities. In the equation above, choosing $y(0)$ and $y(1)$ to be constant selects the appropriate normalizable and infalling behaviour of the fluctuation Φ. In particular, a solution with boundary condition $y(0) =$ const. will be a superposition of solutions with exponents $1 - \delta \leq 0$ and 0 close to the AdS boundary ($x = 1$). The Dirichlet boundary condition $y(1) =$ const. for Φ can be only satisfied for a discrete set of frequencies ω or momenta q. In the preceding chapter we used this approach, and computed these values imposing matching conditions at some intermediate point for the Frobenius series. However, as one considers higher frequencies the number of terms in the expansion needs to be increased and the convergence gets worse.

Fortunately, whenever we can map to the Heun equation there is an alternative method which we can use, based on the improved convergence of the solutions. Normal solutions are convergent for $|x| < 1$, but for some values of the parameters the solutions can converge for $|x| < 2$. This happens when we have two possible solutions for the recursion relations of the Frobenius series at the horizon, such that one can satisfy the requirements for the modes at the AdS boundary. This condition of extended convergence boils down to a

transcendental equation for the frequencies or momenta in the form of a continued fraction (see [94, 115] for more details) using Pincherle's theorem on the existence of minimal solutions to three term recursion relations.

The coefficients of the Frobenius series at $x = 0$ should satisfy the recursion relation

$$a_{n+2} + A_n(\omega, q)\, a_{n+1} + B_n(\omega, q)\, a_n = 0 \ , \quad n \geq 2 \ , \tag{5.9}$$

where

$$A_n(\omega, q) = -\frac{(n+1)(2\delta + \epsilon + 3(n+\gamma)) + Q}{2(n+2)(n+1+\gamma)} \ , \tag{5.10}$$

$$B_n(\omega, q) = \frac{(n+\alpha)(n+\beta)}{2(n+2)(n+1+\gamma)} \ , \tag{5.11}$$

and $a_0 = 1,\ a_1 = Q/2\gamma$. Then one obtains the following recursive definition

$$r_n = \frac{a_{n+1}}{a_n} = -\frac{B_n(\omega, q)}{A_n(\omega, q) + r_{n+1}} \ . \tag{5.12}$$

Pincherle's theorem states that a minimal solution to the three term recursion relation (5.9) exists if and only if the continued fraction on the right hand side in (5.12) converges. Moreover, in this case it converges precisely to a_{n+1}/a_n. In [94, 96] it was pointed out that the minimal solution corresponds precisely to a solution of the Heun equation that is analytic at $x = 1$ therefore fulfilling the correct boundary conditions. Choosing $n = 0$ we find

$$r_0 = \frac{Q}{2\gamma} \ , \tag{5.13}$$

and computing r_0 recursively gives a transcendental equation for q (or ω in the quasinormal case). Using this formula, we can compute numerically the complex momentum modes with high precision. In order to do that, we cut the fraction at a large value $n = n_* = 100$ and use the asymptotic value $r_n = 1/2 - (2 + \omega)/4n_*$. It is important to realize that Pincherle's theorem applies only if we are dealing with genuine three term recursion relations. For some pathological cases it can happen that the recursion relation involves three terms only from a certain value of $n = n_1$ on. This happens for example if either $\alpha = 0$ or $\beta = 0$ when $B_0 = 0$. In such a case one has to use (5.12) with $n = n_1$. We will see that we are faced with this in the cases of the longitudinal vector field perturbations and of the shear mode perturbations at $\omega = 0$. Since $\alpha = 0$ in both cases it is sufficient to take $n_1 = 1$ and use

$$r_1 = \frac{Q^2 + 3Q\gamma - 2\alpha\beta\gamma + 2Q\delta + Q\epsilon}{4Q + 4Q\gamma} \ , \tag{5.14}$$

instead of (5.13).

We have numerically computed the complex momentum eigenvalues using this method. The results for the scalar field perturbations are shown in figure 5.2. The real and imaginary parts of the five lowest complex momenta are plotted as a function of the frequency.

The real parts start out at $q^{\mathrm{R}} = 0$ for zero frequency. The imaginary parts start out at a finite value at $\omega = 0$, develop a shoulder that is more pronounced for the higher modes and then fall off rather fast until they enter a regime of slow decrease for large frequencies. Numerically we found that the lowest mode becomes almost constant at large frequencies with $q^{\mathrm{I}} \approx 0.83$ at $\omega = 100$. Also the higher modes flatten out for high frequencies. As expected, higher frequencies can penetrate farther into the plasma. It is an interesting question if the plasma becomes transparent for some high but finite frequency, if transparency is reached only in the limit $\omega = \infty$ or if the absorption length stays finite. Unfortunately our algorithm does not allow us to explore this asymptotic regime. We can speculate however using the underlying conformal invariance of the $\mathcal{N}=4$ theory. Since for high frequencies the temperature is less and less important we expect that the absorption length diverges as $\omega \to \infty$, i.e. $q^{\mathrm{I}}(\omega = \infty) = 0$. A finite absorption length would point to an underlying scale in the theory. On the other hand, if the plasma were to become transparent at some finite value of ω, we would expect that to happen at a scale that is set by the temperature. However, our numerical results show finite absorption lengths for much higher frequencies.

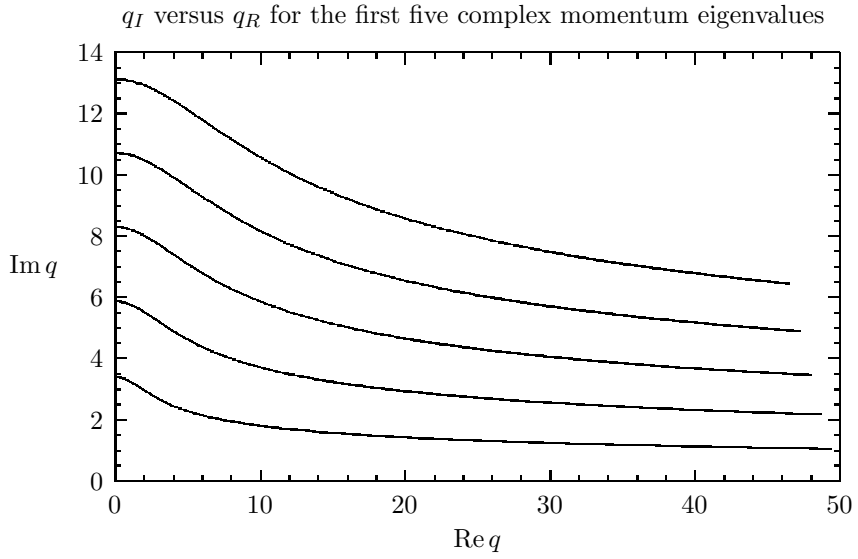

Figure 5.1: *We have traced the locations of the five lowest momentum eigenvalues in the complex q-plane for different frequencies as a function of the frequency out to $\omega = 50$. The momentum eigenvalues vary continuously with the frequency and lie on the analogues of Regge trajectories.*

Glueball masses. Of particular interest are the absorption lengths in the static limit $\omega \to 0$. In this case we will refer to the absorption length as the screening length. The equation (5.4) with $\omega = 0$ has been studied before in [109, 110]. There the interpretation of the eigenvalues in the momentum with $q^2 < 0$ was as masses of glueballs in the three-

dimensional theory that is obtained by reduction on the thermal circle in the Euclidean continuation of the AdS-black hole we saw in section 2.2. The glueball masses can be calculated as the discrete eigenvalues $M_n^2 = -q_n^2$. Our numerical results at $\omega = 0$ for the first ten modes are compiled in table 5.1 and are in good agreement with results given by refs. [109, 110]. It is important to see if the eigenfunctions correspond to the wave

n	q_n^2
1	-11.5877
2	-34.5270
3	-68.9750
4	-114.9104
5	-172.3312
6	-241.2366
7	-321.6265
8	-413.5009
9	-516.8597
10	-631.7028

Table 5.1: *The first ten glueballs of the scalar mode.*

functions of the glueballs too. In [111] the authors observe that for all the glueball masses the correct boundary conditions correspond to demanding analyticity of the wave function at the horizon and the boundary. These are precisely the same boundary conditions that emerge in our case at $\omega = 0$. Therefore, the screening lengths for static fields corresponds precisely to the glueball masses computed earlier in [109–111].

5.3 Numerics II: global currents

In the $\mathcal{N}=4$ theory, the global currents associated to R-charges map to mixed components of the S^5 and AdS_5 metrics, that can be seen as graviphotons after dimensional reduction to AdS_5. In general, any global symmetry in the field theory will map to a local gauge symmetry in the holographic dual. Then, to find the poles of the retarded Green's functions in the plasma

$$G_{\mu\nu}(t-t', \mathbf{x}-\mathbf{y}) = -i\,\theta(t-t')\,\left\langle [J_\mu(t,\mathbf{x}), J_\nu(t',\mathbf{y})] \right\rangle \ , \tag{5.15}$$

we have to compute the complex momentum eigenvalues for vector fields in the AdS-black hole.[2] We will see that there are two decoupled sectors, corresponding to transverse and

[2]We are assuming that the total charge in the equilibrium state vanishes, so there are no chemical potentials.

longitudinal channels. The reason is that temperature breaks four-dimensional Lorentz symmetry to three-dimensional rotational symmetry. In the glueball language, the zero frequency masses correspond to $J^{\rm PC} = 1^{--}$ and 0^{-+} states. However, the states arising from the vector fields are also charged under the global R-symmetry and therefore do not form part of the superselection sector that constitutes QCD$_3$. For simplicity we will refer to these states also as glueballs. The longitudinal channel is special because it also describes the diffusion of the conserved charge through the plasma, that does not appear as a glueball state in the three-dimensional theory because the residue of the diffusion mode vanishes in the zero frequency limit. We will show that the diffusion pole is also captured by complex momentum eigenvalues.

We can compute the complex momentum eigenvalues corresponding to a vector field in the AdS-Schwarzschild background in an analogous way to the scalar field case. The equations of motion for such a field are given in the appendix A.1, equations (A.6) or equations (A.7), which are the ones we will be working with. Notice that there is a choice of gauge invariant variables $E_{\rm L} = qA_0 + \omega A_{\rm L}$ and $\mathbf{E}_{\rm T} = \omega \mathbf{A}_{\rm T}$ that describe the diffusive and transverse channel respectively [99], given by equations (A.8) and which we used in chapter 4. However, the spectrum of complex momentum values (equivalently of quasinormal modes) is gauge invariant, so it should not matter if we choose to work with gauge components, that obey simpler equations and which allow a map to Heun equations. Since the invariant quantity is $E_{\rm L}$, this means that A_0 and $A_{\rm L}$ should have the same spectrum, as the constraint (A.6a) points out.

As promised, in the $x = 1 - z^2$ coordinate and for a suitable factorization of each component, equations (A.7) can be written as Heun equations:

- *Temporal.* The critical exponents at the singularities are

$$\left(0; -i\frac{\omega}{4}, i\frac{\omega}{4}\right) \ , \quad \left(1; \frac{1}{2}, \frac{1}{2}\right) \ , \quad \left(2; -\frac{\omega}{4}, \frac{\omega}{4}\right) \ , \quad \left(\infty; -\frac{1}{2}, \frac{3}{2}\right) \ .$$

$$V_0(x) = x^{-i\omega/4}(x-1)^{1/2}(x-2)^{-\omega/4} y(x) \ . \tag{5.16}$$

- *Longitudinal.* The critical exponents at the singularities are

$$\left(0; -1 - i\frac{\omega}{4}, -1 + i\frac{\omega}{4}\right) \ , \quad \left(1; \frac{1}{2}, \frac{1}{2}\right) \ , \quad \left(2; -1 - \frac{\omega}{4}, -1 + \frac{\omega}{4}\right) \ , \quad \left(\infty; \frac{5}{2} - \sqrt{5}, \frac{5}{2} + \sqrt{5}\right) \ .$$

$$V_{\rm L}(x) = x^{-1-i\omega/4}(x-1)^{1/2}(x-2)^{-1-\omega/4} y(x) \ . \tag{5.17}$$

In both cases we find the same parameters for the Heun equation

$$\begin{aligned} \alpha &= -\frac{\omega}{4}(1+i) \ , \quad \beta = 2 - \left(\frac{\omega}{4}(1+i)\right) \ , \quad Q = \frac{q^2}{4} - (1+3i)\frac{\omega}{4} - (2-i)\frac{\omega^2}{8} \ , \\ \gamma &= 1 - i\frac{\omega}{2} \ , \quad \delta = 1 \ , \quad \epsilon = 1 - \frac{\omega}{2} \ . \end{aligned} \tag{5.18}$$

Notice that the boundary conditions for $V_{\rm L}(x)$ are not infalling ones. They are determined by the constraint (A.6a).

- *Transverse.* The critical exponents at the singularities are

$$\left(0; -i\frac{\omega}{4}, i\frac{\omega}{4}\right) \ , \quad (1;0,1) \ , \quad \left(2; -\frac{\omega}{4}, \frac{\omega}{4}\right) \ , \quad (\infty;0,1) \ .$$

$$A_{\rm T}(x) = x^{-i\omega/4}(x-1)(x-2)^{-\omega/4}y(x) \ , \tag{5.19}$$

with the following parameters in the Heun equation

$$\begin{aligned} \alpha &= 1 - \frac{\omega}{4}(1+i) \ , \quad \beta = 2 - \left(\frac{\omega}{4}(1+i)\right) \ , \quad Q = \frac{q^2}{4} + 2 - (1+5i)\frac{\omega}{4} - (2-i)\frac{\omega^2}{8} \ , \\ \gamma &= 1 - i\frac{\omega}{2} \ , \quad \delta = 2 \ , \quad \epsilon = 1 - \frac{\omega}{2} \ . \end{aligned} \tag{5.20}$$

As we had anticipated, the temporal and longitudinal components have the same spectrum, since they obey the same Heun equation, although this was not evident in equations (A.7a) and (A.7b).

The results are shown in figures 5.3 and 5.4. The real and imaginary parts of the five lowest complex momentum are plotted as a function of the frequency. The behaviour is similar to the one found for the scalar operator. The imaginary parts start out at a finite value at $\omega = 0$, develop a shoulder that is more pronounced for the higher modes and then fall off rather fast until they enter a regime of slow decrease for large frequencies. The real parts start out the $q^{\rm R} = 0$ for zero frequency.

So far, we have described the absorption of R-current excitations in the plasma. However, a conserved global charge cannot be dissipated, it is spread out by the slow process of diffusion. This is described in the hydrodynamic regime $\omega, q \ll T$ by a diffusion pole [93] (units restored)

$$\omega = -i\,\frac{q^2}{2\pi T} \ . \tag{5.21}$$

In our analysis of complex wave numbers we are able to see numerically this mode ($q = (1+i)\sqrt{\omega}$ with our conventions) that fits nicely with the analytic prediction in the hydrodynamical regime; see fig. 5.6.

Glueball masses. In the zero frequency limit, the absorption lengths can be interpreted as the inverse glueball masses of an effective three-dimensional theory. Note however that these states do not lie in the superselection sector that constitutes the holographic dual of QCD$_3$! For the longitudinal channel we have to take into account that $\alpha(\omega = 0) = 0$ so we have to use the modified recursion relation starting at $n = 1$ (5.14). It turns out that the glueball masses of the longitudinal channel coincide with the ones found for the scalar operator, table 5.1. Indeed, at $\omega = 0$ we can transform the Heun equation

n	q_n^2
1	-5.1313
2	-22.4816
3	-51.2098
4	-91.4106
5	-143.0926
6	-206.2577
7	-280.9066
8	-367.0395
9	-464.6566
10	-573.7580

Table 5.2: *The first ten glueballs of the transverse mode.*

with parameters (5.7) into the Heun equation with parameters (5.18). First, make the coordinate transformation $x \to \frac{x-2}{x-1}$, that shuffles the singular points $2 \leftrightarrow 0$, $1 \leftrightarrow \infty$. Then, the redefinition $y(x) \to (x-1)^2 y(x)$ (explained in appendix A.4) shows that both equations are equivalent. Notice that the solutions that are analytic in $[0,1]$ in the transformed equation correspond to solutions that are analytic in $[2,\infty)$ in the original equation, and not to the physical modes. However, such solutions can be generated from the physical ones by conformal transformations on the two-sphere,[3] so both types appear for the same values of the parameters. Notice that both solutions have a similar analytic structure, the only singularity is a branch cut joining two of the singular points. Also the fact that the auxiliary parameters Q of both equations are the same for the particular cases we are considering, allows an immediate identification of the complex momentum numbers.

The transverse channel has different spectrum, whose first modes are in table 5.2. Although the glueballs associated to vector fields have non-zero R-charge, and are usually not considered, our computation shows that the lightest three-dimensional state and hence, the longest correlation length, belongs to this class.[4]

5.4 Numerics III: stress-energy tensor

The stress-energy tensor of the gauge theory encodes important dynamical and thermodynamical properties of the plasma. Correlation functions of the stress-energy tensor

$$G_{\mu\nu,\rho\sigma}(t-t',\mathbf{x}-\mathbf{y}) = -i\,\theta(t-t')\,\left\langle [T_{\mu\nu}(t,\mathbf{x}),T_{\rho\sigma}(t',\mathbf{y})]\right\rangle \ , \tag{5.22}$$

[3] See [116] for an exhaustive list of Heun solutions and their relations.

[4] This state is even lighter than the lightest QCD$_3$ glueball listed in [111].

are related to perturbations of the metric that leave the S^5 factor invariant. Therefore, we want to introduce a small fluctuation of the four-dimensional part of the metric $g_{\mu\nu} = g^0_{\mu\nu} + h_{\mu\nu}$.

In the gauge theory, the breaking of Lorentz symmetry to rotational symmetry by temperature splits the Green's functions in transverse, shear and sound channels, that in the zero frequency limit contain the $J^{PC} = 2^{++}$, 1^{++} and 0^{++} glueball spectrum. This is reflected in the gravity dual, where the perturbations fall into three different classes with decoupled field equations [93, 95, 99]. The associated spin to each of these channels is also 2, 1 and 0, so we will refer to them also as tensor, vector and scalar. In the shear and sound channels there are also hydrodynamical modes that describe the diffusion of conserved momentum and the propagation of sound. We will not study the sound channel since we cannot map its equation to a Heun one, but we will show that complex momentum modes also capture the shear pole.

In this section we will work within the gauge-invariant formalism developed in [117], where we can distinguish among the three different channels named above. The relevant equations —in Schrödinger-like form— are in appendix A.1, given by equations (A.12). By making the change of variable $x = 1-z^2$, the equations for tensor and vector perturbations lead to a Heun equation. For scalar perturbations (related to the sound channel) the situation is not so simple, and it requires a separate analysis that we leave for future work, so in the following we will be concerned only with tensor and vector perturbations.

- *Tensor perturbations.* The characteristic exponents are

$$\left(0; -i\frac{\omega}{4}, i\frac{\omega}{4}\right) \ , \quad \left(1; -\frac{3}{4}, \frac{5}{4}\right) \ , \quad \left(2; -\frac{\omega}{4}, \frac{\omega}{4}\right) \ , \quad \left(\infty; \frac{3}{4}, \frac{3}{4}\right) \ .$$

$$\psi_{\rm T}(x) = x^{-i\omega/4}(x-1)^{5/4}(x-2)^{-\omega/4}y(x) \ . \tag{5.23}$$

$$\begin{aligned} \alpha\beta &= \left(\frac{\omega}{4}(1+i)-2\right)^2 \ , \quad Q = \frac{q^2}{4} + 4 - (2-i)\left((-1+3i)\frac{\omega}{4} + \frac{\omega^2}{8}\right) \ , \\ \gamma &= 1 - i\,\frac{\omega}{2} \ , \quad \delta = 3 \ , \quad \epsilon = 1 - \frac{\omega}{2} \ . \end{aligned} \tag{5.24}$$

- *Vector perturbations.* The characteristic exponents are

$$\left(0; -i\frac{\omega}{4}, i\frac{\omega}{4}\right) \ , \quad \left(1; -\frac{1}{4}, \frac{3}{4}\right) \ , \quad \left(2; -\frac{\omega}{4}, \frac{\omega}{4}\right) \ , \quad \left(\infty; -\frac{3}{4}, \frac{9}{4}\right) \ .$$

$$\psi_{\rm V}(x) = x^{-i\omega/4}(x-1)^{3/4}(x-2)^{-\omega/4}y(x) \ . \tag{5.25}$$

$$\begin{aligned} \alpha\beta &= \frac{\omega}{4}(1+i)\left(\frac{\omega}{4}(1+i)-3\right) \ , \quad Q = \frac{q^2}{4} - (1+5i)\frac{\omega}{4} - (2-i)\frac{\omega^2}{8} \ , \\ \gamma &= 1 - i\,\frac{\omega}{2} \ , \quad \delta = 2 \ , \quad \epsilon = 1 - \frac{\omega}{2} \ . \end{aligned} \tag{5.26}$$

Notice that tensor fluctuations obey the same equations as a massless scalar field, so the first modes of the spectrum are plotted in figure 5.2. The Heun equation we have for the vector perturbations goes over to the one the authors in [96] found for the shear mode after the transformation described in appendix A.4.

As we have commented above, vector fluctuations correspond to the shear channel of the gauge theory. This channel is associated to the momentum of the plasma, that as a conserved quantity is not absorbed but diffused. In the hydrodynamical limit it is possible to find an analytic expression for the diffusion pole [93]

$$\omega = -i\,\frac{q^2}{4\pi T}\ . \tag{5.27}$$

We find good numerical agreement for this mode $q = (1+i)\sqrt{2\omega}$, as can be seen in fig. 5.7.

The results for the shear mode are shown in figure 5.5. The real and imaginary parts of the five lowest complex momentum are plotted as a function of the frequency. Again, we find a similar behaviour to scalar and vector modes. The imaginary parts start out at a finite value at $\omega = 0$, develop a shoulder that is more pronounced for the higher modes and then fall off rather fast until they enter a regime of slow decrease for large frequencies. The real parts start out the $q^{\mathrm{R}} = 0$ for zero frequency.

Glueball masses. We can find the glueball spectrum of the effective three-dimensional theory by taking the static limit $\omega = 0$. Again we have to use the recursion relation starting $n = 1$ (5.14) since $\alpha(\omega = 0) = 0$. The results for the shear channel are compiled in table 5.3. The glueball spectrum for neutral glueballs has been computed using a similar supergravity approach in [111]. The numbers we find differ actually somewhat from the ones quoted in [111] for the 1^{++} glueballs. We attribute this to the different numerical methods that have been used to obtain them.

5.5 Conclusions

In this chapter we have established on more firm grounds the relation between solutions to linearized field equations with complex momenta in an AdS-black hole background and the absorption lengths of a conformal gauge theory in a plasma phase. This was done computing explicitly some simple examples corresponding to scalar, vector and metric fluctuations.

Due to conformal symmetry, all the absorption lengths scale simply with the inverse of the temperature T^{-1}. At zero frequency we find agreement with previous computations of the effective three-dimensional glueball spectrum [109–111]. However, we prefer in this thesis to interpret our results as screening lengths for static fields. This interpretation

n	q_n^2
1	-18.6758
2	-47.4951
3	-87.7228
4	-139.4167
5	-202.5882
6	-277.2408
7	-363.3762
8	-460.9949
9	-570.0974
10	-690.6838

Table 5.3: *The first ten glueballs of the shear mode.*

has also recently and independently been proposed in ref. [114]. Furthermore, we have computed the dependence of the absorption length on the frequency. The results for the first modes are compiled in figures 5.2, 5.3, 5.4 and 5.5. In all the cases, the plasma is less absorptive for higher frequencies. The complex wave numbers also capture the hydrodynamical behaviour for R-charge and momentum diffusion. Our numerical results are in agreement with the simple analytic continuation of the dispersion relation for the hydrodynamic modes. This is shown in figures 5.6 and 5.7.

One of the interesting results of our study is that the longest screening length (the lightest "glueball" mass in the dimensionally reduced theory) corresponds to a state with non-vanishing R-charge. Such a state does not belong to the spectrum of the QCD$_3$ theory, i.e. the mass gap of the effective three-dimensional theory is not the one of QCD$_3$! Glueball masses play an important role in the determination of the Debye screening length. Here one studies the glueball exchange between open strings in the AdS-black hole background. As has been pointed out in [114] the mass gap by itself is not important for the Debye screening, because only specific operators can couple to the open string. Since these open strings are R-charge neutral, the low mass states with non-zero R-charge do not couple to the string. However, the string configuration one considers usually has its endpoints fixed on one point on the S^5 and it is also possible to consider strings that end on different points on the S^5. In such a situation the light non-zero R-charge states might become relevant and could modify the result for the screening length.

In this chapter we have only studied the cases that can be reduced to Heun equations and allow the application of the efficient continued fraction approach to the calculation of the complex momentum eigenvalues. It would certainly be interesting to extend the present investigations to the cases that cannot be reduced to Heun equations. In these cases

one has to resort to the elementary method of Frobenius expansions, which slows down the numerical calculation considerably. Nevertheless we think that this is an interesting problem especially in view of the comparison to the glueball mass calculations.

Another rather intersting point is the question whether the absorption length diverges in the limit of infinite frequency or whether it stays finite. Unfortunately, so far we know only about numerical methods to evaluate the absorption lengths.

A related problem is the calculation of the the absorption lengths in non-conformal holographic theories. Due to the presence of an underlying scale the dependence on the frequency is likely to show a more complicated pattern than the one we have found for the conformal case in this thesis. It will also be of high interest to compute absorption lengths for the meson states that appear in theories with D7-brane embeddings in the AdS-black hole, using the same methods that we employ in chapter 6 in the study of meson quasinormal modes [3]. In [106] it has recently been emphasized that instabilities arise for near critical black hole embeddings. Such instabilities show up as quasinormal modes with positive imaginary part. As we have seen, similar instabilities can also arise in the study of the absorption lengths. Since the instabilities in the screening lengths arise at $\omega = 0$ and for real values of q^2 it might be much easier to search for these instead of unstable quasinormal modes.

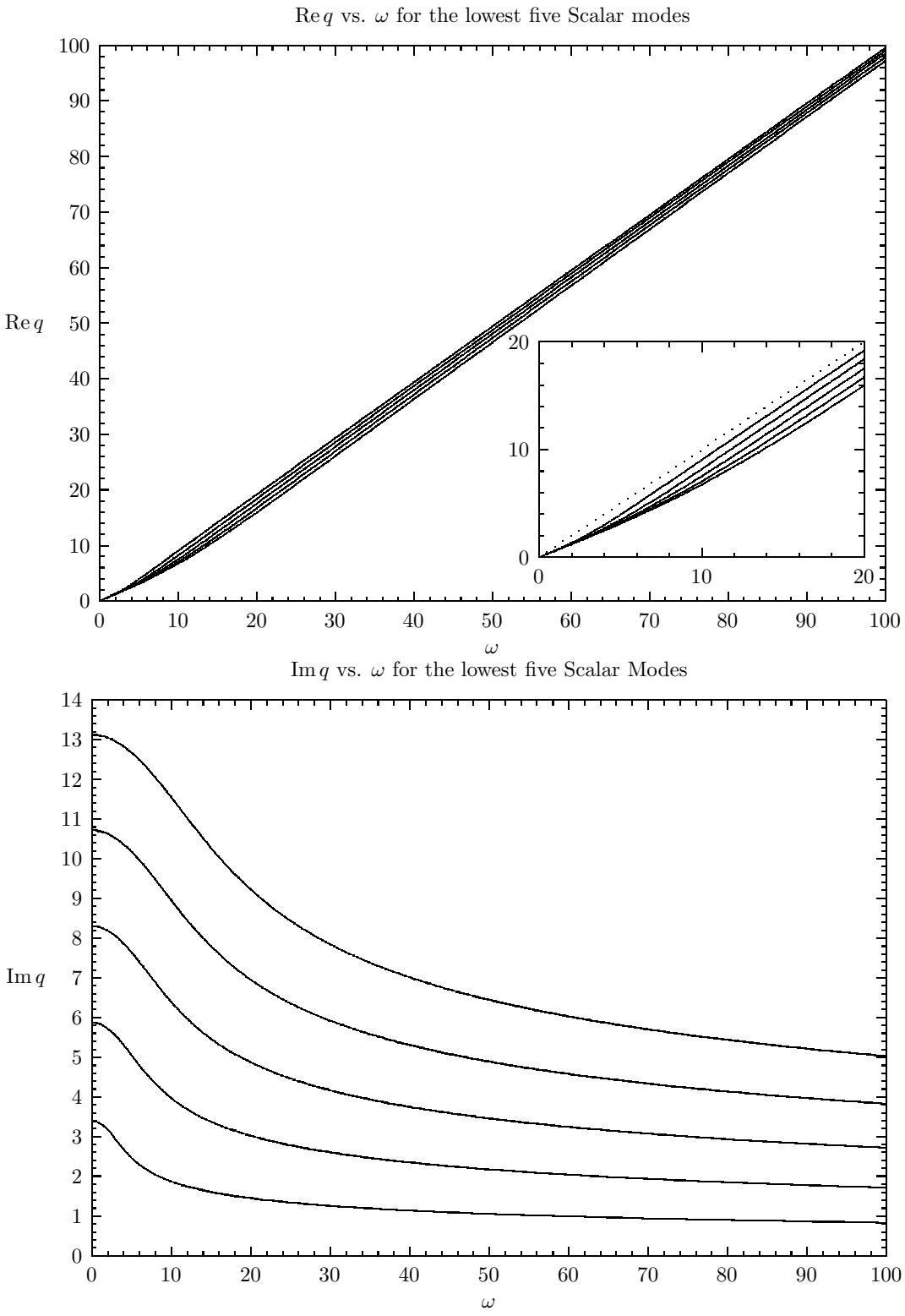

Figure 5.2: *Real and imaginary parts of the lowest five complex momentum eigenvalues versus the frequency. In the lower-right corner of the first figure we have zoomed in to show the separation between the five modes.*

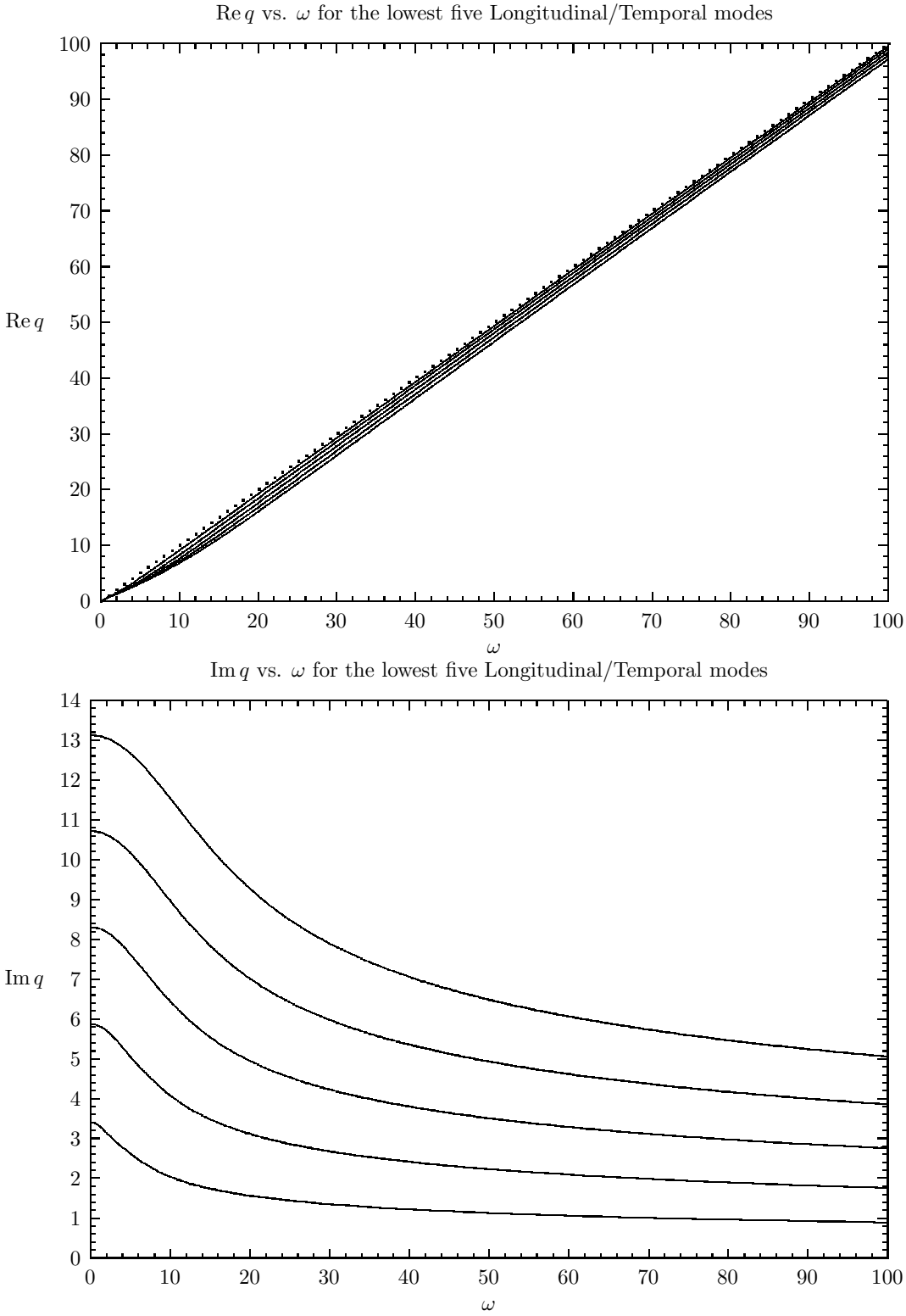

Figure 5.3: *Longitudinal perturbations of the vector field on AdS. At $\omega = 0$ the values coincide with the ones of the scalar field perturbations. For $\omega > 0$ the shape is however different.*

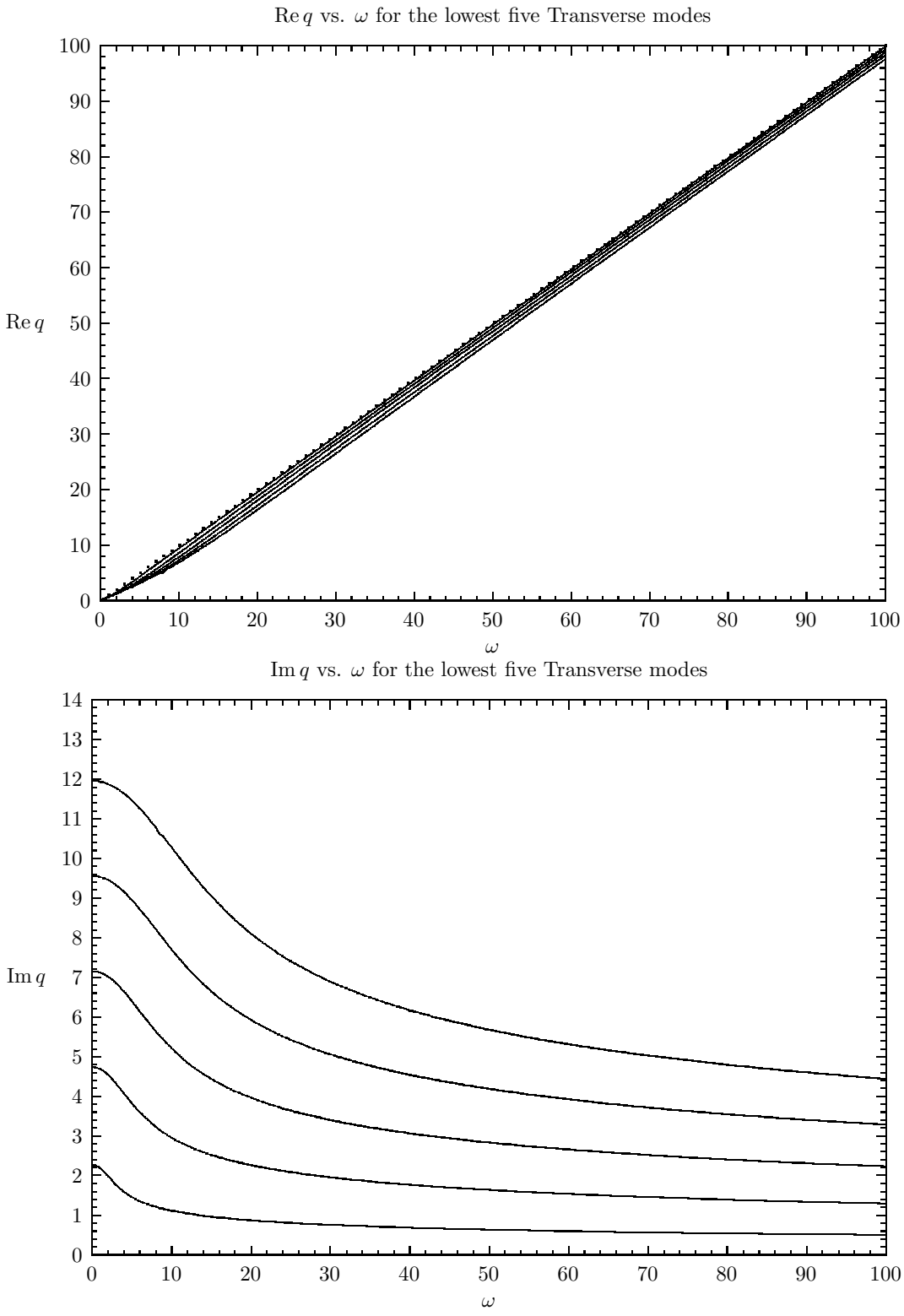

Figure 5.4: *The complex momentum eigenvalues of the transverse vector field components. Note that the lowest mode gives the longest absorbtion length. The plasma is most transparent to transverse vector perturbations.*

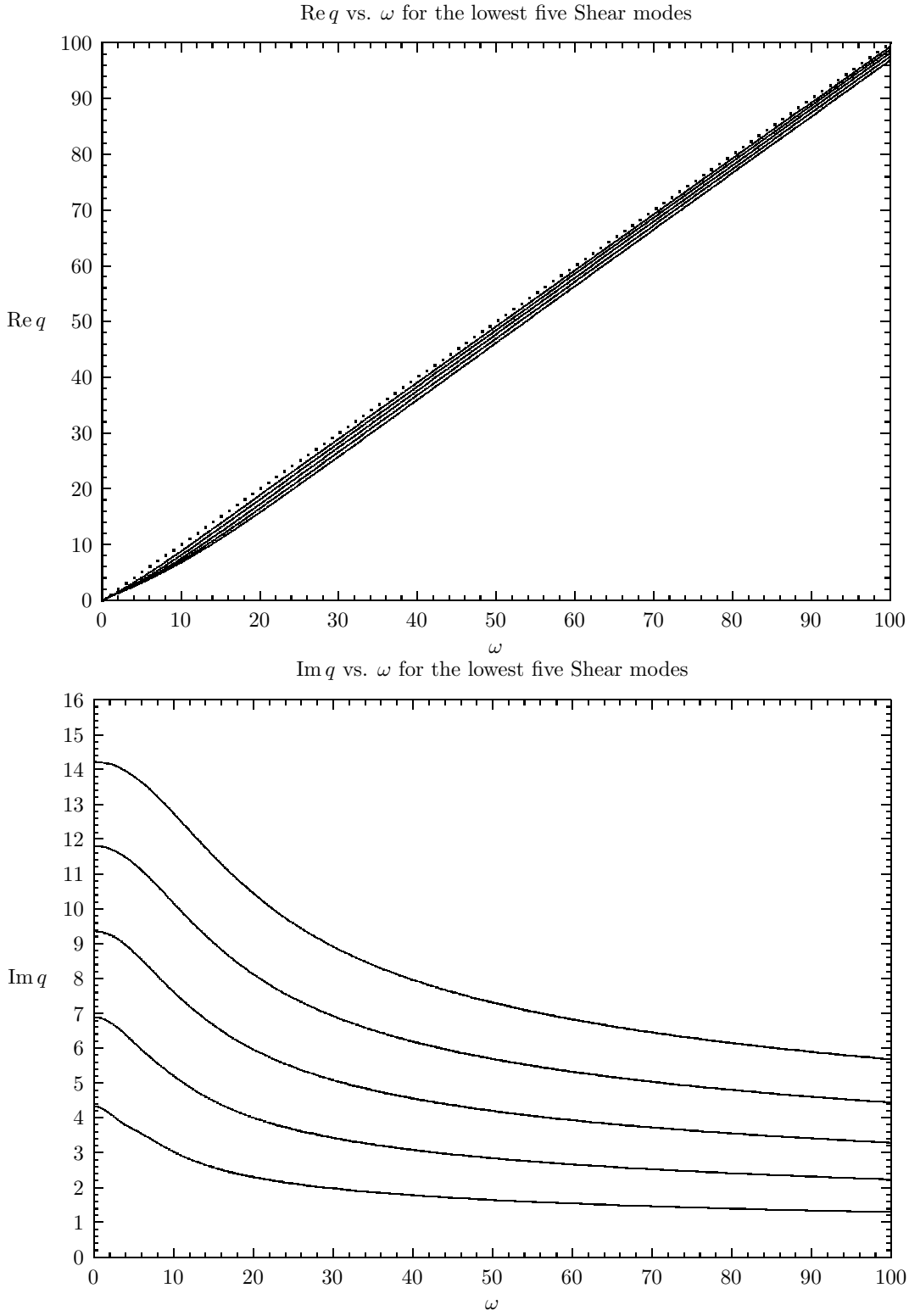

Figure 5.5: *The lowest five complex momentum eigenvalues above the diffuse mode for the shear channel perturbations.*

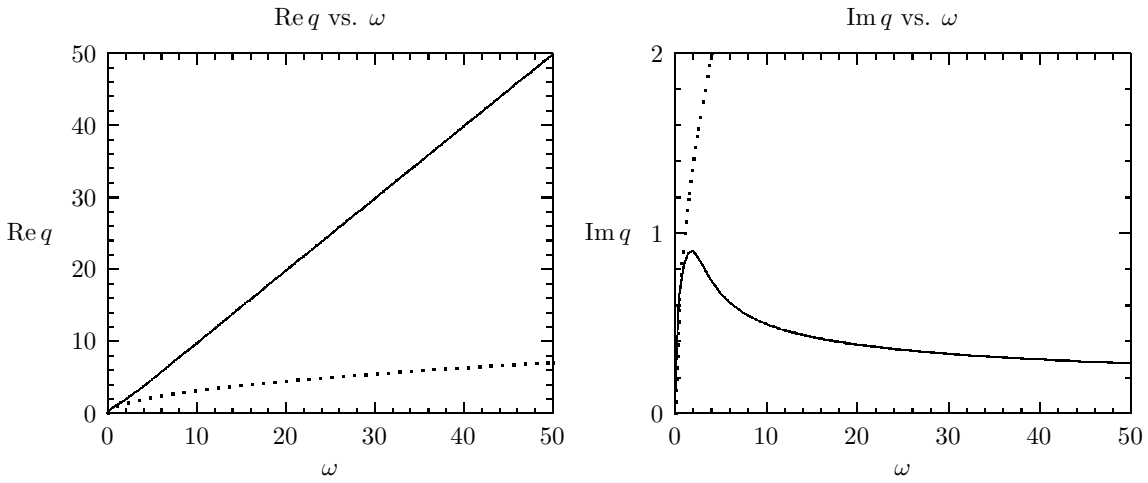

Figure 5.6: *Diffusion mode. The solid line represents the numerical solution while the dotted line is the analytic formula from hydrodynamical analysis.*

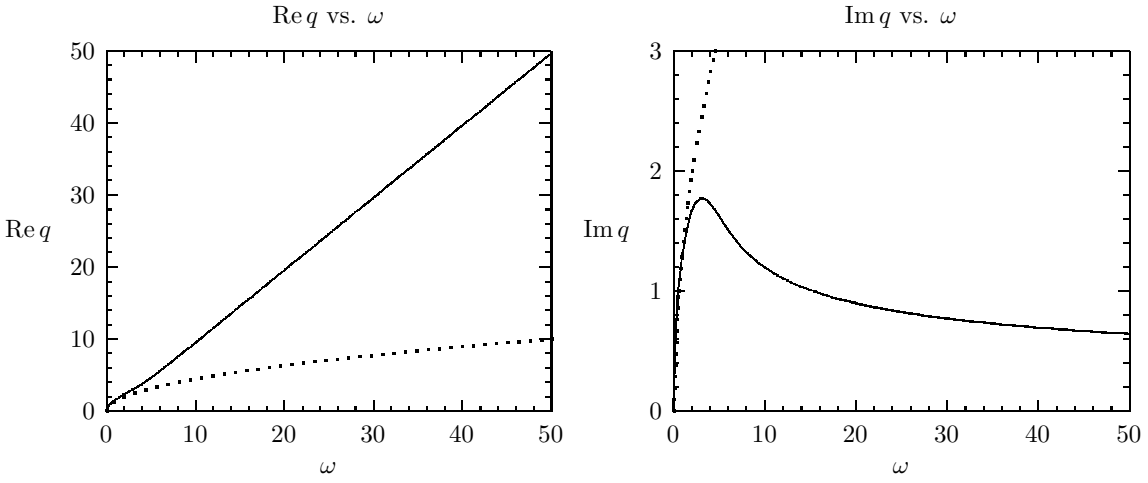

Figure 5.7: *Shear mode. The solid line represents the numerical solution while the dotted line is the analytic formula from hydrodynamical analysis.*

Chapter 6

Meson melting

In this chapter we will be concerned with the dissociation of mesons in a holographic quark-gluon plasma, but so far we have computed properties of gluon plasmas without fundamental matter. These only have particles in the adjoint representation since the $\mathcal{N}=4$ theory is supersymmetric, and all states in a given representation transform equally under the gauge group. However, this limitation can be overcome by giving the strings new places to end on, i.e. introducing a new set of different D-branes. From the point of view of the D3-branes, strings that stretch between them and the new ones represent particles in the fundamental representation of the SU(N) gauge group, i.e. "quarks". In our case, fundamental matter is modelled in this way through the embedding of D7-branes in $\mathrm{AdS}_5 \times \mathrm{S}^5$, where the holographic dictionary in section 2.1 relates the asymptotic behaviour at the conformal boundary of the D7-brane to the quark mass m_q and the quark bilinear condensate $\langle q\bar{q} \rangle$. So far these embeddings have been achieved only in a sort of quenched approximation, where the number of flavours N_f is much less than the number of colours N.[1] In the AdS context it means that the D7-branes are introduced as probe branes in the gravity background, ignoring their backreaction onto the geometry [126].[2]

To have finite temperature one would like to embed them in a black hole geometry. This was studied some time ago in [128,129], where it was found that there are two topologically distinct classes of embeddings. The first class, called the *Minkowski embedding,* stays everywhere outside the black hole whereas the second class, the *black hole embedding,* reaches down to the horizon such that the induced geometry on the brane is itself a black hole. Again focusing in our case, D7-brane embeddings in AdS black hole geometries were first considered in [130]. The two types of embeddings give rise to a first order phase transition where the value of the quark condensate jumps by a finite amount [131–135]; this was generalized to other types of backgrounds and D6- or D8-brane embeddings where there is a chiral U(1) or even a non-Abelian chiral symmetry, with the quark condensate as an order parameter for chiral symmetry breaking [136, 137].

The model we consider in this chapter, IIb supergravity on the AdS-Schwarzschild background with D7-branes partially wrapped on the S^5, is dual to $\mathcal{N}=4$ SU(N) gauge

[1] See however [118–125] for (very) recent and exciting progress beyond the quenched approximation.

[2] A recent review on adding fundamental matter to the gauge/gravity correspondence is [127].

theory at finite temperature T in the large N limit *with* one (or few) $\mathcal{N}=2$ hypermultiplets of mass m_q in the fundamental representation. Because of the underlying conformal symmetry we can either set T or m_q to one. Varying the mass of the quarks is therefore equivalent in this model to varying the temperature, i.e. lowering the mass is the same as rising the temperature. High values of the mass m_q correspond to Minkowski embeddings and low values to black hole embeddings. Therefore we can also think of the two kind of embeddings as being at low temperature (Minkowski embedding) or high temperature (black hole embedding).

Quark anti-quark bound states give rise to mesons. In the holographic dual high-spin mesons are modelled by spinning open strings ending on the probe branes. The decay of high-spin mesons has been studied in [138–141]. We will be concerned with the decay of low-spin mesons in this thesis. Low-spin mesons are represented by the small fluctuations around the equilibrium configuration of the D-brane world-volume. The spectrum of the D-brane fluctuations is very different for the two different classes of embeddings. In the case of the Minkowski embeddings there is a discrete spectrum of modes with eigenvalues that can be identified with the meson masses [126, 142]. Technically one imposes Dirichlet or Neumann boundary conditions for the fluctuations at the endpoints of the embedded brane. A wave travelling along the brane will then get reflected at the endpoint and this gives rise to a discrete set of eigenmodes and eigenfrequencies. If the brane embedding is however such that it touches the horizon, a wave travelling down the brane will eventually reach the horizon, fall through it and not come back again (see figure 6.1). In this case one has to impose purely infalling boundary conditions at the position of the horizon. These boundary conditions give rise to our old friends the *quasinormal modes,* but now on the brane!

Our interpretation of the quasinormal modes on the branes is as follows: they represent the late stages of the melting process of a meson inserted in a plasma at high temperature. The imaginary part of the quasinormal frequency gives the decay constant of the collective mode corresponding to the quasinormal mode in the plasma.[3] In other words: mesons built up of sufficiently light quarks (or equivalently at sufficiently high temperature) inserted in the plasma will melt just as an icecube melts in hot water. At a late stage the typical timescales of this melting process is given by the inverse of the imaginary part of the quasinormal frequencies. We could start for example with a Minkowski type D7-brane embedding in an excited state with a normal mode fluctuation on it representing a stable meson. If we now increase the temperature slowly the D7-brane with the normal mode on

[3]For the $\mathcal{N}=4$ theory, the analysis of refs. [99, 104, 105] shows that these poles can not be automatically given a quasiparticle interpretation. Our case is slightly different in that we are considering an $\mathcal{N}=2$ theory with an additional scale (the quark mass). Nevertheless we do not want to interpret the quasinormal modes as quasiparticles, solely as the collective modes representing the late time stages of the decay of a meson perturbation inserted in the plasma.

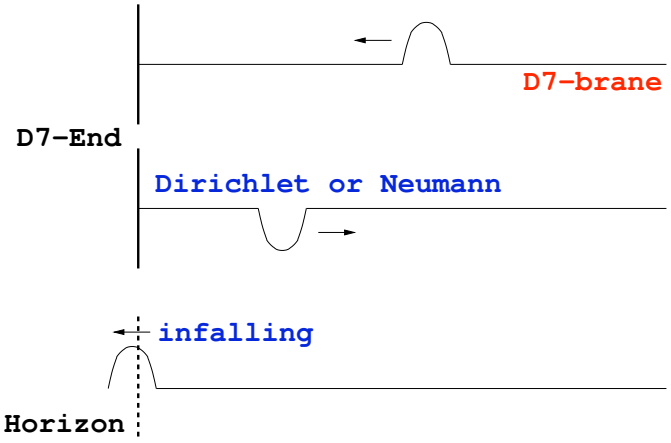

Figure 6.1: *Waves travelling down a D7-brane towards the interior of an* AdS*-black hole. For Minkowski embeddings the wave meets the end of the brane and is reflected there. This gives rise to normal modes and frequencies that are the holographic duals of low-spin mesons and their masses. In the case of the black hole embeddings the wave travels down the brane and through the horizon and simply never comes back. The fluctuation has to obey infalling boundary conditions giving rise to quasinormal modes.*

it will eventually enter the unstable regime and undergo the phase transition to the black hole embedding. Since the fluctuation is considered to be a small perturbation we can assume that the phase transition is basically unchanged from the one that takes place for the ground state of the D7-brane. After the phase transition, the additional energy present due to the meson perturbation will eventually drop into the black hole, with this decay process governed by the quasinormal modes. In this way we can study holographically the melting of the meson at high temperature.

In section 6.2 we first compute the quasinormal modes for the trivial embedding. This is the embedding that corresponds to massless quarks in the dual field theory, for which we present the first ten quasinormal frequencies computed with the Heun method. Then we go over to brane embeddings that correspond to massive quarks. The branes are bent for these embeddings and the embedding itself can be calculated only through numerical integration of a highly non-linear differential equation. This makes the computation of the quasinormal modes around these embeddings much more difficult. We employ two strategies. First we approximate the numerical embedding by an ansatz that is introduced in the differential equation of the fluctuations. We solve the equations at the boundary and at the horizon using series expansions with the right asymptotics. We use the horizon series to give initial values close to the horizon and integrate numerically towards the boundary. We then match the numerical solutions with the boundary series at a point close to the boundary and demand that the resulting solution is smooth. This fixes the quasinormal frequency. We were able to find the three lowest quasinormal modes for a

number of brane embeddings up to masses that actually lie already above the critical mass, where the phase transition to the Minkowski embeddings occurs.

We also employed a second method to find the quasinormal modes. This second method consists in converting the differential equation into a finite difference equation. In this approach one imposes the correct boundary conditions at the endpoints and uses an ansatz solution that is fed into the finite difference equation. An improvement to the ansatz solution y can be computed by demanding that $y + \Delta y$ fulfils the finite difference equations to first order, in an expansion in the correction Δy. This gives a new ansatz solution and therefore it amounts to a recursive algorithm that eventually relaxes to the correct quasinormal mode and frequency within a given accuracy goal. We describe this relaxation method in more detail in appendix A.5. In praxis, it turned out that the relaxation method worked well only for the lowest quasinormal mode. The agreement of the quasinormal frequencies as computed with the relaxation method or with the midpoint shooting algorithm is however excellent and typically of the order of

$$\frac{\left|\omega^{\text{shoot}} - \omega^{\text{relax}}\right|}{\left|\omega^{\text{shoot}} + \omega^{\text{relax}}\right|} \approx 10^{-4} \ ,$$

so we are confident that the quasinormal frequencies are accurate up to the quoted uncertainty, and thus we will state only the results from the midpoint shooting method.

In section 6.3 we briefly discuss the masses of the mesons that are represented by the fluctuations around the Minkowski embeddings and in section 6.4 we conclude.

6.1 D7-brane embeddings

As said in the introduction, there are two qualitatively different embeddings of the D7-brane in this AdS-Schwarzschild geometry. At large $m_q/(\sqrt{\lambda}T)$, with m_q the quark mass, the tension of the D7-brane pulls enough to maintain itself outside of the black hole, ending at a finite value $r_0 > r_+$ of the radial coordinate. This is the so-called *Minkowski* embedding. On the contrary, for small $m_q/(\sqrt{\lambda}T)$ the brane is forced to fall through the horizon, thus inheriting the black hole structure. In this case one calls it the *black hole* embedding.

In our discussion we use the metric in the $z = r_+/r$ coordinate (A.1), with the overall L^2 factor absorbed, and further write the S^5 element as

$$\mathrm{d}\Omega_5^2 = \mathrm{d}\theta^2 + \sin^2\theta\,\mathrm{d}\psi^2 + \cos^2\theta\,\mathrm{d}\Omega_3^2 \ , \tag{6.1}$$

where θ and ψ parametrise the transverse directions to the brane. The D7 wraps all of AdS_5 (either down to the horizon or not) and the S^3 inside the S^5. Its action is the DBI action

$$S_{\text{D7}} = T_{\text{D7}} \int \mathrm{d}^8\xi \, \sqrt{-\det \mathrm{P}[G]} \ , \tag{6.2}$$

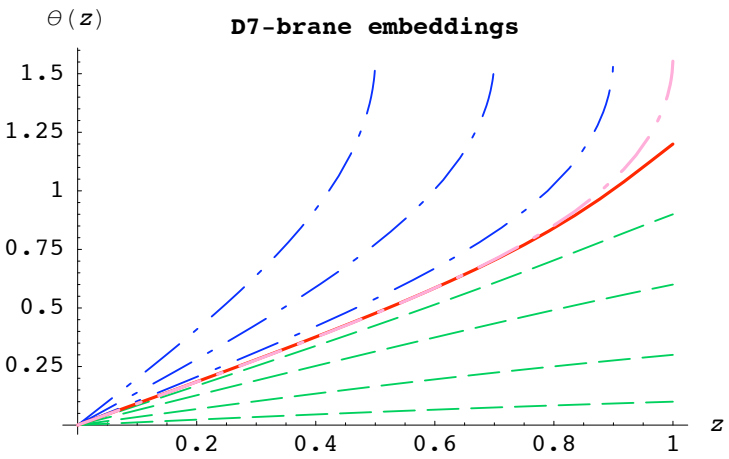

Figure 6.2: *Minkowski (thin and thick dot-dashed) and black hole (dashed) D7-brane embeddings. We have also plotted the critical embedding (solid).*

with P[G] the pullback of the bulk metric G onto the brane. The profile of the embedding is characterised by its shape in the transverse coordinates. We will consider embeddings that have a simple profile characterised by the dependence of the S^3 radius on the $AdS_5 \times S^5$ radial direction ($\theta(z), \psi = \text{const.}$). Absorbing the tension and volume of the S^3 into the normalization, the action is

$$S_{D7} = \int dz \, \frac{\cos^3\theta(z)}{z^5} \sqrt{1 + z^2(1-z^4)\,\theta'(z)^2} \ . \tag{6.3}$$

The embedding is obtained by solving the equation of motion for $\theta(z)$, which after some simplifications is

$$\begin{aligned} 0 \ &= \ 3\sin\theta(z)\left[-1 + z^2\,(-1+z^4)\,\theta'(z)^2\right] \\ &\quad + z\cos\theta(z)\Big[(3+z^4)\,\theta'(z) + 2z^2\,(1-z^4)\,(2-z^4)\,\theta'(z)^3 + z(-1+z^4)\,\theta''(z)\Big] \ . \end{aligned} \tag{6.4}$$

For the Minkowski embedding one demands the brane to end outside the black hole, so the S^3 has to shrink to zero size at z_0. Therefore one imposes $\theta(z_0) = \pi/2$. The second boundary condition comes from the requirement of a smooth ending without conical deficit. This imposes that $\theta'(z_0) \to \infty$ which we simulate in the numerical integration of (6.4) by setting the derivative to 10^4. In the black hole case, one sets the angle to some value $\theta(1) = \theta_0$ at the horizon $z = 1$, whereas the second boundary condition is $\theta'(1) = (3/4)\tan\theta_0$. This can be seen by demanding the embedding to be smooth at the horizon.[4] Figure 6.2 shows the two embeddings for different values of the boundary conditions.

[4]This boundary condition translates to Neumann boundary conditions when Fefferman–Graham coordinates are used as in [135].

The solid curve in figure 6.2 represents the critical embedding which is associated to the fundamental phase transition of the theory. In order to compute the critical embedding one needs to compute separately the free energy of the Minkowski and black hole embeddings which correspond to the *same* quark mass, given by the derivative at the boundary. These free energies need to be renormalised,[5] where a holographic renormalization scheme may be used [143–145]. For this particular setup this was done in [146]. The critical embedding corresponds to the configuration where the difference of free energies changes sign, with the free energy for the embedding given by the action (6.3), and with a discontinuity jump of the quark condensate.

The asymptotic expansion of the embedding

$$\theta(z) = \Theta_0\, z + \Theta_2\, z^3 + \mathcal{O}(z^5) + \dots \ , \tag{6.5}$$

allows to obtain the quark mass

$$m_q = \frac{1}{2}\,\Theta_0 \sqrt{\lambda}\, T \equiv \Theta_0\, \Delta m(T) \ , \tag{6.6}$$

where we introduce the thermal rest mass factor $\Delta m(T) := \frac{1}{2}\sqrt{\lambda}\, T$, and also the condensate through [135][6]

$$\frac{\langle q\bar{q}\,\rangle}{\pi^2 T^2 \Delta m(T)} = \lim_{\epsilon\to 0} \frac{1}{\epsilon^3 \sqrt{-\det \mathrm{P}[G]\Big|_{z=\epsilon}}} \frac{\delta S_{\text{reg.}}}{\delta\, \theta(\epsilon)} = -4\Theta_2 + \frac{2}{3}(\Theta_0)^3 \ . \tag{6.7}$$

This computation has been done in a variety of papers [130, 131, 133]. The value of the quark mass for the critical embedding is $m_{\text{crit.}} \approx 0.92\, \Delta m(T)$. The physical situation corresponds to a discontinuous jump from a black hole embedding to a Minkowski one. It was also studied recently in [135] in the case of a curved boundary $\mathrm{S}^1 \times \mathrm{S}^3$, where the deconfinement transition of the dual gauge theory was also analysed with similar results.

6.2 Quasinormal modes on the flavour brane

According to section 2.2, the black hole geometry corresponds to a strongly interacting quark-gluon plasma. From the point of view of mesons, there has been a deconfinement phase transition so they no longer provide a good description of fundamental degrees of freedom, though we still may introduce a one of them in the plasma with an associated finite lifetime.

The spectrum of mesons turns out to be real and continous, so the associated two-point correlation functions will show a branch cut along the real axis pointing at the

[5] One introduces an effective cutoff integrating down to $z = \epsilon \sim 0$, and later renormalises $\epsilon \to 0$.

[6] We have used a definition of the mass that differs by a factor $\sqrt{2}$ from the one given in [135].

deconfinement of mesons. As we know the poles of such functions can be the quasinormal frequencies; those vanishing with the spatial momentum will correspond to wide and slow fluctuations thus describing the hydrodynamical properties of the plasma. Other quasinormal modes will also describe dissipation processes of the mesons. In principle, quasinormal modes could describe unstable bound states of quarks in the plasma, with the same quantum numbers as the low temperature analog mesons and a finite lifetime. This will be true if distinct resonances appear in the spectral function, with a small enough width and an appropriate dispersion relation $\omega(\mathbf{q})$ so they can be interpreted as quasiparticles. In [99] it is shown that in $\mathcal{N}=4$ plasma the quasinormal poles actually do not lead to resonances and that the high frequency behaviour is dominated by the underlying conformal symmetry. The case studied here is slightly different because for non-zero quark mass, the theory is already non-conformal and the structure of mesonic Green's functions is given by an infinite set of discrete poles localized to the real axis, that we can identify with the stable spectrum of mesons. Also the fact that the plasma is strongly coupled for quarks and gluons does not affect mesons, because their interactions decrease at least as $\sim 1/N$ in the large N limit, so from their point of view the plasma is a weakly coupled gas. This is confirmed by the zero drag force computed for mesons [138–141].

However, the relation between hypothetical bound states in the plasma and the actual mesons in the low temperature phase is not completely clear, since the wavefunction of a meson entering the plasma will probaly suffer strong non-linear effects before diluting. On the other hand, if we consider a single meson or a small number, the process of melting can be seen as a small fluctuation losing energy into the plasma and should be described by linear response theory and the related quasinormal modes.[7]

In the case that interests us, we introduced a set of D7 probes in an $\mathrm{AdS}_5 \times \mathrm{S}^5$ black hole geometry. The fields living on the branes are gauge fields and two scalar fields θ and ψ, parameterising the directions transverse to the brane. According to the correspondence, we can associate them to meson operators in the dual theory. From now on, we will be interested only in fluctuations of θ, a scalar of mass squared $m^2 = -3$, that in the dual theory maps to a meson operator of dimension $\Delta = 3$, a quark bilinear. The normalizable modes of this field should correspond to scalar meson states in the dual theory.

From the two possible situations, let us consider D7-brane embeddings that fall into the black hole. Then, the induced metric on the branes has a horizon and there will be quasinormal modes in the spectrum of fluctuations of the brane. Since the black hole brane configuration corresponds to a deconfined situation for quarks, the meson spectrum associated to normal modes will be continuous [134, 136].

For simplicity, we will consider only singlet states on S^3, and since we are interested

[7] Remember that we are considering low-spin mesons only.

only in the mass and decay width, we will consider space-independent perturbations. However, it could be an interesting issue to see the effect of non-zero momentum with respect to the plasma rest frame on bound states. On general grounds, we expect that the states will be more stable.

Let us write the coordinate θ as $\theta(z,t) = \theta_0(z) + \vartheta(z,t)$, that is, embedding plus fluctuations over it. The action for the fluctuations is the DBI action of the brane

$$S_{\rm D7} \simeq \int \mathrm{d}t\,\mathrm{d}z\,\frac{\cos^3(\theta_0(z)+\vartheta)}{z^5}\sqrt{1-\frac{z^2}{1-z^4}(\partial_t\vartheta)^2+z^2(1-z^4)(\theta_0'(z)+\partial_z\vartheta)^2}\ . \tag{6.8}$$

If we consider small fluctuations, we can use the linearised equations of motion. Using $\vartheta(z,t) = \mathrm{e}^{-i\omega t}\vartheta(z)$, we are left with a second-order differential equation in z

$$\vartheta''(z) + A_1(z)\,\vartheta'(z) + (B(z)^2\,\omega^2 + A_0(z))\,\vartheta(z) = 0\ , \tag{6.9}$$

where using

$$s(z) = 1 + z^2(1-z^4)\,\theta_0'(z)^2\ , \tag{6.10}$$

the coefficients of the differential equation are

$$B(z) = \sqrt{s(z)}\,(1-z^4)^{-1}\ , \tag{6.11a}$$

$$A_0(z) = s(z)\frac{3\sec^2\theta_0(z)}{z^2(1-z^4)}\ , \tag{6.11b}$$

$$A_1(z) = -\frac{3+z^4}{z(1-z^4)} + 6\theta_0'(z)\Big(\tan\theta_0(z) - z(2-z^4)\theta_0'(z)\Big)\ , \tag{6.11c}$$

where we have used the equations of motion of the embedding (6.4) to eliminate $\theta_0''(z)$. As we noted in section 3.1, if $\vartheta(z)$ is a solution for some frequency $\omega = \omega^{\rm R} - i\omega^{\rm I}$, then $\vartheta^*(z)$ is also a solution for a frequency $\widetilde{\omega} = -\omega^*$. This $\mathbf{Z}_2$ symmetry allows to form real combinations of quasinormal modes, that will be true geometric deformations of the brane.

Close to the boundary of AdS ($z \to 0^+$), the differential equation is approximately

$$\vartheta''(z) - \frac{3}{z}\,\vartheta'(z) + \frac{3}{z^2}\,\vartheta(z) = 0\ , \tag{6.12}$$

with solutions $\vartheta(z) \sim a\,z + b\,z^3$. According to the dictionary of the correspondence, we should set $a = 0$ in order to study the spectrum of states. Otherwise, we will be introducing couplings for meson operators in the Lagrangian. Notice that the behaviour is universal for any embedding and frequency ω.

Close to the horizon ($z \to 1^-$), the differential equation becomes

$$\vartheta''(z) + \frac{1}{z-1}\,\vartheta'(z) + \frac{\omega^2}{16(z-1)^2}\,\vartheta(z) = 0\ , \tag{6.13}$$

with solutions $\vartheta(z) \sim a'(1-z)^{i\omega/4} + b'(1-z)^{-i\omega/4}$. In this case, we will impose ingoing boundary conditions $a' = 0$. The asymptotic behaviour is also universal for any embedding.

Equation (6.9) can be transformed into a Schrödinger equation, useful to derive analytic properties of the frequencies [147–149]. Using $\vartheta(z) = \sigma(z) f(z)$ with

$$\frac{\sigma'(z)}{\sigma(z)} = -\frac{1}{2}\left(A_1(z) + \frac{B'(z)}{B(z)}\right) , \tag{6.14}$$

the equation for quasinormal modes is

$$\left(\frac{1}{B(z)}\frac{\mathrm{d}}{\mathrm{d}z}\left(\frac{1}{B(z)}\frac{\mathrm{d}}{\mathrm{d}z}\right) + \omega^2 - V(z)\right) f(z) = 0 , \tag{6.15}$$

so the Schrödinger equation is recovered after changing variables to the 'tortoise' coordinate $\mathrm{d}z_* = \sqrt{s(z)}\mathrm{d}z/(1-z^4)$, that is defined such that the horizon is at $z_* \to \infty$. The potential is

$$V(z) = -\frac{(1-z^4)^2}{s(z)}\left(A_0(z) + A_1(z)\frac{\sigma'(z)}{\sigma(z)} + \left(\frac{\sigma'(z)}{\sigma(z)}\right)^2 + \left(\frac{\sigma'(z)}{\sigma(z)}\right)'\right) . \tag{6.16}$$

Consider now solutions that fall into the horizon, which in the z_* coordinate are $f(z_*) = \exp(+i\omega z_*)\,\psi(z_*)$, multiply equation (6.15) by the conjugate solution $\psi^*(z_*)$ and integrate between the boundary and the horizon

$$\int_{z_*^b}^{\infty} \mathrm{d}z_* \left(-\psi^*(z_*)\,\psi''(z_*) - 2i\omega\,\psi^*(z_*)\,\psi'(z_*) + V(z_*)|\psi(z_*)|^2\right) = 0 . \tag{6.17}$$

The solution $\psi(z_*)$ should vanish at the boundary and go to a constant at the horizon. The second-derivative term can be integrated by parts giving a result proportional to $|\psi'(z_*)|^2$. Taking the imaginary part of this equation and integrating by parts we find the relation

$$2i\mathrm{Im}\,\omega \int_{z_*^b}^{\infty} \mathrm{d}z_*\,\psi^*(z_*)\,\psi'(z_*) = -\omega^*|\psi(\infty)|^2 , \tag{6.18}$$

that can be plugged back into the original equation

$$\int_{z_*^b}^{\infty} \mathrm{d}z_* \left(|\psi'(z_*)|^2 + V(z_*)\,|\psi(z_*)|^2\right) = -\frac{|\omega|^2\,|\psi(\infty)|^2}{\mathrm{Im}\,\omega} . \tag{6.19}$$

If the left hand side is positive, the imaginary part of the frequency must be negative. This depends on the value of the potential. The potential (6.16) is non-negative between the boundary $z = 0$ and the horizon $z = 1$ for the massless case $\theta_0(z) = 0$. For the massive case we found numerically that the potential is non-negative up to values $\theta_0(1) \sim 0.83$. Above this value the potential starts developing a well close to the horizon, so in principle there could be unstable modes of positive imaginary frequency. The numerical plots of the potential are in figure 6.3.

Other qualitative properties of the frequencies can also be deduced from the shape of the potential. The frequencies of brane fluctuations are given by the energy spectrum of the

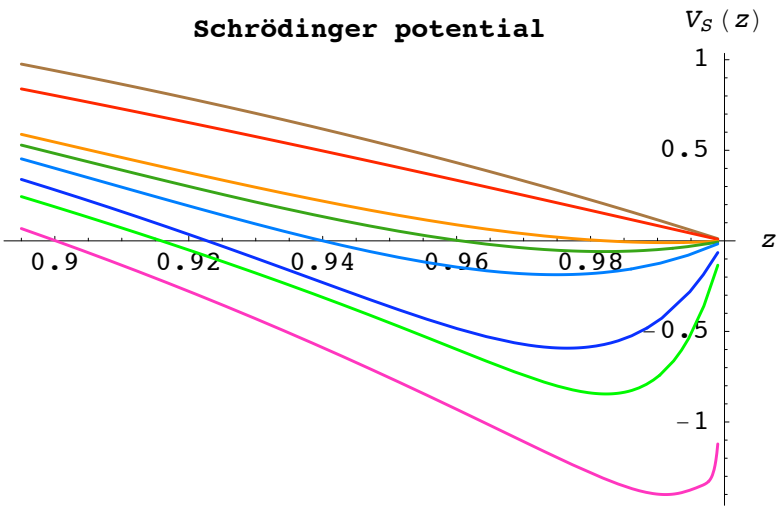

Figure 6.3: *Schrödinger potential close to the horizon for different horizon embeddings, corresponding to* $\theta_0(1) = 0.1, 0.5, 0.83, 0.9, 1.0, 1.2, 1.3$ *and* 1.5*. As* $\theta_0(1)$ *increases, the potential develops a negative-valued well.*

Schrödinger potential. For Minkowski embeddings, the potential is an infinite potential well, so the spectrum is real and discrete. For black hole embeddings, the potential is qualitatively the same close to the boundary, but it vanishes at the horizon. In both cases the potential develops a negative well close to the horizon as the embedding approaches the critical one separating Minkowski and black hole topologies. For Minkowski embeddings, the well starts developing for $z_0 > 0.955$. If the well is deep enough, we expect that negative-energy bound states will appear. Bound states correspond to modes of tachyonic mass on Minkowski slices [150, 151] and they are probably signalling an instability of the brane. We checked the presence of no tachyons up to $z_0 = 0.99$. At $z_0 = 0.999$ we find that there is a single tachyon with $\omega \simeq 0.69\, i$, thus a true instability of the D-brane embedding. For black hole embeddings, the instability appears between $\theta_0(1) = 1.29$ and $\theta_0(1) = 1.295$, where we find a mode with frequency $\omega \simeq 0.0014\, i$. Therefore, the first order transition occurs before these instabilities are present. Near-critical embeddings have been shown to be thermodynamically unstable [152], both instabilities seem to be related because the appearance of tachyonic modes coincide with the onset of the thermodynamical instability, in agreement with [153, 154].

Massless case. We will consider first the simplest case of massless quarks, where the D7 embedding is trivial $\theta_0(z) = 0$. The frequencies of the massless embedding can then be used as a starting point for the search of quasinormal frequencies in the massive case. It is more convenient now to change our coordinate to $x = 1 - z^2$. The equation takes the simpler form

$$\vartheta''(x)+\frac{1+(1-x)^2}{x(1-x)(2-x)}\,\vartheta'(x)+\left(\frac{\omega^2}{4x^2(1-x)(2-x)^2}+\frac{3}{4x(1-x)^2(2-x)}\right)\vartheta(x)=0\ , \tag{6.20}$$

with four regular singularities $x=0,1,2,\infty$, with exponents $\{i\omega/4,-i\omega/4\}$, $\{1/2,3/2\}$, $\{\omega/4,-\omega/4\}$, $\{0,0\}$. Therefore, it is a Heun equation and we can follow the analysis described in [94] and used by us in the preceding chapter for the absorption lengths, now to compute the quasinormal frequencies.

Using the transformation

$$\vartheta(x)=x^{-i\omega/4}(x-1)^{3/2}(x-2)^{-\omega/4}\,y(x)\ , \tag{6.21}$$

we can write the equation in the standard form for a Heun equation

$$y''(x)+\left(\frac{\gamma}{x}+\frac{\delta}{x-1}+\frac{\epsilon}{x-2}\right)y'(x)+\frac{\alpha\beta x-Q}{x(x-1)(x-2)}\,y(x)=0\ , \tag{6.22}$$

with parameters

$$\alpha \;=\; \beta=\frac{3}{2}-\frac{\omega}{4}(1+i)\ ,\quad \gamma=1-i\frac{\omega}{2}\ ,\quad \delta=2\ ,\quad \epsilon=1-\frac{\omega}{2}\ , \tag{6.23}$$

$$Q \;=\; \frac{9}{4}-\frac{\omega}{4}(1+5i)-\frac{\omega^2}{8}(2-i)\ . \tag{6.24}$$

Quasinormal modes correspond to solutions of this equation defined in the interval $[0,1]$ with boundary conditions $y(0)=y(1)=1$, that select the appropriate normalizable and ingoing behaviour of the solution. Back to the Heun method, using formula (5.13), we can easily compute numerically the quasinormal frequencies with high precision, in a totally analogous fashion as for the absorption lengths. It should be noted that in this case we do not encounter problems with false frequencies. For the first ten modes these are compiled in table 6.1. Higher modes $k\gg 1$ seem to have the asymptotic behaviour

$$\omega_k\simeq 1.219-0.779i+(2k-1)(1-i)\ . \tag{6.25}$$

Massive case. When we consider massive quarks, associated to a non-trivial D7 profile $\theta_0(1)\neq 0$, the situation gets much more involved. First of all, we only know the embedding numerically, and second, we know that it is not an analytic function, since its expansion close to AdS boundary involves logarithmic terms. So we have to use mainly a numerical approach to compute the quasinormal frequencies.

We use a shooting method to compute the frequencies. We approximate our numerical embeddings by a power expansion in order to keep computation time bounded. This is our main source of error, typically we trust our results up to the fourth decimal. Close to the

k	Re (ω_k)	Im (ω_k)
1	2.1988	−1.7595
2	4.2119	−3.7749
3	6.2155	−5.7773
4	8.2172	−7.7781
5	10.2181	−9.7785
6	12.2186	−11.7787
7	14.2180	−13.7788
8	16.2193	−15.7789
9	18.2195	−17.7790
10	20.2183	−19.7790

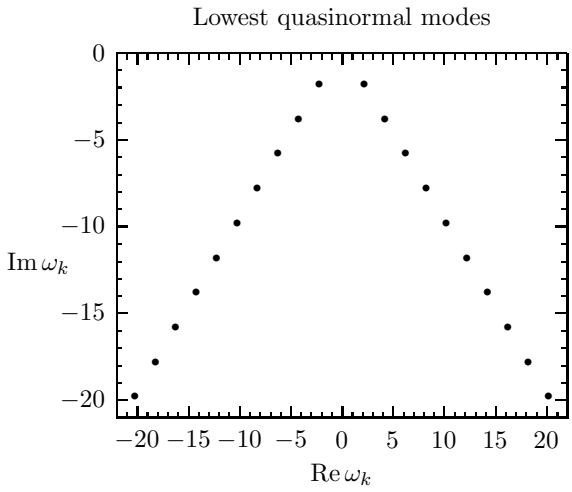

Table 6.1: *Quasinormal frequencies for massless quarks using the convergence method ($n = 200$ for $k < 10$ and $n = 250$ for $k = 10$).*

singular points we approximate the modes by a series expansion with the right behaviour, as z^3 at the AdS boundary ($z = 0$) and like $(1 - z)^{-i\omega/4}$ at the horizon ($z = 1$). We use then the series expansion at the horizon to give initial values for the numerical solution. Close to the boundary, we try to match smoothly the numerical solution with the series expansion at $z = 0$. The matching points between the numerical solution and the series expansions are selected so that the error in the differential equation coming from the series is less than 10^{-8}, all values lying in the intervals $[0.0375, 0.15]$ and $[0.85, 0.9625]$.

The matching can be done only for discrete values of the frequency that we find exploring the complex ω plane. The frequencies that we have found for the massless case are very useful to give a starting point for our search, and we also use them to check the method for the massless case. Since the method becomes quite expensive in terms of CPU time for higher modes, especially when we approach the critical embedding $\theta_0(1) = \pi/2$, we have limited to the first three modes. The results can be found in tables 6.2 and 6.3 and in figure 6.4. We see that the evolution drives the quasinormal frequencies from their values in the massless embedding toward values closer to the real axis. Unfortunately, we are not able to reach the limiting embedding numerically, so we cannot confirm what is the endpoint of the evolution. It would be interesting to make an improved numerical analysis or an analytic computation of quasinormal frequencies for near-limiting embeddings to address this issue.

We have checked the results using the relaxation method. In this method we use the numerical values of the embedding, lowering significantly this source of error. We find that the results for the first mode have a very good agreement; typically the absolute relative error in the frequencies is of order 10^{-4}, as quoted in the introduction to this chapter.

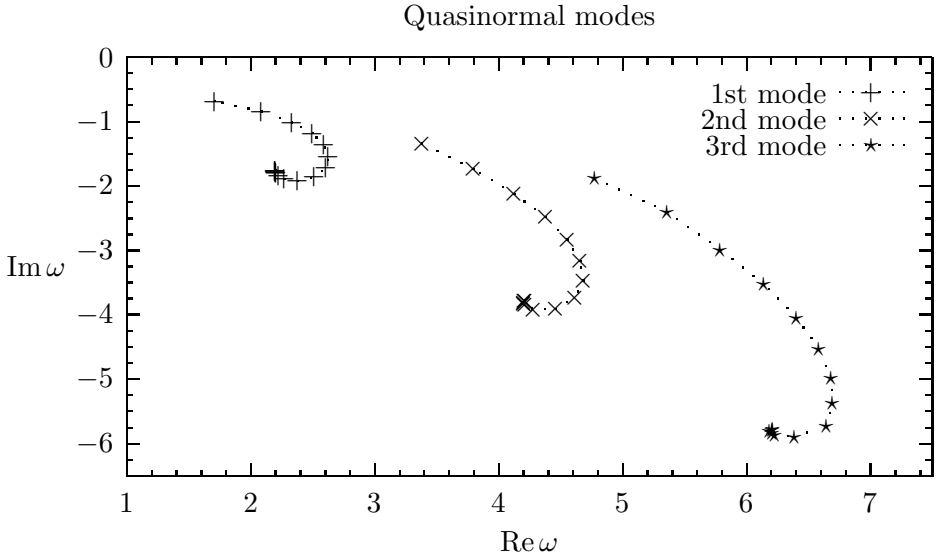

Figure 6.4: *Evolution of the first three quasinormal frequencies in the complex plane as we change the embedding. All of them show the same behaviour when θ_0 is increased: firstly they go to the right to reach a returning point and start moving to the left decreasing their imaginary part.*

$\theta_0(1)$	Re (ω_1)	Im (ω_1)
0.00	2.1988	−1.7595
0.10	2.1989	−1.7636
0.20	2.1999	−1.7765
0.25	2.2016	−1.7868
0.30	2.2051	−1.8001
0.40	2.2225	−1.8371
0.50	2.2712	−1.8855
0.60	2.3785	−1.9133
0.70	2.5153	−1.8546
0.80	2.6057	−1.7172
0.90	2.6299	−1.5454
1.00	2.5935	−1.3665
1.10	2.4972	−1.1867
1.20	2.3342	−1.0135
1.30	2.0866	−0.8488
1.40	1.7078	−0.6846

$\theta_0(1)$	Re (ω_2)	Im (ω_2)
0.00	4.2119	−3.7749
0.10	4.2090	−3.7808
0.20	4.2035	−3.8020
0.25	4.2057	−3.8218
0.30	4.2136	−3.8477
0.40	4.2818	−3.9122
0.50	4.4607	−3.9061
0.60	4.6172	−3.7287
0.70	4.6822	−3.4663
0.80	4.6585	−3.1643
0.90	4.5558	−2.8370
1.00	4.3784	−2.4866
1.10	4.1243	−2.1242
1.20	3.7945	−1.7345
1.30	3.3796	−1.3415

Table 6.2: *(Left) first and (right) second quasinormal frequencies for different D7 embeddings.*

$\theta_0(1)$	Re (ω_3)	Im (ω_3)
0.00	6.2155	−5.7773
0.10	6.2064	−5.7813
0.20	6.1851	−5.8052
0.25	6.2067	−5.8341
0.30	6.2299	−5.8666
0.40	6.3867	−5.8924
0.50	6.6466	−5.7291
0.60	6.6925	−5.3760
0.70	6.6829	−4.9753
0.80	6.5846	−4.5276
0.90	6.4048	−4.0423
1.00	6.1417	−3.5153
1.10	5.7917	−2.9881
1.20	5.3629	−2.4019
1.30	4.7783	−1.8763

Table 6.3: *Third quasinormal frequencies for different D7 embeddings.*

6.3 Meson masses and lifetimes

We have identified small fluctuations of D7-probe branes with the low energy spectrum of mesons. In the zero temperature case ($T = 0$), the spectrum of mesons is given by regular and normalizable modes on the brane. The bare mass of the quarks m_q is identified with the asymptotic properties of the embedding, as in (6.6). If the mass is finite, then the embedding ends at a finite value of the radial coordinate, providing an IR cutoff for the modes on the brane. The spectrum is discrete with a mass gap $M \sim m_q/\sqrt{\lambda}$ and grows linearly [126, 142]. If the bare mass is zero, then the induced metric on the brane is conformal $AdS_5 \times S^3$ and the spectrum becomes continuous.

For Minkowski embeddings, the spectrum will be similar to the zero temperature case for $m_q/\Delta m(T) \gg 1$. We show the first modes of the meson spectrum for several embeddings in table 6.4 and figure 6.5, notice that the mass gap grows linearly with the quark mass for embeddings with $m_q/\Delta m(T) > 1$.

Below the critical mass $m_q \simeq 0.92\,\Delta m(T)$, there can be a first or a second order transition to a black hole embedding [130, 131, 133–135, 154, 155]. Free energy arguments show that the branch of black hole embeddings reached by the first order transition will dominate. However, the second order transition is interesting because its properties are similar to type II critical collapse of black holes and black hole/black string merger tran-

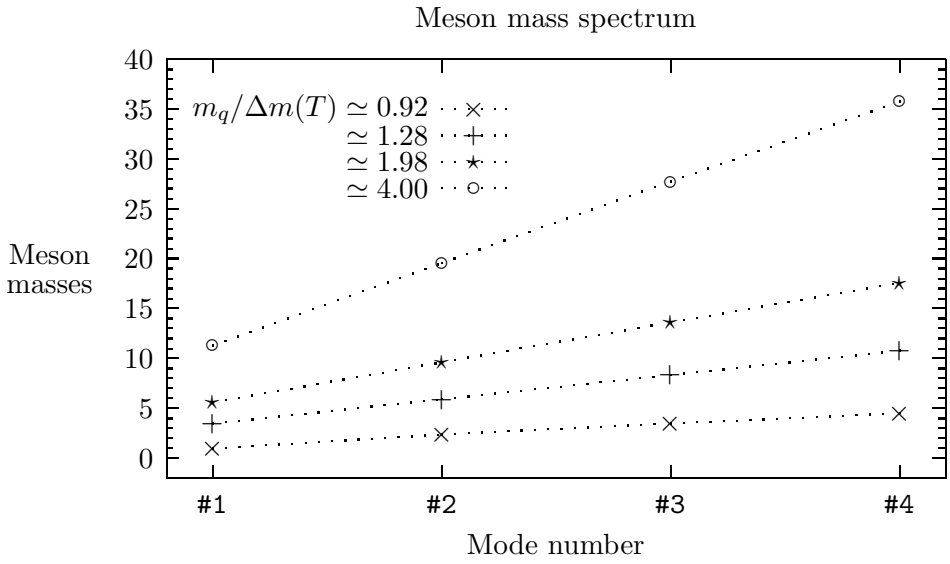

Figure 6.5: *First modes of the meson spectrum for Minkowski embeddings ending at* $z_0 = 0.25, 0.5, 0.75, 0.99$. *We observe that the spectrum grows linearly and the mass gap increases with the distance of the embedding to the horizon* $z_+ = 1$.

sitions [134, 155]. In black hole embeddings, the theory is in a deconfined phase and the spectrum of mesons is continuous. From the geometric point of view, this is due to the presence of a horizon.

$m_q/\Delta m(T)$	1	2	3	4
0.91784	0.9589	2.3411	3.4388	4.5087
1.27999	3.4357	5.9163	8.3647	10.7981
1.98432	5.5717	9.6391	13.6312	17.5994
3.99805	11.3081	19.5905	27.7128	35.7863

Table 6.4: *First meson masses in temperature units for different quark masses in Minkowski embeddings.*

Let us consider the results of the previous section. The mass and the width of quasinormal modes are roughly proportional, and proportional to the temperature (see fig. 6.6). As we increase the quark mass there is some change, close to the critical value where the two branches of black hole embeddings merge. The width decreases appreciably, specially for higher modes, while the mass does not change as much. In any case, before the first order phase transition the mass and the width are of the same order, which makes a quasiparticle interpretation unlikely.

The melting is therefore characterized by the temperature, showing little dependence on the quark mass *after the transition*. This implies that mesons made of light quarks will start melting at lower temperatures but will have longer lifetimes just after the transition.

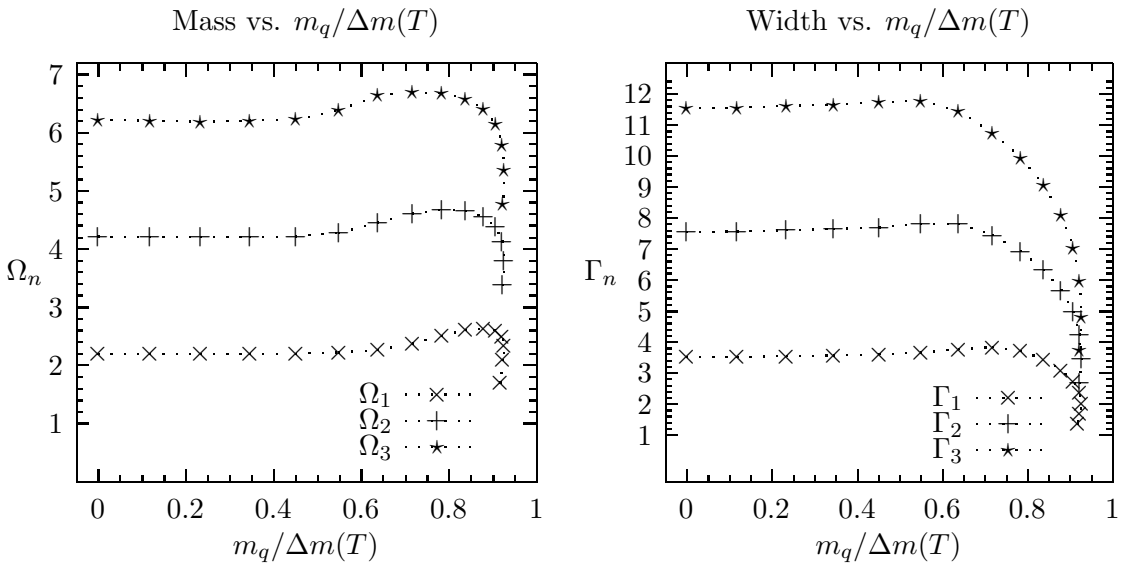

Figure 6.6: *(Left) Quasinormal masses in temperature units for the first three modes as a function of the bare quark masses, and (right) quasinormal widths in temperature units for the first three modes as a function of the bare quark masses. We have defined* $\omega_n := \Omega_n - i\,\Gamma_n/2$.

Considering mesons made of quarks of fixed mass, heavier mesons with the same quantum numbers (in our case, zero spin mesons associated to the scalar operator $\bar{q}q$) will initially decay through higher quasinormal modes, so they will lose energy faster. Then, a heavy meson that goes through a plasma region will usually emerge as a lower mass state. If the meson does not emerge, then the decay is dominated by the lowest quasinormal mode at large times and becomes universal, it is no longer possible to distinguish the original state. This means that any scattering process will in principle increase the energy and entropy of the plasma, as we expect from a dissipative medium.

6.4 Conclusions

We have proposed a holographic picture (of the late stages) of the melting process of low-spin mesons in the quark-gluon plasma. The important ingredient are D7-brane embeddings in AdS-black hole backgrounds that do reach down to the horizon. The induced metric on the world-volume of these D7-branes is itself a black hole and therefore it makes sense to compute the quasinormal modes of the brane fluctuations. These modes describe the dissipation of the energy of mesonic excitations by the plasma, in particular the melting of mesons. One important point is that this process of melting in the holographic plasma is only available for mesons built out of quarks with masses up to $m_q = 0.92\sqrt{\lambda}\,T/2$, where T is the plasma temperature and λ is the 't Hooft coupling. Heavier quarks are represented by D7-branes with no horizon on their world-volume and therefore have stable

meson excitations.

The melting of quarkonium states is of high importance in the physics of the quark-gluon plasma. It has long been regarded to be one of the cleanest signatures of plasma formation. In particular, quarkonium states such as the J/ψ meson are expected to melt in the quark-gluon plasma and therefore the abundance of these particles measured in processes where quark-gluon plasma formation takes place should drop significantly if compared to nuclear collisions without plasma formation.

Although the model we have considered here is quite far from QCD it is still interesting to have a look to this problem from our perspective of holographic meson melting. We found that the melting process takes place only for quarkonium states built out of quarks with masses of at most the order of the temperature of the plasma. The mass of the charm quark is $m_c \approx 1.4$ GeV and the RHIC temperatures is $T_{\text{RHIC}} \lessapprox 300$ MeV. AdS predicts critical mass to temperature ratios of $1-2$ if we use the recent estimates on how to relate $5.5 < \lambda < 6\pi$ to QCD [156]. It is quite interesting that very recently meson melting has been considered in a real time approach in Hard Thermal Loop resummed perturbation theory [157]. There the authors found an imaginary part in the static quark anti-quark potential giving rise to a decay width and that this decay width can be ignored for quarks heavier that $m_q = 12\pi T/g^2$. One is tempted to speculate that this is the weak coupling QCD analog of the holographic value $m_q = 0.92\sqrt{\lambda}T/2$ and that there exists an interpolating function $f(\lambda)$ such that $m_q = f(\lambda)T$, where $f(\lambda) \approx \sqrt{\lambda}$ at strong coupling and $f(\lambda) \approx 1/\lambda$ at weak coupling.

The biggest drawback of the AdS-model is that the background corresponds to plasmas made up only of particles in the adjoint representation. Although in a background with dynamical quarks included one still expects heavy quarks being reasonably well modelled by D-brane embeddings the presence of fundamental quarks in the deconfined plasma might change the dissociation rates even for heavy quarks in a drastic way. In any case, the quasinormal modes on D-branes embedded in gravity duals of gauge theories offer a unique way of studying quarkonium dissociation in a holographic way.

It is of high interest to apply our approach to meson melting also to other models, such as models with non-Abelian chiral symmetries [137] or the phenomenological holographic models of QCD developed in [158, 159]. In view of the above mentioned problem of J/ψ suppression it would be of extreme interest to have a phenomenological holographic QCD model that includes heavy flavours such as the charm quark.

In this thesis we have only considered modes with vanishing momentum on the S^3 as well as on $\mathbf{R}^3$. Especially, the dependence of the quasinormal modes on momentum relative to the rest frame of the plasma should be quite interesting. Furthermore one could study the modes of the other fields on the D7-brane world-volume, such as the

vector fields whose excitations correspond to vector mesons. We also have found evidence that quasinormal modes show an interesting behaviour when the system goes through the second order phase transition, allowing a continuous connection of both phases.

Outlook

As a summary of some of the suggested continuations of this work we may think of

- Going to the tensor channel and compute the residues for those quasinormal modes. Following the shear and sound hydrodynamic modes is interesting, since they describe the flow of momentum and energy, and thus provide a truly direct connection with thermalization time in the plasma. Actually this is work in progress,
- Again, concerning the residues and merging with the next chapter one could compute them for absorption lengths. This allows to see distances where damping of collective excitations becomes important,
- One could also overcome the inability to map the sound mode (scalar part of tensor) in the absorption lengths to a Heun equation, by doing a full numerical treatment like those performed in chapters 4 for the residues and in chapter 6 for the massive embedding of the D7-brane,
- Since one expects the mesons to be moving in the plasma, it would be nice to introduce the dependence on momentum for them. Even more so, this could be done for other kinds of perturbations in the D7 embeddings apart from the scalars in chapter 6,
- Provided the potential of these methods as applied to more realistic phenomena, it would be very much desirable to do these analyses for more phenomenological setups, like the Sakai–Sugimoto model [137], or string theory completions that have recently appeared.

At this level, but with a different target

- One could consider expanding and not static plasmas using time-dependent backgrounds,
- Our plasmas have infinite extent, but real ones are finite, so this feature could be a nice add on,
- We have complexified the frequency and momentum, but one still could complexify the angular momentum corresponding to modes on the S^5.

Finally on more theoretical grounds

- we could try to go to next orders in linear response theory to see if there are noticeable corrections,
- there have been very recently papers on second order hydrodynamics, so it could be nice to see how these field theory computations might match the string theory results.

Appendix

A.1 Conventions and equations of motion

In the main text we have obtained the backgrounds for supergravity fields dual to the gauge theories at both zero and finite temperature. These were given by the metrics (2.3) and (2.8), respectively. In general we work with the AdS part only, except for chapter 6 were we put a D7-brane that wraps also part of the S^5.

The conformal symmetry of the underlying AdS spacetime can be used to set r_+ to one. We will do this implicitly in the following by using the coordinate $z = r_+/r$ and rescaling gauge theory coordinates as $r_+ L^{-2}(t, \mathbf{x}) \mapsto (t, \mathbf{x})$

$$\mathrm{d}s^2 = \frac{L^2}{z^2}\left(-f(z)\,\mathrm{d}t^2 + \mathrm{d}\mathbf{x}^2 + \frac{\mathrm{d}z^2}{f(z)}\right) + L^2\,\mathrm{d}\Omega_5^2 \ . \tag{A.1}$$

The boundary is now located at $z = 0$, the horizon at $z = 1$ and the black hole factor is just $f(z) = 1 - z^4$.

Scalar fields. The equation of motion for a minimally coupled scalar of mass m follows from its action in the background (A.1), and reads

$$\phi''(t, \mathbf{x}, z) + \left(\frac{f'(z)}{f(z)} - \frac{3}{z}\right)\phi' - \frac{\ddot{\phi}}{f(z)^2} + \frac{\Delta\phi}{f(z)} - \frac{(mL)^2}{z^2\, f(z)}\,\phi = 0 \ . \tag{A.2}$$

It is now fair to assume that rotational as well as translational invariance are unbroken in the boundary theory, so one may express ϕ in terms of its Fourier transform

$$\phi(t, \mathbf{x}, z) = \int \frac{\mathrm{d}^4 k}{(2\pi)^4}\, \mathrm{e}^{-i\omega t + i\mathbf{k}\mathbf{x}}\, \Phi_k(z)\, \phi_0(k) \ , \tag{A.3}$$

where as usual in the AdS/CFT correspondence we demand $\Phi_k(z = 0) := 1$ to reproduce the boundary condition for the supergravity field, $\phi|_\partial = \phi_0(x)$. Through this transformation one obtains the final form of the equation of motion in terms of $\Phi_k(z)$

$$\Phi_k''(z) + \left(\frac{f'(z)}{f(z)} - \frac{3}{z}\right)\Phi_k'(z) + \left(\frac{\omega^2}{f(z)^2} - \frac{\mathbf{k}^2}{f(z)} - \frac{(mL)^2}{z^2 f(z)}\right)\Phi_k(z) = 0 \ . \tag{A.4}$$

Usually we will throw away the L^2 factor in front of the metric by setting it to one. At the level of equations of motion it only leaves a fingerprint on the mass term as seen above. Besides, in the main body we only consider massive scalars on (a) the arguments of stability for absorption lengths in section 3.2 and (b) in the discussion of massive scalar mesons of section 6.2. In both cases setting $L = 1$ plays no important role.

Vector fields. In this case the equations of motion for such a field are given by the Maxwell equations

$$\frac{1}{\sqrt{-g}}\,\partial_\nu\Big(\sqrt{-g}\,g^{\mu\rho}g^{\nu\sigma}F_{\rho\sigma}\Big)=0\ , \tag{A.5}$$

where $F_{\mu\nu}=\partial_\mu A_\nu-\partial_\nu A_\mu$. We can choose the $A_z=0$ gauge in the metric (A.1) and expand in plane waves A_μ as we did for the scalar field. Separating the vector field in longitudinal and transverse components, $A_{\rm L}(z)=\frac{\mathfrak{q}}{q}\cdot\mathbf{A}(z)$ and $\mathbf{q}\cdot\mathbf{A}_{\rm T}(z)=0$, the equations of motion are

$$\begin{aligned}
0 &= \omega A_0'(z)+q\,f(z)A_{\rm L}'(z)\ , && \text{(A.6a)}\\
0 &= A_0''(z)-\frac{1}{z}A_0'(z)-\frac{1}{f(z)}\Big(\omega q A_{\rm L}(z)+q^2A_0(z)\Big)\ , && \text{(A.6b)}\\
0 &= A_{\rm L}''(z)+\frac{z}{f(z)}\left(\frac{f(z)}{z}\right)'A_{\rm L}'(z)+\frac{\omega}{f(z)^2}\Big(qA_0(z)+\omega A_{\rm L}(z)\Big)\ , && \text{(A.6c)}\\
0 &= \mathbf{A}_{\rm T}''(z)+\frac{z}{f(z)}\left(\frac{f(z)}{z}\right)'\mathbf{A}_{\rm T}'(z)+\left(\frac{\omega^2}{f(z)^2}-\frac{q^2}{f(z)}\right)\mathbf{A}_{\rm T}(z)\ . && \text{(A.6d)}
\end{aligned}$$

The first three equations are not independent so we can use the first one to write decoupled equations for $A_0'(z)$ and $A_{\rm L}'(z)$. Then the relevant equations for the temporal, longitudinal and transverse components of the vector field read

$$\begin{aligned}
0 &= V_0''+\left(\frac{f'}{f}-\frac{1}{z}\right)V_0'+\left(\frac{\omega^2}{f^2}-\frac{q^2}{f}-\frac{f'}{zf}+\frac{1}{z^2}\right)V_0(z)\ , && \text{(A.7a)}\\
0 &= V_{\rm L}''+\left(3\frac{f'}{f}-\frac{1}{z}\right)V_{\rm L}'+\left(\frac{\omega^2}{f^2}-\frac{q^2}{f}+\left(\frac{f'}{f}\right)^2+\frac{f''}{f}-2\frac{f'}{zf}+\frac{1}{z^2}\right)V_{\rm L}(z)\ , && \text{(A.7b)}\\
0 &= \mathbf{A}_{\rm T}''+\left(\frac{f'}{f}-\frac{1}{z}\right)\mathbf{A}_{\rm T}'+\left(\frac{\omega^2}{f^2}-\frac{q^2}{f}\right)\mathbf{A}_{\rm T}(z)\ , && \text{(A.7c)}
\end{aligned}$$

where we defined $V_0(z)=A_0'(z)$ and $V_{\rm L}(z)=A_{\rm L}'(z)$. These will be used in chapter 5.

Notice that there is also a choice of gauge-invariant variables $E_{\rm L}=qA_0+\omega A_{\rm L}$ and $\mathbf{E}_{\rm T}=\omega\mathbf{A}_{\rm T}$, which we will use in chapter 4 for the analysis of residues of retarded Green's functions. In this case they are written in the coordinate $x=1-z^2=1-r_+^2/r^2$, such that the horizon sits at $x=0$ and the boundary at $x=1$. Introducing the dimensionless frequency and momentum $2\pi T(\mathfrak{w},\mathfrak{q}):=(\omega,q)$, the equations of motion for these gauge invariant combinations of the vector field perturbations with frequency ω and momentum q are [99]

$$\begin{aligned}
E_{\rm T}''+\frac{f'(x)}{f(x)}\,E_{\rm T}'+\frac{\mathfrak{w}^2-\mathfrak{q}^2f(x)}{(1-x)f(x)^2}\,E_{\rm T}(x) &= 0\ , && \text{(A.8a)}\\
E_{\rm L}''+\frac{\mathfrak{w}^2f'(x)}{f(x)(\mathfrak{w}^2-\mathfrak{q}^2f(x))}\,E_{\rm L}'+\frac{\mathfrak{w}^2-\mathfrak{q}^2f(x)}{(1-x)f(x)^2}\,E_{\rm L}(x) &= 0\ . && \text{(A.8b)}
\end{aligned}$$

The metric. In chapter 5 we analyze perturbations of the metric. In this case we work with a set of gauge-invariant variables, following [117]. There, the authors consider general metrics of the form

$$\mathrm{d}s^2 = -\mathsf{F}(r)\,\mathrm{d}t^2 + \frac{\mathrm{d}r^2}{\mathsf{F}(r)} + r^2\mathrm{d}\sigma_n^2 \ , \tag{A.9}$$

where $\mathrm{d}\sigma_n^2$ corresponds to a metric of a n-dimensional space of constant sectional curvature $K = 0, \pm 1$, and

$$\mathsf{F}(r) = K - \frac{2M}{r^{n-1}} - \lambda r^2 \ . \tag{A.10}$$

In our case, $K = 0$, $n = 3$, $\lambda = -1$ and $M = r_+^4/2$.

The Einstein equations are decomposed in tensor, vector and scalar components relative to the three-dimensional metric. It is thus possible to define three different gauge-invariant quantities to which we can associate a Schrödinger-like equation of motion [117]. In the z coordinate they read

$$-f(z)\,\frac{\mathrm{d}}{\mathrm{d}z}\left(f(z)\,\frac{\mathrm{d}\psi_I}{\mathrm{d}z}\right) + V_I(z)\,\psi_I = \omega^2\,\psi_I \ , \quad I \equiv \{\mathrm{T},\mathrm{V},\mathrm{S}\} \ , \tag{A.11}$$

where for each perturbation we will have a different potential. Rewriting the Schrödinger equation by shifting $(\omega, q) \mapsto r_+(\omega, q)$, the potentials V are given by

$$\begin{aligned}
V_{\mathrm{T}}(z) &= \frac{f(z)}{4z^2}\,(15 + 4\,q^2z^2 + 9z^4) \ , \\
V_{\mathrm{V}}(z) &= \frac{f(z)}{4z^2}\,(\,3 + 4\,q^2z^2 - 27z^4) \ , \\
V_{\mathrm{S}}(z) &= \frac{f(z)}{4z^2}\,\frac{1}{(1+6q^{-2}z^2)^2}\left(-1 + 4\,q^2z^2 + 9z^4 + 156z^6 - 108\frac{z^2}{q^2} + 540\frac{z^4}{q^4} + 324\frac{z^8}{q^4}\right) \ ,
\end{aligned} \tag{A.12}$$

for tensor, vector and scalar perturbations, respectively.

A.2 Residues from the connection coefficients

We have seen in the main text that the retarded Green's functions can be expressed in terms of the connection coefficients as $\Pi^{(\alpha)} \propto \mathcal{B}_{(\alpha)}/\mathcal{A}_{(\alpha)}$, for (α) a given channel (which will be hidden except for the last equation) and modulo a prefactor associated to the precise $G_{\mu\nu}$. How can we extract the expression for the residues from it? In the main text we have motivated that *close to the poles* the Green's function can be decomposed basically as a "peak", so

$$\Pi(\mathfrak{w}, \mathfrak{q}) = \sum_n \frac{\mathfrak{R}_n(\mathfrak{w}, \mathfrak{q})}{\mathfrak{w} - \mathfrak{w}_n(\mathfrak{q})} \ ,$$

and therefore its inverse can be rewritten as

$$\begin{aligned}\Pi^{-1}(\mathfrak{w},\mathfrak{q}) &= \frac{1}{\sum_n \frac{\mathfrak{R}_n}{\mathfrak{w}-\mathfrak{w}_n}} = \frac{1}{\prod_n(\mathfrak{w}-\mathfrak{w}_n)^{-1}\sum_i\Big(\mathfrak{R}_i\prod_{j\neq i}(\mathfrak{w}-\mathfrak{w}_j)\Big)} \\ &= \frac{\prod_n(\mathfrak{w}-\mathfrak{w}_n)}{\sum_i\Big(\mathfrak{R}_i\prod_{j\neq i}(\mathfrak{w}-\mathfrak{w}_j)\Big)}\ . \end{aligned} \tag{A.13}$$

We can extract the poles differentiating with respect to $\mathfrak{w}$ and evaluating at the quasinormal modes. For example, if there were just two poles

$$\partial_{\mathfrak{w}}\,\Pi^{-1} = \frac{(\mathfrak{w}-\mathfrak{w}_1)+(\mathfrak{w}-\mathfrak{w}_2)}{\mathfrak{R}_1(\mathfrak{w}-\mathfrak{w}_2)+\mathfrak{R}_2(\mathfrak{w}-\mathfrak{w}_1)} - (\mathfrak{w}-\mathfrak{w}_1)(\mathfrak{w}-\mathfrak{w}_2)\,\frac{\mathfrak{R}_1+\mathfrak{R}_2}{\Big(\mathfrak{R}_1(\mathfrak{w}-\mathfrak{w}_2)+\mathfrak{R}_2(\mathfrak{w}-\mathfrak{w}_1)\Big)^2}\ ,$$

and particularizing to $\mathfrak{w}=\mathfrak{w}_1$ gives $\mathfrak{R}_1^{-1}$. In the general case of interest to us, the derivative reads

$$\partial_{\mathfrak{w}}\,\Pi^{-1} = \frac{\sum_i\prod_{j\neq i}(\mathfrak{w}-\mathfrak{w}_j)}{\sum_i\mathfrak{R}_i\prod_{j\neq i}(\mathfrak{w}-\mathfrak{w}_j)} - \prod_n^{\text{all}}(\mathfrak{w}-\mathfrak{w}_n)\times\text{term}\ . \tag{A.14}$$

Since the second term contains *all* the quasinormal modes, evaluating $\mathfrak{w}$ at any of them will make it automatically vanish. Thus,

$$\partial_{\mathfrak{w}}\,\Pi^{-1}\big|_{\mathfrak{w}=\mathfrak{w}_n} = \frac{\prod_{j\neq n}(\mathfrak{w}_n-\mathfrak{w}_j)}{\mathfrak{R}_n\prod_{j\neq n}(\mathfrak{w}_n-\mathfrak{w}_j)} = \frac{1}{\mathfrak{R}_n}\ , \tag{A.15}$$

or, equivalently,

$$\mathfrak{R}_n^{(\alpha)} = \left[\frac{\partial}{\partial\mathfrak{w}}\,\Pi^{-1}_{(\alpha)}\Big|_{\mathfrak{w}=\mathfrak{w}_n}\right]^{-1} = \text{factor}\times\left[\frac{\partial}{\partial\mathfrak{w}}\left(\frac{\mathcal{A}_{(\alpha)}}{\mathcal{B}_{(\alpha)}}\right)\Big|_{\mathfrak{w}=\mathfrak{w}_n}\right]^{-1}\ , \tag{A.16}$$

where "factor" is dependent on the type of perturbation, for instance $-N^2\,T^2/8$ for the vectors —see (4.11).

A.3 Effective potentials

In section 3.2 we have presented the stability analysis for a scalar field but it can be generalized for any field component $\varphi(z)$ satisfying a decoupled linear second order differential equation

$$\varphi''(z) + A_1(z)\,\varphi'(z) + A_0(z)\,\varphi(z) + B(z)^2\omega^2\varphi(z) = 0\ . \tag{A.17}$$

Factorizing $\varphi(z)=\sigma(z)\,\phi(z)$ and normalizing the ϕ'' term

$$\phi'' + \left(2\frac{\sigma'}{\sigma}+A_1\right)\phi' + \left(A_0 + A_1\,\frac{\sigma'}{\sigma} + \frac{\sigma''}{\sigma}\right)\phi + B(z)^2\omega^2\,f = 0\ . \tag{A.18}$$

We now change $B(z)\mathrm{d}z = \mathrm{d}z_*$ and divide by $B(z)^2$

$$\partial_{z_*}^2\phi+\omega^2\phi+\frac{1}{B(z)}\left(2\frac{\sigma'}{\sigma}+A_1+\frac{B'(z)}{B(z)}\right)\partial_{z_*}\phi+\frac{1}{B(z)^2}\left(A_0+A_1\frac{\sigma'}{\sigma}+\frac{\sigma''}{\sigma}\right)\phi=0\ . \tag{A.19}$$

This expression becomes a Schrödinger equation when σ satisfies

$$2\frac{\sigma'}{\sigma}+A_1+\frac{B'(z)}{B(z)}=0\ . \tag{A.20}$$

Then, the same stability arguments can be applied with the proper identification of the potential

$$V_0(z)=-\frac{1}{B(z)^2}\left(A_0+\frac{1}{4}\left(\left(\frac{B'}{B}\right)^2-A_1^2\right)-\frac{1}{2}\left(A_1'+\left(\frac{B'}{B}\right)'\right)\right)\ . \tag{A.21}$$

We will now apply this to the other equations under consideration in this paper.

- transverse vector components

$$V_0=\frac{f(z)}{4z^2}\left(3+5z^4+4q^2z^2\right) \tag{A.22}$$

- longitudinal and temporal vector components

$$V_0=-\frac{f(z)}{4z^2}\left(1+7z^4-4q^2z^2\right) \tag{A.23}$$

- gravitational vector perturbation (shear mode)

$$V_0=\frac{f(z)}{4z^2}\left(3-27z^4+4q^2z^2\right) \tag{A.24}$$

Due to the underlying analyticity of the solution of the corresponding Heun equation all fields, $\mathbf{A}_\mathrm{T}, V_\mathrm{L}, V_0, \Phi_\mathrm{V}$, fulfill the boundary conditions leading to (3.15) and (3.16). The effective potential is positive in the case of the transverse vector fields. For the longitudinal and temporal vector field components it is negative and therefore the stability argument presented in section 3.2 does not apply. We note that the asymptotic behavior at the boundary is the same as that of a scalar field saturating the Breitenlohner–Freedman bound. We take this as an indication for stability, in the original analysis in AdS a positive energy condition is satisfied even for fields with negative potential [160]. The asymptotic behavior of the fields is restricted by the condition of having a well-defined conserved energy. In turn, the positive contribution of the kinetic energy always overcomes the negative contribution from the potential. A formal analysis [161] can be applied that shows the stability of vector perturbations. The 'Hamiltonian' operator $H=-\partial_{z_*}^2+V_0$ must be positive definite over the set of normalizable solutions

$$\int_{z_*^b}^{\infty} dz_*\chi^* H\chi>0\ . \tag{A.25}$$

We can rewrite (A.25) as

$$-\left[\chi^* D_\rho \chi\right]_{z_*^b}^{\infty} + \int_{z_*^b}^{\infty} dz_* \left(|D_\rho \chi|^2 + V_\rho |\chi|^2\right) > 0 \ , \tag{A.26}$$

where we have introduced an auxiliary function ρ, such that $D_\rho = \partial_{z_*} + \rho$ and

$$V_\rho = V_0 + \partial_{z_*}\rho - \rho^2 \ . \tag{A.27}$$

A convenient election that makes $V_\rho \geq 0$ for vector fluctuations is $\rho = -f(z)/2z$. We can easily see that there is no contribution from the boundary term at the horizon, since $\chi(\infty) \to$ const. and $\rho(\infty) \to 0$. Therefore, we are left with the condition

$$\lim_{z\to 0} \chi^* \left(\partial_z - \frac{1}{2z}\right) \chi = 0 \ . \tag{A.28}$$

Close to the boundary, $V_0 \simeq -1/4z^2$, so the solution is a combination of Bessel functions $\chi \sim a\sqrt{z} J_0(\omega z) + b\sqrt{z}\, Y_0(\omega z)$. Then, the condition (A.28) satisfied when $b = 0$, that is equivalent to choose the normalizable solution at the boundary.

The effective potential of the shear mode is also interesting. It is negative close to the horizon. Equation (3.16) shows that this is a necessary requirement for existence of the hydrodynamic shear mode with $\mathrm{Re}\,(q^2) = 0$. We would expect that if the potential is deep enough, instabilities will appear. This is in agreement with other analysis that exhibit a negative well in the interior. Purely imaginary frequencies have been found in the study of electromagnetic and gravitational perturbations in global AdS [90,162]. In the extremal limit, the frequencies seem to reach the real axis at $\omega = 0$, and the geometry was conjectured to be marginally unstable. Recent works also suggest that instabilities of D7 probe branes in AdS appear when a quasinormal mode cross the real axis at $\omega = 0$ [3,106].

A.4 Changing parameters in a Heun equation

In this appendix we show how to map a given Heun equation with given parameters into another Heun equation for a different function with a different set of parameters. This will allow in some cases to avoid the problem with "fake" modes.

Let us start with a Heun equation for $y(x)$

$$y'' + \left(\frac{\gamma}{x} + \frac{\delta}{x-1} + \frac{\epsilon}{x-2}\right) y' + \frac{\alpha\beta x - Q}{x(x-1)(x-2)}\ y(x) = 0 \ , \tag{A.29}$$

where the parameters are subject to the condition $\alpha+\beta+1 = \gamma+\delta+\epsilon$. The characteristic exponents at the AdS boundary ($x = 1$) are in general

$$\{1; 0, 1-\delta\} \ ,$$

for $y(x)$. In the cases where $\delta \in \{0 \cup \mathbb{Z}^-\}$, the first solution is logarithmic, but the logarithm might accidentally vanish at the "false frequencies"

$$y(x) = \mathcal{A}[1 + (1-x) + \ldots + h(1-x)^{(1-\delta)} \log(1-x) + \ldots] + \mathcal{B}[(1-x)^{(1-\delta)} + \ldots] \ , \quad \text{(A.30)}$$

where $h = 0$. According to [96] and as seen in section 2.3, the Green's function is proportional to the ratio $\mathcal{B}/\mathcal{A}$, and the false frequencies are the ones for which accidentally $h = 0$.

Now we would like to change the function $y(x)$ such that we find a related Heun equation with different parameters. Let us define

$$y(x) = (1-x)^{\varrho} Y(x) \ . \quad \text{(A.31)}$$

This allows us to find a Heun equation for $Y(x)$, *provided* $\varrho = 1 - \delta$, and where the new set is

$$\begin{aligned} \widetilde{\alpha} &= \alpha + \varrho = \alpha + 1 - \delta \ , \\ \widetilde{\beta} &= \beta + \varrho = \beta + 1 - \delta \ , \\ \widetilde{Q} &= Q + 2\gamma\varrho = Q + 2\gamma(1-\delta) \ , \\ \widetilde{\delta} &= \delta + 2\varrho = 2 - \delta \ , \\ \widetilde{\gamma} &= \gamma \ , \quad \widetilde{\epsilon} = \epsilon \ . \end{aligned} \quad \text{(A.32)}$$

The interesting thing about this shift is that we can find a positive $\widetilde{\delta} \in \mathbb{Z}^+$ when in the original Heun equation we encounter fake frequencies. This always eliminates the false frequencies since the second solution is never analytic but goes like $(1-x)^{(\delta-1)}$, which is a negative (or zero) exponent for $\widetilde{\delta} \in \mathbb{Z}^+$. Now, the Frobenius solution is

$$Y(x) = \mathcal{A}[(1-x)^{-\varrho} + \ldots + h(1-x)^{(1-\delta-\varrho)} \log(1-x) + \ldots] + \mathcal{B}[(1-x)^{(1-\delta-\varrho)} + \ldots] \ . \quad \text{(A.33)}$$

The recursion algorithm of Leaver [115] and its adaption to the Heun equation by Starinets [94] computes when the solution of the Heun equation is analytic at $x = 1$. Now the solution that goes with the coefficient $\mathcal{A}$ is never analytic, and therefore the false frequencies do not appear.

A.5 Relaxation method

It is common practice to use the shooting method to solve two-point boundary value differential equations. Indeed, we have used this method to compute the first three quasinormal modes of the massive embedding for a variety of bare quark masses at the horizon. However, in order to check at least those results for the first mode, we follow the spirit

of *"always shoot first and only then relax"*. The reference for this appendix is Numerical Recipes [163].

The idea behind this method consists in replacing the differential equations by a finite-difference system (FDE) on a grid. One will then modify the value of the dependent variables at each point *relaxing* to the configuration which solves the differential equation. In our case, we will convert our second order complex ODE into a set of four first order equations, with the real and imaginary parts separated, and then into an FDE.

In general one has the set of N ODE's

$$\frac{\mathrm{d}y_i(x)}{\mathrm{d}x} = g_i(x, y_1, \ldots, y_N; \lambda) \ , \tag{A.34}$$

where each dependent variable depends on the others and itself, on the independent variable x, and possibly on additional parameters, like λ above. In our case this (complex) parameter takes the role of the quasinormal frequency. Those extra parameters can be embedded in the problem giving equations for them too

$$\begin{cases} y_{N+1} & \equiv & \lambda \ , \\ \dfrac{\mathrm{d}y_{N+1}}{\mathrm{d}x} & = & 0 \ , \quad \text{since it is constant} \ . \end{cases} \tag{A.35}$$

The solution to the problem involves $N \times M$ values, for the N dependent variables in a grid of M points. Concerning boundary conditions, for the system to be determined one needs N of them, supplying it with extra boundary conditions for the extra parameters if present.

The system is discretized as usual

$$x \to \frac{1}{2}(x_k + x_{k-1}) \ , \quad y \to \frac{1}{2}(y_k + y_{k-1}) \ , \tag{A.36}$$

for points in the bulk (not in the boundaries). One may arrange the whole set of y_i's in a column vector $\mathbf{y}_k = (y_1, \ldots, y_N, y_{N+1})_k{}^T$, where the subscript k refers to evaluation at the point x_k, $k = 1, \ldots, M$. With this matrix notation, the system (A.34) is rewritten as

$$0 = \mathbf{E}_k \equiv \mathbf{y}_k - \mathbf{y}_{k-1} - (x_k - x_{k-1})\, \mathbf{g}_k(x_k, x_{k-1}, \mathbf{y}_k, \mathbf{y}_{k-1}) \ , \quad k = 2, \ldots, M \ , \tag{A.37}$$

where the $\mathbf{E}_k$ are the aforementioned FDE's. These are the equations that we need to fulfil. Notice there are N equations at $M-1$ points, so the remaining N equations are just given by the boundary conditions. We will set n_1 of them on the left at x_1, called $\mathbf{E}_1$, and the rest $n_2 = N - n_1$ at x_M, called $\mathbf{E}_{M+1}$ (no typo in the subscript!).

Now one is set with all the necessary material. Suppose one has a good ansatz that nearly solves the FDE's $\mathbf{E}_k$. By shifting each solution $\mathbf{y}_k \to \mathbf{y}_k + \Delta\mathbf{y}_k$ and Taylor expanding

in the shift, one obtains a relation

$$0 = \mathbf{E}_k(\mathbf{y} + \Delta\mathbf{y}) \simeq \mathbf{E}_k(\mathbf{y}_k, \mathbf{y}_{k-1}) + \sum_{n=1}^{N} \frac{\partial \mathbf{E}_k}{\partial y_{n,k-1}} \Delta y_{n,k-1} + \sum_{n=1}^{N} \frac{\partial \mathbf{E}_k}{\partial y_{n,k}} \Delta y_{n,k} \ , \quad \text{(A.38)}$$

$$\Rightarrow \ -E_{j,k} = \sum_{n=1}^{N} \Big(S_{j,n} \, \Delta y_{n,k-1} \Big) + \sum_{n=N+1}^{2N} \Big(S_{j,n} \, \Delta y_{n-N,k} \Big) \ , \quad \text{(A.39)}$$

which by inverting it allows to find the $\Delta\mathbf{y}_k$ that improve the solution. This is done by merging the two differentials

$$S_{j,n} = \frac{\partial E_{j,k}}{\partial y_{n,k-1}} \ , \quad S_{j,n+N} = \frac{\partial E_{j,k}}{\partial y_{n,k}} \ , \quad n = 1, \ldots, N \ , \quad \text{(A.40)}$$

in a $N \times 2N$ matrix, for each bulk grid position x_k. For the boundaries the expressions follow equally

$$-E_{j,1} = \sum_{n=1}^{N} S_{j,n} \, \Delta y_{n,1} = \sum_{n=1}^{N} \frac{\partial E_{j,1}}{\partial y_{n,1}} \Delta y_{n,1} \ , \quad j_2 + 1, \ldots, N \ , \quad \text{(A.41)}$$

$$-E_{j,M+1} = \sum_{n=1}^{N} S_{j,n} \, \Delta y_{n,M} = \sum_{n=1}^{N} \frac{\partial E_{j,M+1}}{\partial y_{n,M}} \Delta y_{n,M} \ , \quad j = 1, \ldots, n_2 \ , \quad \text{(A.42)}$$

where n runs in both from 1 to N. The whole $(NM \times NM)$ S matrix possess a block diagonal structure. This allows for a somewhat fast Gaussian elimination, since off-diagonal entries are already zero, and forms the basis of an iterative process which can be put to run until one reaches a desired accuracy in the result. Concerning this last point, we computed the error of our solution as

$$\texttt{err} = \frac{1}{MN} \sum_{k=1}^{M} \sum_{j=1}^{N} \left| \frac{\Delta y[j][k]}{\texttt{scalevar}[j]} \right| < \texttt{conv} \ , \quad \text{(A.43)}$$

where $\texttt{scalevar}[j]$ is an associated scale for each of the dependent variables (e.g. the value at the midpoint or so). The idea is that when that averaged value of the shift to get a better solution is smaller than conv, we accept the former values we had as the actual solution. In our computations we set $\texttt{conv} = 10^{-6}$.

Part III

Secciones en castellano

Introducción

En esta tesis nos encontramos en una situación difícil: es claramente un trabajo de teoría de cuerdas, pero con una fuerte motivación y *relación directa* con el mundo experimental. Siendo ésta tal mezcla, deberíamos decir que es igualmente un desafío y muy divertido trabajar en ella. Esperamos haber sido capaces de presentar las cosas con profundidad, sin conflictos con los conocimientos que poseemos hoy en día.

Esta tesis versa sobre cómo calcular ciertas propiedades de un plasma, cuando éste resulta ser no-Abeliano y, de forma más importante, cuando está acoplado fuertemente. Diremos en este párrafo que la teoría de cuerdas y en particular la correspondencia Anti-deSitter/Teoría Conforme de Campos (AdS/CFT por sus siglas en inglés) ha resultado ser una herramienta como poco muy interesante. Esto es así porque utilizando dicha correspondencia uno puede realizar cálculos cuantitativos que, en algunos casos, dan incluso resultados muy cercanos a los obtenidos en el experimento. En este sentido podemos conectar la parte experimental con la teoría de cuerdas. Aún así, veremos que esta aproximación cuerdosa al problema todavía necesita desarrollarse más hasta alcanzar la madurez.

Siguiendo con lo anterior, ¿por qué plasmas no-Abelianos fuertemente acoplados? Hay muchos motivos para estudiar este tipo de plasmas, siendo el mejor ejemplo los primeros microsegundos después del Big Bang. La historia temporal del Universo tiene una serie de periodos distintos, comenzando con los primeros 10^{-43} segundos donde los efectos de gravedad cuántica dominaron. Antes del inicio de inflación alrededor de 10^{-35} segundos el medio ya era una especie de sopa extremadamente caliente y densa hecha de quarks y gluones *libres*, entre otras partículas. Según evolucionó y expandió desde el estado inicial se enfrió (y aún lo hace), perdiendo parte de sus simetrías. Como consecuencia de ello pasó por una serie de transiciones de fase. La primera tuvo lugar alrededor de los 10^{-11} segundos tras el estallido y es conocida como transición de fase electrodébil, lo cual significa que las fuerzas electromagnética y débil se observaban por separado. El plasma de quarks y gluones continuó enfriándose llegando a la siguiente transición, esta mucho más importante para nosotros: la transición quark/hadrón, también conocida en el mundo más teórico como la *transición confinamiento/deconfinamiento.* Ésta fijó la escala de formación de materia hadrónica, donde los protones y neutrones tales y como los conocemos aparecieron, y donde los quarks y gluones dejaron de ser libres en condiciones "normales", i.e. aquellas del medio que los rodea. La transición ocurrió tras los primeros diez microsegundos, cuando la temperatura era de unos 200 MeV. Esta forma tan moderna de medir temperaturas puede traducirse en Kelvins usando la constante de Boltzmann,

dando unos 2×10^{12} K; un medio realmente caliente. Tras un par de minutos los neutrones y protones formaron deuterio y núcleos de helio, i.e. se inició la nucleosíntesis, aunque la mayor parte de los protones quedaron sin combinarse formando núcleos de hidrógeno. Unos 380 000 años más tarde se vió el desacoplo de radiación de la materia y la formación de átomos neutros, y después básicamente todo lo que hemos tenido ha sido formación de estructuras como estrellas, galaxias, etc.

Así, volviendo más o menos al periodo entre inflación y la transición de deconfinamiento, estudiar plasmas no-Abelianos de quarks y gluones es nada más y nada menos que estudiar parcialmente los primeros microsegundos de nuestro Universo.

Por supuesto hay aproximaciones a esta cuestión más terrenales, que son los llamados "pequeños Bangs". Estas explosiones con materia muy caliente y densa han sido producidas haciendo chocar núcleos en el Colisionador de Iones Pesados Relativistas (RHIC de sus siglas en inglés) en el Brookhaven National Laboratory, en EE.UU. El resultado es una *bola de fuego* hecha en gran parte de quarks y gluones, que termaliza y enfría en su expansión. Este plasma ha sido llamado el Plasma de Quark-Gluón (QGP del inglés), y ciertamente guarda un parecido con el proceso descrito dos párrafos arriba. El estudio de estas bolas de fuego nos ha mostrado ya muchas cosas sobre la teoría subyacente, la Cromodinámica Cuántica (QCD), por encima de la transición de deconfinamiento. Su comprensión puede igualmente jugar un papel clave en nuestra comprensión del plasma primordial.

Sin embargo, resulta que la descripción del QGP es una dura tarea. No es sencillo extraer información *dinámica* de él, por ejemplo los parámetros de transporte. Grandes fenómenos colectivos en él parecen mostrar que está fuertemente acoplado, reforzando la idea de que cálculos desde primeros principios —cálculos en QCD— son difíciles de llevar a cabo. Y de hecho esto puede ser una oportunidad para la teoría de cuerdas, como trataremos de probar.

Nuestro objetivo en esta tesis es doble. En primer lugar, no queremos hacer el camino largo. Esto significa que no planeamos hablar sobre cada detalle, mucha más información y partes técnicas pueden encontrarse en la extensísima literatura. Eso nos lleva al segundo objetivo, que no es más que esa falta de información sea equilibrada con pedagogía y simplicidad. Esperamos haber conseguido esto.

El trabajo que presentamos está dividido en dos partes. En la primera presentamos el caso a estudiar y proporcionamos las herramientas que utilizaremos para obtener resultados también

Capítulo 1: está dedicado a presentar una motivación para el QGP a través de la transición deconfinante; explicando algunas nociones básicas de los plasmas como la introducción de temperatura, la descripción de pequeñas perturbaciones y algunos de los modos colectivos que pueden encontrarse; y finalmente mostrar en mayor pro-

fundidad el experimento en RHIC, que es nuestra nueva herramienta experimental para estudiar la fase de plasma.

Capítulo 2: se explica lo básico de la conjetura de Maldacena y sus generalizaciones más relevantes para este trabajo, es decir (a) cómo poner la teoría gauge a temperatura finita mediante la adición de un agujero negro al background y (b) cómo calcular cantidades que vienen de funciones a dos puntos en un formalismo en tiempo real y su relación con los llamados *modos cuasi-normales*. Éstos son modos de frecuencia compleja asociados a ecuaciones diferenciales con valores en la frontera sujetos a condiciones muy peculiares en ella.

Capítulo 3: en él analizamos todas las ligauras que pueden imponerse formalmente en las funciones de Green retardadas y en el espectro cuasi-normal. También hacemos un análisis de estabilidad para diferentes perturbaciones del background.

Nuestros resultados son analizados y comentados en la segunda parte, que consisten en:

Capítulo 4: presentamos resultados de la contribución de cada modo colectivo a un plasma de gluones. En este sentido calculamos los residuos de la función espectral para los primeros cuatro modos cuasi-normales de perturbaciones vectoriales, con diferentes valores del momento. Siempre que existen hacemos un seguimiento de los modos hidrodinámicos, que son modos cuasi-normales puramente imaginarios. Estos resultados tienen una interpretación interesante como tiempo de termalización τ_{therm} del plasma.

Capítulo 5: se muestra el cálculo de longitudes de absorción en un plasma de gluones. El punto clave es hacer complejo el momento en lugar de la frecuencia; así uno tiene modos de momento complejo como función de la frecuencia ω en lugar de modos cuasi-normales como función del momento q. Las longitudes de absorción vienen dadas por el inverso de la parte imaginaria del momento complejo, mostrándose que decaen exponencialmente. En el límite de frecuencia cero, los modos de momento complejo están conectados con el espectro de masas de glubolas en QCD_3, de quienes obtenemos los valores en algunos casos.

Capítulo 6: se considera un plasma más fenomenológico a través de la adición de grados de libertad en la fundamental, i.e. "quarks". Nuestros resultados modelizan las etapas finales del proceso de disociación de excitaciones colectivas en tal plasma. Este proceso se construye en el dual gravitatorio mediante una brana que cae en el agujero negro. Se argumenta que la descripción puede ser útil para el estudio de supresión de charmonium en RHIC.

El trabajo original presentado en esta tesis concierne al preprint [1] y a nuestros artículos publicados [2–4].

Conclusiones

En esta tesis se han estudiado tres aspectos de la física de plasmas en acoplo fuerte desde una perspectiva holográfica. En lo que sigue damos las conclusiones sobre cada uno de ellos.

Capítulo 4. Hemos encontrado una estructura analítica para el correlador de la carga-R a temperatura finita muy interesante. Cuando el momento es cero, una propiedad genérica de los correladores es la existencia de un conjunto infinito de polos equiespaciados en el plano de frecuencias complejas. A acoplo débil éstos se colocan sobre el eje imaginario [102], pero de acuerdo con el cálculo en AdS/CFT se alejan de él en acoplo fuerte. El comportamiento correcto en el ultravioleta, que se puede obtener analíticamente a temperatura cero, se recupera sumando la contribución de todos los polos. El valor de los residuos es crucial, especialmente el hecho de que el modo hidrodinámico se anule a momento cero. Cuando consideramos dependencia en el momento, la forma analítica del residuo para el modo difusivo en la aproximación hidrodinámica, proporcional a q^2, inducirá una singularidad en el correlador a tiempos pequeños, a añadir a la singularidad ultravioleta usual. Esto claramente no puede ser la respuesta correcta, y se entiende como una limitación a la validez de la aproximación. El comportamiento amortiguado y oscilatorio del residuo hidrodinámico puede curar este problema, haciendo que la contribución del modo difusivo sea suave a tiempos pequeños. De hecho, el modo hidrodinámico se desacopla para momentos $q > 1$ y de esa forma se comporta como los modos colectivos presentes a acoplo débil. En este sentido nuestros resultados van más allá de la aproximación hidrodinámica. En principio esperamos que otros modos hidrodinámicos que aparecen en el correlador a dos puntos del tensor de esfuerzos —los modos sónico y de cizalladura— presentados en la sección 1.2 tengan un comportamiento colectivo similar.

Observamos también que según aumenta el momento, la difusión se hace menos importante y las otras excitaciones colectivas de los modos longitudinales describen las fluctuaciones de la densidad de carga. En contraste con los partones vestidos por interacciones en el regimen de acoplo débil, éstos no desacoplan a gran momento. El comportamiento es también diferente del de los polos encontrados para operadores invariantes gauge. En acoplo débil estos polos se convierten en cortes de ramificación en posiciones fijas del eje imaginario, mientras que el cálculo holográfico predice a acoplo infinito que las únicas singularidades existentes son polos que se acercan al eje real. Finalmente un nuevo pico aparece en la función espectral, localizado cerca de $\mathfrak{w} = \mathfrak{q}$. Este pico sobrevive a momento

más grande, y puede ser interpretado como una excitación de tipo cuasi-partícula de las fluctuaciones de la densidad de carga, lo cual muestra un cambio de comportamiento del sistema según se aumenta el momento, de difusivo a reactivo. Por contra, las fluctuaciones transversas apenas tienen propiedades características, así que no aparecen cuasi-partículas para ellas; esto refleja el hecho de que no hay modos que se propaguen en la teoría conforme a temperatura cero.

Tal y como se sugirió en la introducción del capítulo 4 podemos aplicar nuestros resultados al cálculo de una escala de tiempo hidrodinámica τ_{H}. Recordando la ecuación (3.4) podemos estimar el momento en el que la contribución del modo difusivo está a la par con el primer modo cuasi-normal

$$|R_{\mathrm{H}}(q)\,\mathrm{e}^{-i\Omega_{\mathrm{H}}(q)\tau_{\mathrm{H}}-\Gamma_{\mathrm{H}}(q)\tau_{\mathrm{H}}}| \simeq |R_1(q)\,\mathrm{e}^{-i\Omega_1(q)\tau_{\mathrm{H}}-\Gamma_1(q)\tau_{\mathrm{H}}}|\ ,$$

que tras un poco de álgebra lleva a la fórmula dependiente de q

$$\tau_{\mathrm{H}} = \frac{\log|R_{\mathrm{H}}/R_1|}{\Gamma_{\mathrm{H}}-\Gamma_1} = \frac{1}{2\pi T}\,\frac{\log|\mathfrak{R}_{\mathrm{H}}/\mathfrak{R}_1|}{\mathrm{Im}\,(\mathfrak{w}_1-\mathfrak{w}_{\mathrm{H}})}\ .$$

Usando nuestros resultados numéricos representamos τ_{H} como función de $\mathfrak{q}$, para encontrar que en unidades de $(2\pi T)^{-1}$ la escala temporal mínima es $\tau_{\mathrm{H}} = 3.7 - 3.2$ en el rango $\mathfrak{q} = 0.3 - 0.48$, aumentando rápidamente para valores más grandes del momento. Para valores más bajos también crece, pero esto es debido al hecho de que la distribución de carga ya es bastante uniforme, de manera que podemos tomar esos valores como aquellos donde comienza la difusión. De hecho, la relación de dispersión comienza a desviarse de la aproximación hidrodinámica para $\mathfrak{q} \approx 0.45$, que corresponde a longitudes de onda Compton de 1.2 fm, básicamente el tamaño del protón. Como un modelo para el sQGP en RHIC descrito en la sección 1.3, cojamos $T \simeq 2\,T_c \simeq 350\,\mathrm{MeV}$. La escala temporal hidrodinámica es entonces $\tau_{\mathrm{H}} \approx 0.3\,\mathrm{fm}/c$. Es un tiempo notablemente pequeño, incluso un poco menor que τ_{form}. De hecho indica que la aproximación hidrodinámica es válida desde tiempos muy pequeños. Recordemos que en RHIC el tiempo de termalización es $\tau_{\mathrm{therm}} \approx 0.6 - 1.0\,\mathrm{fm}/c$ y que la aproximación hidrodinámica es por tanto válida ya en $t \lesssim 1\,\mathrm{fm}/c$ [108]. Esperamos que los valores para los modos sónico y de cizalladura relacionados con el flujo de momento y energía cambien un tanto, pero es tranquilizador encontrar los órdenes de magnitud correctos incluso para la teoría $\mathcal{N}=4$.

Capítulo 5. En este capítulo hemos puesto en piso firme la relación entre las soluciones a las ecuaciones de campo linealizadas con momento complejo en un background de agujero negro en AdS y las longitudes de absorción en una teoría gauge conforme en la fase de plasma. Esto se realizó calculando explícitamente algunos ejemplos sencillos correspondientes a fluctuaciones escalares, vectoriales y de la métrica.

Debido a la simetría conforme subyacente, todas las longitudes de absorción escalean simplemente como el inverso de la temperatura T^{-1}. A frecuencia cero encontramos acuerdo con cálculos previos del espectro de glubolas en la teoría efectiva tridimensional [109–111]. Sin embargo, preferimos en esta tesis interpretar nuestros resultados como longitudes de apantallamiento para campos estáticos. Esta interpretación ha sido propuesta recientemente y de manera independiente en la referencia [114]. Es más, también hemos calculado la dependencia de la longitud de absorción con la frecuencia. Los resultados para los primeros modos se muestran en las figuras 5.2, 5.3, 5.4 y 5.5. En todos los casos, el plasma es menos absorbente a frecuencias mayores. Los números de onda complejos capturan igualmente el comportamiento hidrodinámico para la difusión de carga-R y para el momento. Nuestros resultados numéricos están de acuerdo con la simple continuación analítica de las relaciones de dispersión para los modos hidrodinámicos. Esto se muestra en las figuras 5.6 y 5.7.

Uno de los resultados interesantes de nuestro estudio el que la longitud de apantallamiento más larga (la masa de "glubola" más liviana en la teoría reducida dimensionalmente) corresponde a un estado con carga-R no cero. Tal estado no pertenece al espectro de QCD$_3$, i.e. ¡el *mass gap* de la teoría efectiva tridimensional no es el de QCD$_3$! Las masas de glubola juegan un papel importante en la determinación de la longitud de apantallamiento de Debye. En tal caso uno estudia el intercambio de glubolas entre cuerdas abiertas en el background de agujero negro en AdS. Tal y como se hizo notar en [114] el mass gap por sí solo no es importante para el apantallamiento de Debye, dado que sólo ciertos operadores pueden acoplarse a la cuerda abierta. Puesto que estas cuerdas abiertas son neutras bajo carga-R, los estados de masa baja con carga-R no cero no se acoplan a la cuerda. Sin embargo, la configuración de cuerdas que uno normalmente considera tiene sus extremos fijados en un punto de la S^5, o también es posible considerar cuerdas que acaban en puntos diferentes de la S^5. En tal situación los estados de carga-R no cero ligeros pueden volverse importantes y modificar el resultado para la longitud de apantallamiento.

En este capítulo hemos estudiado tan sólo los casos que pueden reducirse a la ecuación de Heun permitiendo aplicar el método eficiente de fracciones continuas para el cálculo de los autovalores del momento complejo. Sería ciertamente interesante extender estas investigaciones a los casos que no son reducibles a la ecuación de Heun. En éstos uno debe utilizar métodos elementales como el de Frobenius, que hace que los cálculos numéricos sean más lentos. Aún así creemos que es un problema interesante, especialmente teniendo en cuenta la comparación con los cálculos de las masas de glubola.

Otro punto interesante es la cuestión acerca de si las longitudes de absorción divergen en el límite de frecuencia infinita o si permanecen finitas. Desafortunadamente hasta ahora los métodos numéricos no permiten acceder a ese regimen.

Un problema relacionado es el cálculo de las longitudes de absorción en teorías holográficas puramente no conformes. Debido a la presencia de una escala subyacente la dependencia en frecuencia probablemente mostrará un patrón más complicado que el encontrado en el caso conforme. También será de gran interés el cálculo de las longitudes de absorción para estados mesónicos que aparecen en teorías con D7-branas embebidas en el agujero negro en AdS, usando los mismos métodos que empleamos en el capítulo 6 para el estudio de los modos cuasi-normales para mesones [3]. En [106] se ha enfatizado recientemente que aparecen inestabilidades para embebimientos con horizonte cercanos al crítico. Tales inestabilidades aparecen como modos cuasi-normales de parte imaginaria positiva. Como hemos visto, inestabilidades similares pueden aparecer igualmente en el estudio de las longitudes de absorción. Puesto que éstas aparecen para las longitudes de apantallamiento a $\omega = 0$ y para valores reales de q^2, puede que sea mucho más sencillo buscar éstas en lugar de las asociadas a modos cuasi-normales inestables.

Capítulo 6. Hemos propuesto una descripción holográfica (de las etapas finales) del proceso de disociación de mesones con espín bajo en el plasma de quarks y gluones. El ingrediente clave es el embebimiento de D7-branas en el background de agujero negro en AdS que caen en el horizonte. La métrica inducida en el volumen de mundo de estas D7-branas es igualmente un agujero negro, y por tanto tiene sentido calcular modos cuasi-normales para las fluctuaciones de la brana. Estos modos describen la disipación de energía de excitaciones mesónicas en el plasma, en particular la disociación de mesones. Un punto importante es que el proceso de disociación en el plasma holográfico es sólo accesible para mesones formados por quarks de masas hasta $m_q = 0.92\sqrt{\lambda}T/2$, donde T es la temperatura en el plasma y λ es el acoplo de 't Hooft. Quarks más pesados vienen representados por D7-branas sin horizonte en su volumen de mundo y por ello tienen excitaciones mesónicas estables.

La disociación de estados de quarkonium es de gran importancia para la física del plasma de quarks y gluones. Desde hace tiempo se le ha considerado como una de las pruebas más limpias de la formación del plasma. En particular, estados de quarkonium tales como el mesón J/ψ se espera que se derritan en el plasma, y por tanto su abundancia medida en los procesos donde hay formación de plasma se vea reducida significativamente en comparación con colisiones nucleares donde no hay formación de plasma.

Aunque el modelo que hemos considerado está bastante lejos de QCD es aún así interesante mirar al problema de la disociación de mesones desde nuestra perspectiva holográfica. Encontramos que el proceso se da para estados de quarkonium hechos de quarks con masas como mucho del orden de la temperatura del plasma. La masa del quark *charm* es $m_c \approx 1.4$ GeV y la temperatura en RHIC es $T_{\rm RHIC} \lessapprox 300$ MeV. AdS predice ratios de masa crítica respecto de la temperatura de $1 - 2$ si usamos estimaciones recientes sobre cómo rela-

cionar $5.5 < \lambda < 6\pi$ con QCD [156]. Es muy interesante que recientemente la disociación de mesones ha sido considerada en un contexto de teoría de perturbaciones *Hard Thermal Loop* [157]. En él los autores encontraron una parte imaginaria para la parte estática del potencial quark-antiquark, dando lugar a una anchura de desintegración que puede ser ignorada para quarks más pesados que $m_q = 12\pi T/g^2$. Uno se siente tentado a interpretar esto como el análogo a acoplo débil de QCD para el valor holográfico $m_q = 0.92\sqrt{\lambda}T/2$, y que existe una función de interpolación $f(\lambda)$ tal que $m_q = f(\lambda)T$, donde $f(\lambda) \approx \sqrt{\lambda}$ en acoplo fuerte y $f(\lambda) \approx 1/\lambda$ en acoplo débil.

El inconveniente más importante del modelo AdS es que el background corresponde a plasmas hechos con quarks sólo en la representación adjunta. Aunque en un background con quarks dinámicos uno espera aún que los quarks pesados estén bien modelizados por embebimientos de D-brana, la presencia de quarks en la fundamental en el plasma deconfinado puede cambiar las tasas de disociación incluso para quarks pesados de manera drástica. En cualquier caso, los modos cuasi-normales en D-branas embebidas en duales gravitacionales de teorías gauge ofrecen una manera única de estudiar la disociación de quarkonium de forma holográfica.

Es de gran interés aplicar nuestro método a la disociación de mesones en otros modelos, tales como aquellos con simetrías quirales no-Abelianas [137] o a modelos holográficos fenomenológicos de QCD desarrollados en [158, 159]. En vista del problema mencionado arriba de la supresión del J/ψ, sería de interés grandísimo tener un dual holográfico fenomenológico de QCD que incluyera sabores pesados como el quark charm.

En esta tesis hemos considerado únicamente modos con momento cero en la S^3 así como en $\mathbf{R}^3$. En especial, la dependencia de los modos cuasi-normales con el momento en relación al sistema de referencia en reposo debería ser muy interesante. Aún más, uno podría estudiar otros campos en el volumen de mundo de la D7-brana, como por ejemplo excitaciones correspondientes a mesones vectoriales. Hemos encontrado igualmente evidencia de que los modos cuasi-normales muestran un comportamiento interesante cuando el sistema sufre la transición de fase de segundo orden, permitiendo una conexión continua entre ambas fases.

Agradecimientos

¡Qué raro es este momento! Llegados a este punto uno desearía que la tesis la escribiese otro para poder dedicarse durante dos meses a esta parte. Pues bien Karl, ¡hemos llegado al final del camino! Increíble. Ha sido un placer trabajar contigo y, aunque la gente no siempre me crea, sí que te sueles explicar muy bien. Creo que eres un Gran Físico, así, con mayúsculas, y me alegro de que finalmente te hayas visto recompensado con el regalo de la estabilidad. De una manera casi más personal, quiero agradecerte sobre todo esa muestra general de honestidad que te caracteriza, tan difícil de encontrar hoy en día. A no ser que me tengas muy engañado . . . ;-)

En esta aventura que es el doctorado uno nunca está solo, aunque a veces lo parezca. Quiero acordarme aquí de mis dos padrinos oficiales, César y Enrique, tan importantes en estas lides. Muchas gracias a los dos, por las clases y por los congresos tan surrealistas en los que nos hemos encontrado, respectivamente. Igualmente quiero agradecer a todos los miembros del tribunal su disponibilidad para fijar el día D y la hora H de la lectura de tesis; sé que ha sido difícil. A nivel de financiación, ha sido inestimable la ayuda prestada por la Comunidad de Madrid, representada por una beca —ahora por fin contrato— de Formación de Personal Investigador. Esto por supuesto no sería posible sin el estimable pago de impuestos de (la mayoría de) los ciudadanos de la Unión Europea. A ellos también van un "gracias". También gracias a la financiación propia del IFT pude estar de estancia en Swansea, un lugar curioso con un departamento lleno de gente maravillosa.

La burrocracia estos años ha sido más llevadera gracias a la fantástica ayuda de Isabel. No puedo imaginarme a nadie tan competente y responsable, quien además se ha convertido en una mini-mami. Juan Carlos y Lola en el departamento también se han portado rebien. Y a Patricia la informática.

A todos los mayores del IFT les agradezco su cercanía y explicaciones, Ángel, Tomás, Esperanza, Pepe, Marga, Ana María, Andrea, Stefano, etc. y sobre todo a Patrick. Espero que el gruñón tenga mucha suerte en su futuro, jeje. Eso sí, lo mejor aparte de poderme haber dedicado a la física estos años ha sido indudablemente la calidad humana y juerguil de todos los estudiantes y algún que otro post-doc (ese Parmesano). Me he encontrado con gente que ha hecho grandes lugares del IFT y de los países que hemos visitado. No sé cómo organizar esto, así que me quedo con TODOS, no sin subrayar a los que me han aguantado a mí y a mi música como compañeros de despacho: Natxo, Juanjo, JP, Bellorín (cuánto hemos vivido), Antón, Irene y los frustrados del zulo II, quienes me han enseñado mucha física, no sin olvidarme de Montañez y del Choyos, dos grandísimos físicos. A tí

Carlos también te agradezco todos los consejos y correcciones de esta tesis.

Un lugar especial ocupan Ernesto y Nico, con quienes estoy condenado a no entenderme. Creo que he aprendido a haceros un huequito en el corazón. Y también mis compañeros de piso, Maferio y Tomás. ¡Cuánto hemos sufrido Tomás! Ahora ya sólo queda lo bueno...

Ya fuera de la física he tenido muchos apoyos. Esa bicicleta Carlos, ¡qué hay que recuperarla! Y a más Carlos, Diego, María, Irene, Ainara, Sergi, etc. Y por supuesto a Sara, quien ha mostrado siempre una curiosidad sincera por lo que estaba haciendo.

También fuera de la física, aunque con una sensibilidad especial hacia los precarios, está *Forges,* por ser una persona con gran relevancia pública que sin embargo no se ha apoltronado en su sillón ni convertido en un hipócrita, y que sigue diciendo las cosas claras y políticamente incorrectas sin, además, ser un exaltado. A *El Roto* igualmente, por su humor tan negro. Y, por qué no, a *El Jueves* por seguir "tocando los borbones..."

Y a toda mi familia, particularmente a mis padres, que aunque nunca han sabido de qué va todo este *embolao* siempre me han apoyado. Muchas de las rentas intelectuales de las que vivo se deben a ellos y su empeño porque la cultura es algo importante. A los que estuvieron y ya no están.

Y, por último, Gema. La fiera devoradora de libros. Aunque esta vez he encontrado uno que no vas a catar apenas: ¡éste, jajaja! Cayendo en los tópicos, que es lo que ocurre con la gente que se quiere de verdad, pues que es un placer tenerte al ladito, aunque eso ya lo sabías por los *acknowledgements* de todos los peipers, y por muchas cosas más.

Me he despertado, casi a las diez
y me he quedado en la cama, más de tres cuartos de hora
y ha merecido la pena

Hoy sí que es un buen día.

Bibliography

[1] Irene Amado, Carlos Hoyos, Karl Landsteiner, and Sergio Montero. *Residues of Correlators in the Strongly Coupled N=4 Plasma*. 2007. `arXiv:0710.4458 [hep-th]`.

[2] Irene Amado, Carlos Hoyos, Karl Landsteiner, and Sergio Montero. *Absorption Lengths in the Holographic Plasma*. *JHEP*, **09**:057, 2007. `arXiv:0706.2750 [hep-th]`.

[3] Carlos Hoyos, Karl Landsteiner, and Sergio Montero. *Holographic Meson Melting*. *JHEP*, **04**:031, 2007. `hep-th/0612169`.

[4] Carlos Hoyos, Karl Landsteiner, and Sergio Montero. *Quasinormal modes and meson decay rates*. *Fortsch. Phys.*, **55**:760–764, 2007.

[5] L. H. Ryder. *Quantum Field Theory*. Cambridge, UK: Univ. Pr. 2nd edition (1996) 507 p.

[6] Sidney R. Coleman and David J. Gross. *Price of asymptotic freedom*. *Phys. Rev. Lett.*, **31**:851–854, 1973.

[7] D. J. Gross and Frank Wilczek. *Ultraviolet Behavior of Non-Abelian Gauge Theories*. *Phys. Rev. Lett.*, **30**:1343–1346, 1973.

[8] H. David Politzer. *Reliable Perturbative Results For Strong Interactions?* *Phys. Rev. Lett.*, **30**:1346–1349, 1973.

[9] Yao, W. -M. et al. *Review of particle physics*. *J. Phys.*, **G33**:1–1232, 2006.

[10] I. Ya. Pomeranchuk. *On the theory of multiple particle production in a single collision*. *Dokl. Akad. Nauk Ser. Fiz.*, **78**:889–891, 1951.

[11] R. Hagedorn. *Statistical thermodynamics of strong interactions at high-energies*. *Nuovo Cim. Suppl.*, **3**:147–186, 1965.

[12] N. Cabibbo and G. Parisi. *Exponential Hadronic Spectrum and Quark Liberation*. *Phys. Lett.*, **B59**:67, 1975.

[13] John C. Collins and M. J. Perry. *Superdense Matter: Neutrons Or Asymptotically Free Quarks?* *Phys. Rev. Lett.*, **34**:1353, 1975.

[14] Edward V. Shuryak. *Quark-Gluon Plasma and Hadronic Production of Leptons, Photons and Psions*. *Phys. Lett.*, **B78**:150, 1978.

[15] O. K. Kalashnikov and V. V. Klimov. *Phase Transition in Quark-Gluon Plasma*. *Phys. Lett.*, **B88**:328, 1979.

[16] Joseph I. Kapusta. *Quantum Chromodynamics at High Temperature*. *Nucl. Phys.*, **B148**:461–498, 1979.

[17] Y. Aoki, G. Endrodi, Z. Fodor, S. D. Katz, and K. K. Szabo. *The order of the quantum chromodynamics transition predicted by the standard model of particle physics*. *Nature*, **443**:675–678, 2006. `hep-lat/0611014`.

[18] Y. Aoki, Z. Fodor, S. D. Katz, and K. K. Szabo. *The equation of state in lattice QCD: With physical quark masses towards the continuum limit*. *JHEP*, **01**:089, 2006. `hep-lat/0510084`.

[19] Y. Aoki, Z. Fodor, S. D. Katz, and K. K. Szabo. *The QCD transition temperature: Results with physical masses in the continuum limit.* *Phys. Lett.*, **B643**:46–54, 2006. hep-lat/0609068.

[20] Frithjof Karsch. *Lattice QCD at high temperature and density.* *Lect. Notes Phys.*, **583**:209–249, 2002. hep-lat/0106019.

[21] D. A. Gurnett and A. Bhattacharjee. *Introduction to Plasma Physics: With Space and Laboratory Applications.* Cambridge, UK: Univ. Pr. (2005) 462 p.

[22] J. L. Nagle. *The letter 's' (and the sQGP).* *Eur. Phys. J.*, **C49**:275–279, 2007. nucl-th/0608070.

[23] T. D. Lee. *A possible new form of matter at high density.* (talk). Prepared for Symposium on Physics on Our World, Cambridge, Mass., 17-18 Oct 1974.

[24] T. D. Lee and G. C. Wick. *Vacuum Stability and Vacuum Excitation in a Spin 0 Field Theory.* *Phys. Rev.*, **D9**:2291, 1974.

[25] J. Hofmann, Horst Stoecker, W. Scheid, and W. Greiner. *On the Possibility of nuclear shock waves in relativistic heavy ion collisions.* Report of the Workshop on BeV/nucleon Collisions of Heavy Ions: How and Why, Bear Mountain, New York, 29 Nov - 1 Dec 1974.

[26] Baumgardt, H. G. et al. *Shock Waves and MACH Cones in Fast Nucleus-Nucleus Collisions.* *Z. Phys.*, **A273**:359–371, 1975.

[27] John Adams et al. *Experimental and theoretical challenges in the search for the quark gluon plasma: The STAR collaboration's critical assessment of the evidence from RHIC collisions.* *Nucl. Phys.*, **A757**:102–183, 2005. nucl-ex/0501009.

[28] K. Adcox et al. *Formation of dense partonic matter in relativistic nucleus nucleus collisions at RHIC: Experimental evaluation by the PHENIX collaboration.* *Nucl. Phys.*, **A757**:184–283, 2005. nucl-ex/0410003.

[29] B. B. Back et al. *The PHOBOS perspective on discoveries at RHIC.* *Nucl. Phys.*, **A757**:28–101, 2005. nucl-ex/0410022.

[30] I. Arsene et al. *Quark gluon plasma and color glass condensate at RHIC? The perspective from the BRAHMS experiment.* *Nucl. Phys.*, **A757**:1–27, 2005. nucl-ex/0410020.

[31] J. D. Bjorken. *Highly Relativistic Nucleus-Nucleus Collisions: The Central Rapidity Region.* *Phys. Rev.*, **D27**:140–151, 1983.

[32] Peter F. Kolb, Josef Sollfrank, and Ulrich W. Heinz. *Anisotropic transverse flow and the quark-hadron phase transition.* *Phys. Rev.*, **C62**:054909, 2000. hep-ph/0006129.

[33] Ulrich W. Heinz and Peter F. Kolb. *Early thermalization at RHIC.* *Nucl. Phys.*, **A702**:269–280, 2002. hep-ph/0111075.

[34] D. Teaney, J. Lauret, and E. V. Shuryak. *A hydrodynamic description of heavy ion collisions at the SPS and RHIC.* 2001. nucl-th/0110037.

[35] Pasi Huovinen. *Anisotropy of flow and the order of phase transition in relativistic heavy ion collisions.* *Nucl. Phys.*, **A761**:296–312, 2005. nucl-th/0505036.

[36] Derek Teaney. *Effect of shear viscosity on spectra, elliptic flow, and Hanbury Brown-Twiss radii.* *Phys. Rev.*, **C68**:034913, 2003. nucl-th/0301099.

[37] Obtained at www.opensciencegrid.org/cms/?pid=1000135.

[38] Talk by B. Jacak, *"Plasma physics of the quark gluon plasma"*, Boulder, May 2006. Available at http://www4.rcf.bnl.gov/∼steinber/boulder2006/.

[39] Stanislaw Mrowczynski. *Early stage thermalization via instabilities. PoS*, C**POD2006**:042, 2006. hep-ph/0611067.

[40] Peter Arnold, Jonathan Lenaghan, and Guy D. Moore. *QCD plasma instabilities and bottom-up thermalization. JHEP*, **08**:002, 2003. hep-ph/0307325.

[41] Peter Arnold, Guy D. Moore, and Laurence G. Yaffe. *The fate of non-abelian plasma instabilities in 3+1 dimensions. Phys. Rev.*, **D72**:054003, 2005. hep-ph/0505212.

[42] Anton Rebhan, Paul Romatschke, and Michael Strickland. *Dynamics of quark-gluon plasma instabilities in discretized hard-loop approximation. JHEP*, **09**:041, 2005. hep-ph/0505261.

[43] Peter Arnold and Guy D. Moore. *QCD plasma instabilities: The nonabelian cascade. Phys. Rev.*, **D73**:025006, 2006. hep-ph/0509206.

[44] Dietrich Bodeker. *The impact of QCD plasma instabilities on bottom-up thermalization. JHEP*, **10**:092, 2005. hep-ph/0508223.

[45] Peter Arnold and Guy D. Moore. *Non-Abelian Plasma Instabilities for Extreme Anisotropy. Phys. Rev.*, **D76**:045009, 2007. arXiv:0706.0490 [hep-ph].

[46] Dietrich Bodeker and Kari Rummukainen. *Non-abelian plasma instabilities for strong anisotropy. JHEP*, **07**:022, 2007. arXiv:0705.0180 [hep-ph].

[47] A. K. Rebhan. *The NonAbelian Debye mass at next-to-leading order. Phys. Rev.*, **D48**:3967–3970, 1993. hep-ph/9308232.

[48] Anton K. Rebhan. *NonAbelian Debye screening in one loop resummed perturbation theory. Nucl. Phys.*, **B430**:319–344, 1994. hep-ph/9408262.

[49] Peter Arnold and Laurence G. Yaffe. *The NonAbelian Debye screening length beyond leading order. Phys. Rev.*, **D52**:7208–7219, 1995. hep-ph/9508280.

[50] A. Hart, M. Laine, and O. Philipsen. *Static correlation lengths in QCD at high temperatures and finite densities. Nucl. Phys.*, **B586**:443–474, 2000. hep-ph/0004060.

[51] G. Baym, H. Monien, C. J. Pethick, and D. G. Ravenhall. *Transverse interactions and transport in relativistic quark-gluon and electromagnetic plasmas. Phys. Rev. Lett.*, **64**:1867–1870, 1990.

[52] H. Heiselberg. *Viscosities of quark - gluon plasmas. Phys. Rev.*, **D49**:4739–4750, 1994. hep-ph/9401309.

[53] Peter Arnold, Guy D. Moore, and Laurence G. Yaffe. *Transport coefficients in high temperature gauge theories. I: Leading-log results. JHEP*, **11**:001, 2000. hep-ph/0010177.

[54] Laszlo P. Csernai, Joseph. I. Kapusta, and Larry D. McLerran. *On the strongly-interacting low-viscosity matter created in relativistic nuclear collisions. Phys. Rev. Lett.*, **97**:152303, 2006. nucl-th/0604032.

[55] Simon C. Huot, Sangyong Jeon, and Guy D. Moore. *Shear viscosity in weakly coupled $N = 4$ super Yang-Mills theory compared to QCD. Phys. Rev. Lett.*, **98**:172303, 2007. hep-ph/0608062.

[56] M. Asakawa, T. Hatsuda, and Y. Nakahara. *Maximum entropy analysis of the spectral functions in lattice QCD. Prog. Part. Nucl. Phys.*, **46**:459–508, 2001. `hep-lat/0011040`.

[57] F. Karsch, E. Laermann, P. Petreczky, S. Stickan, and I. Wetzorke. *A lattice calculation of thermal dilepton rates. Phys. Lett.*, **B530**:147–152, 2002. `hep-lat/0110208`.

[58] Jean-Paul Blaizot and Francois Gelis. *Photon and dilepton production in the quark-gluon plasma: Perturbation theory vs lattice QCD. Eur. Phys. J.*, **C43**:375–380, 2005. `hep-ph/0504144`.

[59] Gerard 't Hooft. *Dimensional reduction in quantum gravity*. 1993. `gr-qc/9310026`.

[60] Leonard Susskind. *The World as a hologram. J. Math. Phys.*, **36**:6377–6396, 1995. `hep-th/9409089`.

[61] Gerard Hooft. *A Planar Diagram Theory For Strong Interactions. Nucl. Phys.*, **B72**:461, 1974.

[62] Juan Martin Maldacena. *The large N limit of superconformal field theories and supergravity. Adv. Theor. Math. Phys.*, **2**:231–252, 1998. `hep-th/9711200`.

[63] S. S. Gubser, Igor R. Klebanov, and Alexander M. Polyakov. *Gauge theory correlators from non-critical string theory. Phys. Lett.*, **B428**:105–114, 1998. `hep-th/9802109`.

[64] Edward Witten. *Anti-de Sitter space and holography. Adv. Theor. Math. Phys.*, **2**:253–291, 1998. `hep-th/9802150`.

[65] Spires (`http://www.slac.stanford.edu/spires/`) is a nice way to search for them.

[66] S. S. Gubser, Igor R. Klebanov, and A. W. Peet. *Entropy and Temperature of Black 3-Branes. Phys. Rev.*, **D54**:3915–3919, 1996. `hep-th/9602135`.

[67] Igor R. Klebanov and A. A. Tseytlin. *Entropy of Near-Extremal Black p-branes. Nucl. Phys.*, **B475**:164–178, 1996. `hep-th/9604089`.

[68] Edward Witten. *Anti-de Sitter space, thermal phase transition, and confinement in gauge theories. Adv. Theor. Math. Phys.*, **2**:505–532, 1998. `hep-th/9803131`.

[69] S. W. Hawking and Don N. Page. *Thermodynamics of Black Holes in anti-De Sitter Space. Commun. Math. Phys.*, **87**:577, 1983.

[70] Juan Martin Maldacena. *Wilson loops in large N field theories. Phys. Rev. Lett.*, **80**:4859–4862, 1998. `hep-th/9803002`.

[71] Vijay Balasubramanian, Per Kraus, Albion E. Lawrence, and Sandip P. Trivedi. *Holographic probes of anti-de Sitter space-times. Phys. Rev.*, **D59**:104021, 1999. `hep-th/9808017`.

[72] Vijay Balasubramanian, Steven B. Giddings, and Albion E. Lawrence. *What do CFTs tell us about anti-de Sitter spacetimes? JHEP*, **03**:001, 1999. `hep-th/9902052`.

[73] Vijay Balasubramanian, Per Kraus, and Albion E. Lawrence. *Bulk vs. boundary dynamics in anti-de Sitter spacetime. Phys. Rev.*, **D59**:046003, 1999. `hep-th/9805171`.

[74] Ulf H. Danielsson, Esko Keski-Vakkuri, and Martin Kruczenski. *Vacua, propagators, and holographic probes in AdS/CFT. JHEP*, **01**:002, 1999. `hep-th/9812007`.

[75] Shijong Ryang. *The Hadamard function and the Feynman propagator in the AdS/CFT correspondence. Phys. Lett.*, **B469**:87–95, 1999. `hep-th/9909186`.

[76] Dam T. Son and Andrei O. Starinets. *Minkowski-space correlators in AdS/CFT correspondence: Recipe and applications. JHEP*, **09**:042, 2002. hep-th/0205051.

[77] C. P. Herzog and D. T. Son. *Schwinger-Keldysh propagators from AdS/CFT correspondence. JHEP*, **03**:046, 2003. hep-th/0212072.

[78] Igor R. Klebanov. *World-volume approach to absorption by non-dilatonic branes. Nucl. Phys.*, **B496**:231–242, 1997. hep-th/9702076.

[79] Edward Witten. *String theory dynamics in various dimensions. Nucl. Phys.*, **B443**:85–126, 1995. hep-th/9503124.

[80] J. A. Minahan and K. Zarembo. *The Bethe-ansatz for N = 4 super Yang-Mills. JHEP*, **03**:013, 2003. hep-th/0212208.

[81] Niklas Beisert, Burkhard Eden, and Matthias Staudacher. *Transcendentality and crossing. J. Stat. Mech.*, **0701**:P021, 2007. hep-th/0610251.

[82] Niklas Beisert, Rafael Hernandez, and Esperanza Lopez. *A crossing-symmetric phase for AdS(5) x S**5 strings. JHEP*, **11**:070, 2006. hep-th/0609044.

[83] S. Moch, J. A. M. Vermaseren, and A. Vogt. *The three-loop splitting functions in QCD: The non-singlet case. Nucl. Phys.*, **B688**:101–134, 2004. hep-ph/0403192.

[84] A. V. Kotikov, L. N. Lipatov, A. I. Onishchenko, and V. N. Velizhanin. *Three-loop universal anomalous dimension of the Wilson operators in N = 4 SUSY Yang-Mills model. Phys. Lett.*, **B595**:521–529, 2004. hep-th/0404092.

[85] Zvi Bern, Michael Czakon, Lance J. Dixon, David A. Kosower, and Vladimir A. Smirnov. *The Four-Loop Planar Amplitude and Cusp Anomalous Dimension in Maximally Supersymmetric Yang-Mills Theory. Phys. Rev.*, **D75**:085010, 2007. hep-th/0610248.

[86] Juan Martin Maldacena. *Eternal black holes in Anti-de-Sitter. JHEP*, **04**:021, 2003. hep-th/0106112.

[87] Kostas D. Kokkotas and Bernd G. Schmidt. *Quasi-normal modes of stars and black holes. Living Rev. Rel.*, **2**:2, 1999. gr-qc/9909058.

[88] Hans-Peter Nollert. *Topical Review: Quasinormal modes: the characteristic 'sound' of black holes and neutron stars. Class. Quant. Grav.*, **16**:R159–R216, 1999.

[89] Gary T. Horowitz and Veronika E. Hubeny. *Quasinormal modes of AdS black holes and the approach to thermal equilibrium. Phys. Rev.*, **D62**:024027, 2000. hep-th/9909056.

[90] Vitor Cardoso and Jose P. S. Lemos. *Quasi-normal modes of Schwarzschild anti-de Sitter black holes: Electromagnetic and gravitational perturbations. Phys. Rev.*, **D64**:084017, 2001. gr-qc/0105103.

[91] Danny Birmingham, Ivo Sachs, and Sergey N. Solodukhin. *Conformal field theory interpretation of black hole quasi-normal modes. Phys. Rev. Lett.*, **88**:151301, 2002. hep-th/0112055.

[92] Ian G. Moss and James P. Norman. *Gravitational quasinormal modes for anti-de Sitter black holes. Class. Quant. Grav.*, **19**:2323–2332, 2002. gr-qc/0201016.

[93] Giuseppe Policastro, Dam T. Son, and Andrei O. Starinets. *From AdS/CFT correspondence to hydrodynamics. JHEP*, **09**:043, 2002. hep-th/0205052.

[94] Andrei O. Starinets. *Quasinormal modes of near extremal black branes. Phys. Rev.*, **D66**:124013, 2002. hep-th/0207133.

[95] Giuseppe Policastro, Dam T. Son, and Andrei O. Starinets. *From AdS/CFT correspondence to hydrodynamics. II: Sound waves. JHEP*, **12**:054, 2002. `hep-th/0210220`.

[96] Alvaro Nunez and Andrei O. Starinets. *AdS/CFT correspondence, quasinormal modes, and thermal correlators in N = 4 SYM. Phys. Rev.*, **D67**:124013, 2003. `hep-th/0302026`.

[97] Vitor Cardoso, Roman Konoplya, and Jose P. S. Lemos. *Quasinormal frequencies of Schwarzschild black holes in anti-de Sitter spacetimes: A complete study on the asymptotic behavior. Phys. Rev.*, **D68**:044024, 2003. `gr-qc/0305037`.

[98] R. A. Konoplya. *Gravitational quasinormal radiation of higher-dimensional black holes. Phys. Rev.*, **D68**:124017, 2003. `hep-th/0309030`.

[99] Pavel K. Kovtun and Andrei O. Starinets. *Quasinormal modes and holography. Phys. Rev.*, **D72**:086009, 2005. `hep-th/0506184`.

[100] Joshua J. Friess, Steven S. Gubser, Georgios Michalogiorgakis, and Silviu S. Pufu. *Expanding plasmas and quasinormal modes of anti-de Sitter black holes. JHEP*, **04**:080, 2007. `hep-th/0611005`.

[101] N. Andersson and K. E. Thylwe. *Complex angular momentum approach to black hole scattering. Class. Quant. Grav.*, **11**:2991–3001, 1994.

[102] Sean A. Hartnoll and S. Prem Kumar. *AdS black holes and thermal Yang-Mills correlators. JHEP*, **12**:036, 2005. `hep-th/0508092`.

[103] Michel Le Bellac. *Thermal Field Theory*. Cambridge, UK: Univ. Pr. (2000) 270 p.

[104] Derek Teaney. *Finite temperature spectral densities of momentum and R-charge correlators in N = 4 Yang Mills theory. Phys. Rev.*, **D74**:045025, 2006. `hep-ph/0602044`.

[105] Pavel Kovtun and Andrei Starinets. *Thermal spectral functions of strongly coupled N = 4 supersymmetric Yang-Mills theory. Phys. Rev. Lett.*, **96**:131601, 2006. `hep-th/0602059`.

[106] Robert C. Myers, Andrei O. Starinets, and Rowan M. Thomson. *Holographic spectral functions and diffusion constants for fundamental matter. JHEP*, **11**:091, 2007. `arXiv:0706.0162 [hep-th]`.

[107] Johanna Erdmenger, Matthias Kaminski, and Felix Rust. *Holographic vector mesons from spectral functions at finite baryon or isospin density*. 2007. `arXiv:0710.0334 [hep-th]`.

[108] Berndt Muller and James L. Nagle. *Results from the Relativistic Heavy Ion Collider. Ann. Rev. Nucl. Part. Sci.*, **56**:93–135, 2006. `nucl-th/0602029`.

[109] Csaba Csaki, Hirosi Ooguri, Yaron Oz, and John Terning. *Glueball mass spectrum from supergravity. JHEP*, **01**:017, 1999. `hep-th/9806021`.

[110] Robert de Mello Koch, Antal Jevicki, Mihail Mihailescu, and Joao P. Nunes. *Evaluation of glueball masses from supergravity. Phys. Rev.*, **D58**:105009, 1998. `hep-th/9806125`.

[111] Richard C. Brower, Samir D. Mathur, and Chung-I Tan. *Glueball spectrum for QCD from AdS supergravity duality. Nucl. Phys.*, **B587**:249–276, 2000. `hep-th/0003115`.

[112] Vitor Cardoso, Jose Natario, and Ricardo Schiappa. *Asymptotic quasinormal frequencies for black holes in non- asymptotically flat spacetimes. J. Math. Phys.*, **45**:4698–4713, 2004. `hep-th/0403132`.

[113] Jose Natario and Ricardo Schiappa. *On the classification of asymptotic quasinormal frequencies for d-dimensional black holes and quantum gravity*. *Adv. Theor. Math. Phys.*, **8**:1001–1131, 2004. hep-th/0411267.

[114] Dongsu Bak, Andreas Karch, and Laurence G. Yaffe. *Debye screening in strongly coupled N=4 supersymmetric Yang-Mills plasma*. *JHEP*, **08**:049, 2007. arXiv:0705.0994 [hep-th].

[115] E. W. Leaver. *An Analytic representation for the quasi normal modes of Kerr black holes*. *Proc. Roy. Soc. Lond.*, **A402**:285–298, 1985.

[116] R. S. Maier. *The 192 Solutions of the Heun Equation*. *Math. Comp.*, **76**:811–843, 2007. arXiv:math/0408317 [math.CA].

[117] Hideo Kodama and Akihiro Ishibashi. *A master equation for gravitational perturbations of maximally symmetric black holes in higher dimensions*. *Prog. Theor. Phys.*, **110**:701–722, 2003. hep-th/0305147.

[118] Sergey A. Cherkis and Akikazu Hashimoto. *Supergravity solution of intersecting branes and AdS/CFT with flavor*. *JHEP*, **11**:036, 2002. hep-th/0210105.

[119] Horatiu Nastase. *On Dp-Dp+4 systems, QCD dual and phenomenology*. 2003. hep-th/0305069.

[120] Benjamin A. Burrington, James T. Liu, Leopoldo A. Pando Zayas, and Diana Vaman. *Holographic duals of flavored N = 1 super Yang-Mills: Beyond the probe approximation*. *JHEP*, **02**:022, 2005. hep-th/0406207.

[121] Johanna Erdmenger and Ingo Kirsch. *Mesons in gauge / gravity dual with large number of fundamental fields*. *JHEP*, **12**:025, 2004. hep-th/0408113.

[122] Ingo Kirsch and Diana Vaman. *The D3/D7 background and flavor dependence of Regge trajectories*. *Phys. Rev.*, **D72**:026007, 2005. hep-th/0505164.

[123] Roberto Casero, Carlos Nunez, and Angel Paredes. *Towards the string dual of N = 1 SQCD-like theories*. *Phys. Rev.*, **D73**:086005, 2006. hep-th/0602027.

[124] Francesco Benini, Felipe Canoura, Stefano Cremonesi, Carlos Nunez, and Alfonso V. Ramallo. *Unquenched flavors in the Klebanov-Witten model*. *JHEP*, **02**:090, 2007. hep-th/0612118.

[125] Francesco Benini, Felipe Canoura, Stefano Cremonesi, Carlos Nunez, and Alfonso V. Ramallo. *Backreacting Flavors in the Klebanov-Strassler Background*. *JHEP*, **09**:109, 2007. arXiv:0706.1238 [hep-th].

[126] Andreas Karch and Emanuel Katz. *Adding flavor to AdS/CFT*. *JHEP*, **06**:043, 2002. hep-th/0205236.

[127] Alfonso V. Ramallo. *Adding open string modes to the gauge / gravity correspondence*. *Mod. Phys. Lett.*, **A21**:1481–1494, 2006. hep-th/0605261.

[128] M. Christensen, Valeri P. Frolov, and A. L. Larsen. *Soap bubbles in outer space: Interaction of a domain wall with a black hole*. *Phys. Rev.*, **D58**:085008, 1998. hep-th/9803158.

[129] Valeri P. Frolov, A. L. Larsen, and M. Christensen. *Domain wall interacting with a black hole: A new example of critical phenomena*. *Phys. Rev.*, **D59**:125008, 1999. hep-th/9811148.

[130] J. Babington, J. Erdmenger, Nick J. Evans, Z. Guralnik, and I. Kirsch. *Chiral symmetry breaking and pions in non-supersymmetric gauge/gravity duals*. *Phys. Rev.*, **D69**:066007, 2004. hep-th/0306018.

[131] Ingo Kirsch. *Generalizations of the AdS/CFT correspondence*. *Fortsch. Phys.*, **52**:727–826, 2004. hep-th/0406274.

[132] Riccardo Apreda, Johanna Erdmenger, Nick Evans, and Zachary Guralnik. *Strong coupling effective Higgs potential and a first order thermal phase transition from AdS/CFT duality*. *Phys. Rev.*, **D71**:126002, 2005. hep-th/0504151.

[133] Tameem Albash, Veselin G. Filev, Clifford V. Johnson, and Arnab Kundu. *A topology-changing phase transition and the dynamics of flavour*. 2006. hep-th/0605088.

[134] David Mateos, Robert C. Myers, and Rowan M. Thomson. *Holographic phase transitions with fundamental matter*. *Phys. Rev. Lett.*, **97**:091601, 2006. hep-th/0605046.

[135] Andreas Karch and Andy O'Bannon. *Chiral transition of $N = 4$ super Yang-Mills with flavor on a 3-sphere*. *Phys. Rev.*, **D74**:085033, 2006. hep-th/0605120.

[136] Martin Kruczenski, David Mateos, Robert C. Myers, and David J. Winters. *Towards a holographic dual of large-N(c) QCD*. *JHEP*, **05**:041, 2004. hep-th/0311270.

[137] Tadakatsu Sakai and Shigeki Sugimoto. *Low energy hadron physics in holographic QCD*. *Prog. Theor. Phys.*, **113**:843–882, 2005. hep-th/0412141.

[138] Kasper Peeters, Jacob Sonnenschein, and Marija Zamaklar. *Holographic decays of large-spin mesons*. *JHEP*, **02**:009, 2006. hep-th/0511044.

[139] A. L. Cotrone, L. Martucci, and W. Troost. *String splitting and strong coupling meson decay*. *Phys. Rev. Lett.*, **96**:141601, 2006. hep-th/0511045.

[140] F. Bigazzi and A. L. Cotrone. *New predictions on meson decays from string splitting*. *JHEP*, **11**:066, 2006. hep-th/0606059.

[141] Kasper Peeters, Jacob Sonnenschein, and Marija Zamaklar. *Holographic melting and related properties of mesons in a quark gluon plasma*. *Phys. Rev.*, **D74**:106008, 2006. hep-th/0606195.

[142] Martin Kruczenski, David Mateos, Robert C. Myers, and David J. Winters. *Meson spectroscopy in AdS/CFT with flavour*. *JHEP*, **07**:049, 2003. hep-th/0304032.

[143] M. Henningson and K. Skenderis. *The holographic Weyl anomaly*. *JHEP*, **07**:023, 1998. hep-th/9806087.

[144] Vijay Balasubramanian and Per Kraus. *A stress tensor for anti-de Sitter gravity*. *Commun. Math. Phys.*, **208**:413–428, 1999. hep-th/9902121.

[145] Sebastian de Haro, Sergey N. Solodukhin, and Kostas Skenderis. *Holographic reconstruction of spacetime and renormalization in the AdS/CFT correspondence*. *Commun. Math. Phys.*, **217**:595–622, 2001. hep-th/0002230.

[146] Andreas Karch, Andy O'Bannon, and Kostas Skenderis. *Holographic renormalization of probe D-branes in AdS/CFT*. *JHEP*, **04**:015, 2006. hep-th/0512125.

[147] Sai Iyer and Clifford M. Will. *Black Hole Normal Modes: A Wkb Approach. 1. Foundations And Application Of A Higher Order Wkb Analysis Of Potential Barrier Scattering*. *Phys. Rev.*, **D35**:3621, 1987.

[148] Sai Iyer. *Black Hole Normal Modes: A Wkb Approach. 2. Schwarzschild Black Holes. Phys. Rev.*, **D35**:3632, 1987.

[149] Kostas Glampedakis and Nils Andersson. *Quick and dirty methods for studying black-hole resonances. Class. Quant. Grav.*, **20**:3441–3464, 2003. gr-qc/0304030.

[150] Jan Troost. *A note on causality in the bulk and stability on the boundary. Phys. Lett.*, **B578**:210–214, 2004. hep-th/0308044.

[151] Pablo Minces. *Bound states in the AdS/CFT correspondence. Phys. Rev.*, **D70**:025011, 2004. hep-th/0402161.

[152] David Mateos, Robert C. Myers, and Rowan M. Thomson. *Thermodynamics of the brane. JHEP*, **05**:067, 2007. hep-th/0701132.

[153] Alex Buchel. *A holographic perspective on Gubser-Mitra conjecture. Nucl. Phys.*, **B731**:109–124, 2005. hep-th/0507275.

[154] Kazuo Ghoroku, Tomohiko Sakaguchi, Nobuhiro Uekusa, and Masanobu Yahiro. *Flavor quark at high temperature from a holographic model. Phys. Rev.*, **D71**:106002, 2005. hep-th/0502088.

[155] Valeri P. Frolov. *Merger transitions in brane-black-hole systems: Criticality, scaling, and self-similarity. Phys. Rev.*, **D74**:044006, 2006. gr-qc/0604114.

[156] Steven S. Gubser. *Comparing the drag force on heavy quarks in $N = 4$ super-Yang-Mills theory and QCD. Phys. Rev.*, **D76**:126003, 2007. hep-th/0611272.

[157] M. Laine, O. Philipsen, P. Romatschke, and M. Tassler. *Real-time static potential in hot QCD. JHEP*, **03**:054, 2007. hep-ph/0611300.

[158] Joshua Erlich, Emanuel Katz, Dam T. Son, and Mikhail A. Stephanov. *QCD and a holographic model of hadrons. Phys. Rev. Lett.*, **95**:261602, 2005. hep-ph/0501128.

[159] Leandro Da Rold and Alex Pomarol. *Chiral symmetry breaking from five dimensional spaces. Nucl. Phys.*, **B721**:79–97, 2005. hep-ph/0501218.

[160] Peter Breitenlohner and Daniel Z. Freedman. *Positive Energy in anti-De Sitter Backgrounds and Gauged Extended Supergravity. Phys. Lett.*, **B115**:197, 1982.

[161] Akihiro Ishibashi and Hideo Kodama. *Stability of higher-dimensional Schwarzschild black holes. Prog. Theor. Phys.*, **110**:901–919, 2003. hep-th/0305185.

[162] E. Berti and K. D. Kokkotas. *Quasinormal modes of Reissner-Nordstroem-anti-de Sitter black holes: Scalar, electromagnetic and gravitational perturbations. Phys. Rev.*, **D67**:064020, 2003. gr-qc/0301052.

[163] W. H. Press, S. A. Teukolsky, W. T. Vetterling, and B. P. Flannery. *Numerical Recipes in C*. Cambridge, UK: Univ. Pr. (2002) 1020 p.